Studying the Solution Behavior of DNA and DNA Sliding Clamps Using Various

Fluorescence Techniques

by

Suman Ranjit

A Dissertation Presented in Partial Fulfillment
of the Requirements for the Degree
Doctor of Philosophy

Approved April 2013 by the
Graduate Supervisory Committee:

Marcia Levitus, Chair
Stuart Lindsay
Hao Yan

ARIZONA STATE UNIVERSITY

May 2013

ABSTRACT

Solution conformations and dynamics of proteins and protein-DNA complexes are often difficult to predict from their crystal structures. The crystal structure only shows a snapshot of the different conformations these biological molecules can have in solution. Multiple different conformations can exist in solution and potentially have more importance in the biological activity. DNA sliding clamps are a family of proteins with known crystal structures. These clamps encircle the DNA and enable other proteins to interact more efficiently with the DNA. Eukaryotic PCNA and prokaryotic β clamp are two of these clamps, some of the most stable homo-oligomers known. However, their solution stability and conformational equilibrium have not been investigated in depth before. Presented here are the studies involving two sliding clamps: yeast PCNA and bacterial β clamp. These studies show that the β clamp has a very different solution stability than PCNA. These conclusions were reached through various different fluorescence-based experiments, including fluorescence correlation spectroscopy (FCS), Förster resonance energy transfer (FRET), single molecule fluorescence, and various time resolved fluorescence techniques.

Interpretations of these, and all other, fluorescence-based experiments are often affected by the properties of the fluorophores employed. Often the fluorescence properties of these fluorophores are influenced by their microenvironments. Fluorophores are known to sometimes interact with biological molecules, and this can have pronounced effects on the rotational mobility and photophysical properties of the dye. Misunderstanding the effect of these photophysical and rotational properties can lead to a misinterpretation of the obtained data. In this thesis, photophysical behaviors of various

organic dyes were studied in the presence of deoxymononucleotides to examine more closely how interactions between fluorophores and DNA bases can affect fluorescent properties. Furthermore, the properties of cyanine dyes when bound to DNA and the effect of restricted rotation on FRET are presented in this thesis. This thesis involves studying fluorophore photophysics in various microenvironments and then expanding into the solution stability and dynamics of the DNA sliding clamps.

ACKNOWLEDGEMENTS

First, I would like to thank my parents, without whom I would not be where I am today. Their dedication toward my education and help and support throughout the years have been instrumental in every single one of my accomplishments. I would like to thank my baby sister, Debapriya, who has been the greatest sibling and partner in crime one can ever imagine.

I want to acknowledge my mentor, Dr. Marcia Levitus. The personal and professional support she has provided for the last six years has been way above the norm and instrumental in my development in the field of science. Her dedication to science and her work ethic have been a great inspiration to me. I am also grateful to the members of my committee, Dr. Stuart Lindsay and Dr. Hao Yan, for their time and guidance. I want to thank Dr. Kaushik Gurunathan for all the help and scientific discussions when I started in the lab. I want to also thank Elana Stennett for the help with this manuscript. Finally, I want to thank all the past and present graduate and undergraduate students who I have interacted with along the way. Their advice and support have been very helpful throughout the years.

TABLE OF CONTENTS

LIST OF TABLES

LIST OF FIGURES

Chapter 1

DNA, deoxymononucleotides, sliding clamps and the different fluorescent

methodologies used for deciphering the interactions

Structures of proteins and protein-DNA complexes are often known but

understanding their function in solution is often elusive. For example, the crystal

structure of DNA sliding clamp was first discovered in 1991.[1] Since that time, any

organism, from viruses to humans, that uses DNA to hold its genetic code has been found

to have these sliding clamps to facilitate DNA replication and repairs. These clamps are

some of the most stable homo-oligomers found in nature, yet they need to open to bind

around DNA. How does this happen? Is the presence of accessory proteins necessary? Do

the clamps have some inherent dynamic behavior that facilitates this binding? The crystal

structures of these clamps do not provide any insight into these questions. As a result,

another technique is needed to look at the conformational dynamics of biological

molecules, in this case the dynamics of the DNA sliding clamps. Fluorescence is such a

technique to investigate these questions on various different timescales so a bigger,

broader picture can be developed.

The conformational dynamics of a biomolecule can be monitored using various

distance-dependent fluorescence methods, including Förster resonance energy transfer

(FRET) and quenching, which makes fluorescence techniques very beneficial.

Interpretation of the data collected from fluorescence experiments are often dependent on

various environmental factors, making these techniques a bit more challenging. Not only

does the fluorescence properties of the fluorophore depend on the micro-environment it is

in, but also the fluorophore can interact with the biological molecule, changing the

properties of the dye. As a result, this can lead to misinterpretation of the data. Therefore,

the photophysics of the systems must be studied in more detail. This thesis is a

compilation of studying fluorophore photophysics in various micro-environments and

then expanding into the solution stability and dynamics of DNA sliding clamps.

1.1 Introduction

Deoxyribonucleic acid (DNA) is one of the most important biological molecules because it contains all of the necessary genetic information. With the help of different accessory proteins, the genome is carried forward for future generations by the DNA replication machinery.[2] A single strand of DNA is a polymer of repeating deoxymononucleotide monomers. The combination of repeating deoxymononucleotides and specific base pair interactions result in DNA forming a rigid double-stranded structure. These characteristics of DNA also allow for one strand to be used as a template for replication. DNA replication involves the use of many different proteins, for example DNA polymerase. DNA polymerase itself is a set of different individual proteins that, when combined, copy the DNA code. One of the important proteins in the DNA polymerase is the DNA sliding clamp.[3] This clamp encircles the DNA with the help of clamp loader proteins and allows the replication machinery to attach to the DNA, resulting in an increase in replication processivity.[4]

The projects described in this thesis involve studying the interactions of DNA and deoxymononucleotides with different fluorophores, as well as using the rigid structure of B form DNA to study different photophysical properties of the dyes. The second chapter of this thesis explains how the structure and geometry of B form DNA was used to control the orientation of two cyanine dyes, Cy3 and Cy5, during FRET. The third chapter of this thesis describes the specific interactions of three different dyes (TAMRA, Cy3B and Alexa 546) with the four DNA mononucleotide phosphates. Further studies

have looked at the solution stability and dynamics of DNA sliding clamps, as the fourth chapter describes.

All of these projects were investigated using various different fluorescence processes and experimental techniques including FRET, quenching of fluorescence, fluorescence correlation spectroscopy (FCS), time resolved fluorescence techniques, single molecule fluorescence, and steady state fluorescence techniques. These techniques and methods are described later in this chapter.

1.2. DNA, deoxynucleotides and sliding clamps

1.2.1. DNA and nucleotide monophosphates. DNA is one of the most important molecule in the history of life. Double-stranded DNA consists of two anti-parallel single DNA strands. The two DNA strands are held together by hydrogen bonding between two DNA bases from the two complementary strands and stacking interactions between adjacent base pairs. The order of the nucleotides determines the primary structure of DNA. This involves the nucleobases, the deoxyribose sugar and the phosphate backbone (shown in red, black, blue in panel A of Figure. 1.1). The attachment of the nucleobase with the deoxyribose sugar is called a nucleoside and the nucleosides are attached to each other using a phosphodiester linkage. DNA contains four different bases: two purines (adenine and guanine) and two pyrimidines (thymine and cytosine). The secondary structure of DNA can vary depending on the conditions. At physiological conditions, DNA is in the B form of the helix.[5] This is the structure that was originally discussed by Watson and Crick in their pioneering work.[6] In this form, two anti-parallel strands are attached by hydrophobic interactions and base pairing between adenine and thymine and between guanine and cytosine (known as Watson-Crick base pairs). This creates the helical structure of DNA (shown in panel B of Figure. 1.1). The B-form of the helix consists of a hydrophobic interior, which is created from the hydrogen-bonded base pairs, and a hydrophilic exterior, consisting of the negatively charged phosphate backbone. The stacked base pairs are virtually perpendicular to the helical axis of DNA and have a separation of 3.4 Å. The adjacent base pairs have a 36° angle between them. This results in a helical pitch of 34 Å and about 10 base pairs per complete turn of DNA. The hydrophilic phosphate backbone imparts a negative charge on the DNA while the

hydrogen bonding and the stacking interactions provide the necessary stabilization required to form the helical structure. B-DNA has a characteristically wider major groove and a narrower minor groove.[5] The B-form of the DNA has a persistence length of about ~50 nm (or approximately 150 bp). This structure of B-DNA was used as a scaffold to attach a modified Cy3 and Cy5 to control their relative orientation during the FRET (see chapter 2).

Deoxynucleotide monophosphates (dNMPs) are the moieties consisting of the DNA bases, deoxyribose sugar, and a 5'-phosphate group (shown in red, black, and blue, respectively, in panel C of Figure. 1.1). There are four different dNMPs corresponding to the four different nucleobases. These are deoxyadenosine monophosphate (dAMP), deoxygunaosine monophosphate (dGMP), deoxycytidine monophospahate (dCMP) and deoxythymidine monophosphate (dTMP) (left to right in panel C of Figure 1.1). The interactions of these nucleotides with different fluorescent dyes (Cy3B, TAMRA, Alexa 546) are presented in chapter 3 of this thesis.
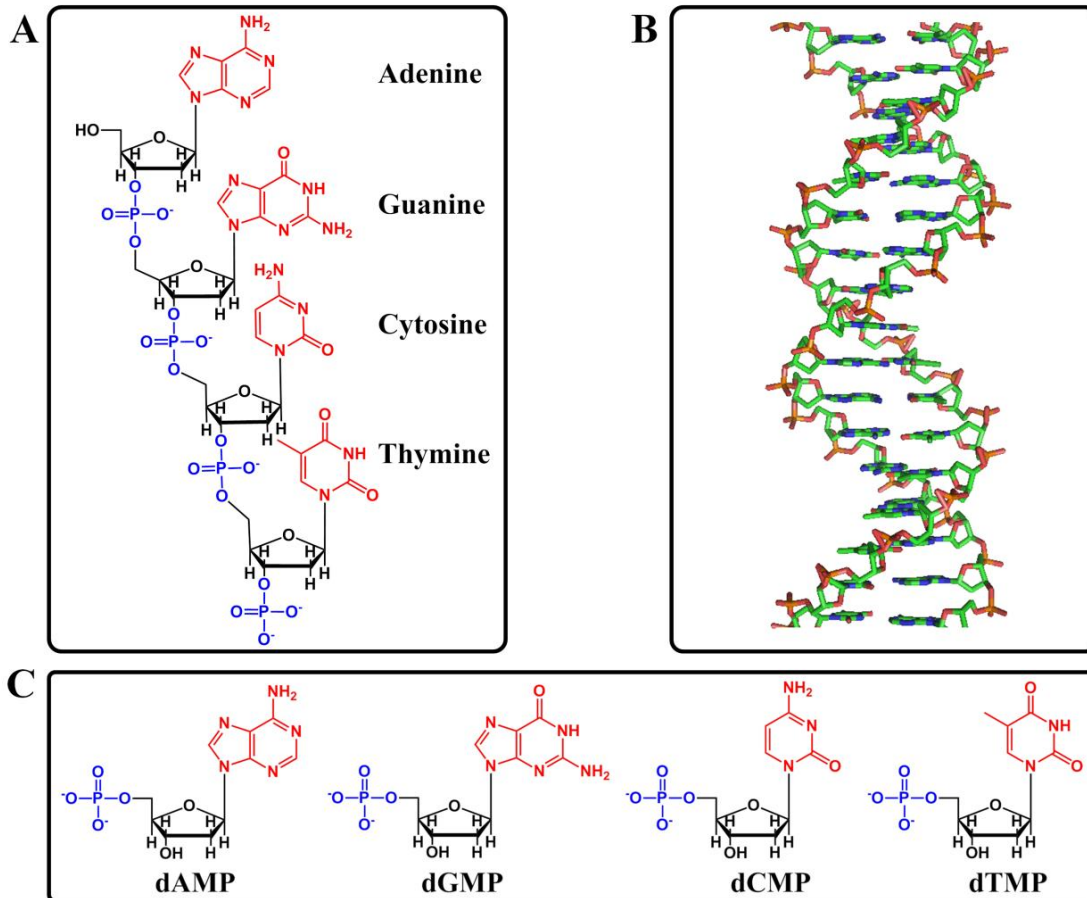
Figure 1.1. Structure of DNA and deoxymononucleotides. Panel A illustrates the primary structure of DNA. The nucleobases (shown in red) are connected to a deoxyribose sugar (shown in black) and form nucleosides. These nucleosides are connected by phosphodiester bonds (shown in blue). The structures of four different nucleobases are also shown in the same figure. Panel B describes the secondary structure of DNA under physiological conditions - B form. This figure was created using the software hyperchem[7] and visualized using pymol. Panel C represents the structures of deoxymononucleotides. The nucleobases, deoxyribose sugar and the 5'phosphate are represented in red, black and blue respectively. The four nucleotides are deoxyadenosine monophopsphate (dAMP), deoxyguanosine monophopsphate (dGMP), deoxycytidine monophopsphate (dCMP) and deoxythymidine monophopsphate (dTMP) (from left to right).

1.2.2. Sliding clamps. Sliding clamps are part of the DNA replication machinery.[3] They are ring-shaped proteins that encircle the DNA and also bind to DNA polymerase and DNA repair proteins. The crystal structures of the sliding clamps show

these ring-like structures in absence of DNA and the rings encircling the DNA when DNA is present.[8-11] The presence of sliding clamps allows the replication proteins to be in closer proximity to DNA, resulting in an increase in the speed and processivity of replication by many orders of magnitude.[12] Sliding clamps are found in various different organisms including T4 phage, bacteria, and eukaryotic cells.[12] Although the sequence homology between the different sliding clamps is very little, they have very similar topology. The structure of various different clamps are visualized using the software Chimera and are represented in Figure. 1.2.[13] These include (A) the β-clamp from *E. coli* (a bacteria), (B) the PCNA from *S. cerevisiae* (baker's yeast, an eukaryote), (C) PCNA from *S. solfataricus* (an archaea), and (D) gp45 from T4 phage virus.

(A)- β-clamp from *E. Coli*.   **(B)- PCNA from *S. cerevisiae*.**   **(C)- PCNA from *S. solfataricus*.**   **(D)- gp45 from T4 - phage**
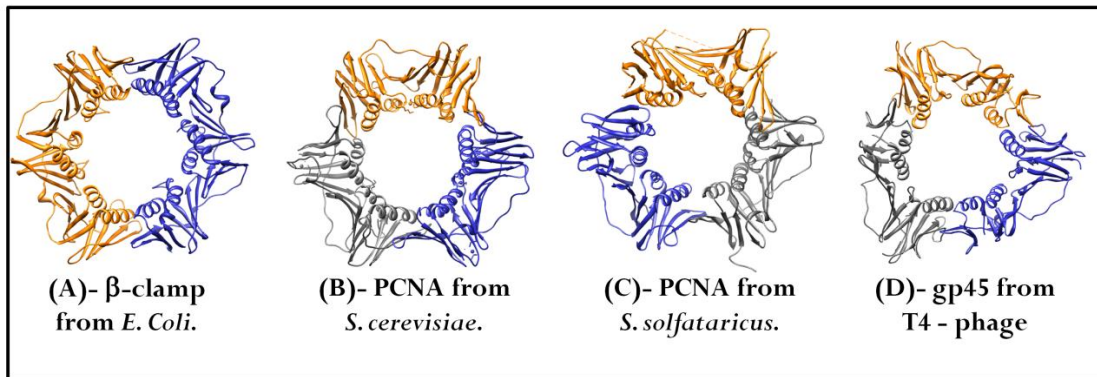
Figure 1.2. Crystal structure of the sliding clamps from different organisms - (A) *Escherichia coli* β (PDB ID. 1MMI), (B) Eukaryotic PCNA from *Saccharomyces cerevisiae* (PDB ID. 1PLQ), (C) archeal PCNA from *Sulfolobus solfataricus* (PDB ID. 2IX2) and (D) gp45 protein from T4 phage virus (PDB ID. 1CZD). These structures were visualized using Chimera.

Chapter 4 of this thesis describes the experiments and results obtained to answer questions about the solution structure, stability, and dynamics of the sliding clamps. In

this chapter, two different sliding clamps - β-clamp from *Escherichia Coli* and PCNA from *Saccharomyces cerevisiae* (Baker's yeast) - are looked at. The crystal structures of both of these proteins are established[9, 11] and the structures of the clamps while encircling the DNA are represented in Figure 1.3.[8, 14] β-clamp is a homodimer consisting of two identical monomeric protein units attached in a head-to-tail fashion. Each monomer has six α helices on the inside surface of the ring and six β sheets on the outside of the ring. In contrast, PCNA is a homotrimer, with each monomer having four α helices and four β clamps. When the sliding clamps encircle the DNA, the central axis of the clamp creates an angle with the helical axis of the DNA. These angles are ~22˚ and ~40˚ for the β-clamp and the PCNA, respectively.[8, 14] Although the crystal structures of these proteins are known, the solution stability and the presence or absence of a rapid spontaneous equilibrium between an open and a closed structure of the clamps have not been investigated previously. To study these properties, both types of clamps were modified and fluorescently labeled with TAMRA. In one type of modification, each monomeric subunit contains one fluorophore. In the other type of the modification, there are two fluorophores attached to the head and the tail portion of each subunit. The positions of these fluorophores in the second sample are such that one fluorophore from one subunit is in very close proximity to another fluorophore (~5 Å) of the adjacent unit. This results in a H-dimer formation and quenching of fluorescence. The reason behind this self quenching is described in detail later in section 1.3.2.5 of this chapter. The opening of the ring or dissociation of the trimer/dimer to monomer results in increased distance between these adjacent dyes and increase of fluorescence. The fluorescence intensity of the sample with only one fluorophore per subunit is independent of the dissociation or ring

9

opening-closing. These two different types of modified clamps were used to study the

ring opening and closing dynamics of β clamp and monomerization equilibria of the

PCNA and β clamp.
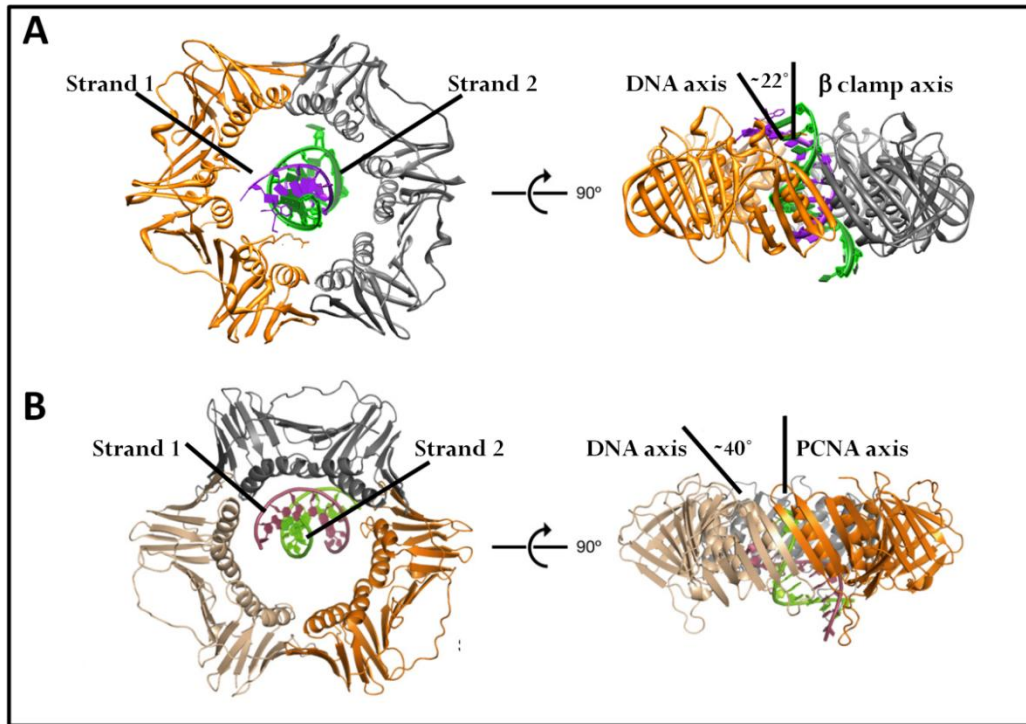
Figure 1.3. The crystal structure of the (A) β-clamp and the (B) PCNA when co-crystallized with the DNA. The β-clamp contains two monomeric subunits (orange and grey in panel A) and PCNA contains three monomeric subunits (orange, grey and brown in panel B). The helical axis of the double stranded DNA creates an angle of ~22˚ and ~40˚ with the central axis of the sliding clamp for the β-clamp and the PCNA, respectively. These pictures were modified from reference 11 and 12 using the software chimera.[8, 13, 14]

1.3. Fluorescence methods and techniques:

1.3.1. Förster resonance energy transfer (FRET). Förster resonance energy transfer, or FRET, is a process where energy from the excited state of one molecule, called the donor, is non-radiatively transferred to the ground state of another molecule, called the acceptor. In FRET, the acceptor has a lower energy gap between the ground state and the first excited state compared to the donor and accepts energy from the donor to become excited itself. The acceptor then can de-excite by transmitting fluorescence.[15, 16] By monitoring the increase in fluorescence of the acceptor or the decrease in fluorescence of the donor, the extent of FRET that occurs in a system can be monitored. These processes can be pictorially described by a Jablonski diagram (Figure 1.4). In this figure, the solid and the dashed arrows represent the radiative and non-radiative pathways, respectively. The fluorescence of the donor and the acceptor are represented by the green and brown arrows, respectively. FRET is shown in red and the de-excitation of the donor by FRET is shown in purple. In FRET, the interaction between the donor point transition emission dipole moment and the acceptor point transition excitation dipole moment results in non-radiative transfer of energy, donor de-excitation and acceptor excitation.
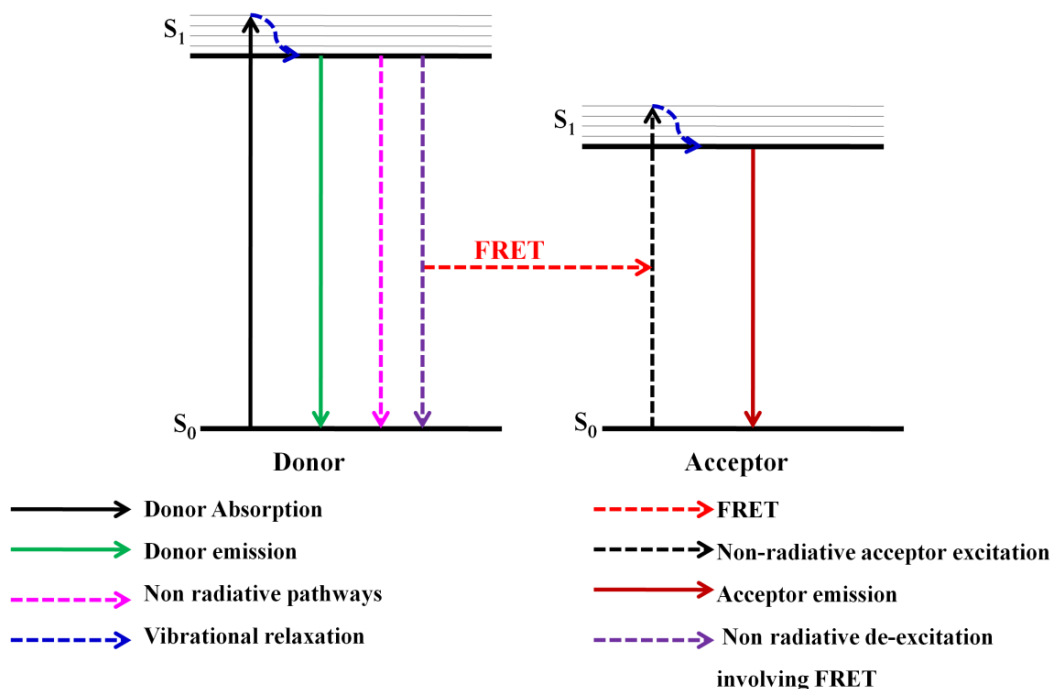
Figure 1.4. A simplified Jablonski diagram describing FRET. After the donor is excited from S_0 to S_1 (black, solid), it comes back to the lowest vibrational state of S_1 by vibrational relaxation (blue, dashed). From the lowest vibrational state of S_1, the molecule can come back to the ground state by radiative emission called fluorescence (green, solid), or via various different non-radiative pathways (magenta, dashed) including internal conversion and FRET (purple, dashed). In FRET, the non-radiative energy transfer (red, dashed) results in the excitation of the acceptor (black, dashed) and subsequent emission of the acceptor (brown, solid) In this diagram, the radiative processes are shown by the solid arrows and the non-radiative processes are depicted with the dashed arrows.

The efficiency of energy transfer depends on the distance between the donor and the acceptor dye (R_{DA}), and hence FRET can be used to measure distances in biological molecules when tagged with a donor-acceptor pair of fluorescent probes.[17-21] Since its discovery, FRET has been one of the most widely used techniques to study structural and functional properties of various biological systems because of the dependence of FRET efficiency on the distance. Stryer first introduced this technique as a tool for measuring

12

distances in biological systems and termed this technique 'spectroscopic ruler'.[22] Lately,

with the advancements in the field of optical detection, newer brighter light sources and

the development of stable, bright organic fluorophores have resulted in the detection of

FRET in the single molecule level.[21, 23-26] Single molecule FRET has increased the

popularity of this already popular technique considerably.

The efficiency of FRET is dependent on the distance between the donor and the

acceptor molecule (R_{DA}). Förster's theory connects this distance (R_{DA}) to the measured

efficiency of energy transfer. This theory treats the donor and acceptor molecules as point

transition dipole moments and according to this theory, the efficiency of the transfer is

given by,[15]

$$E_{FRET} = \frac{R_0^6}{R_0^6 + R_{DA}^6} \tag{1.1}$$

In the above equation R_0 is a term known as the Förster's radius. Hence, if R_0 is

known, the distance between the donor and the acceptor molecules (R_{DA}) can be

calculated. Förster's radius is defined as the distance where the efficiency of the energy

transfer is 50%. Figure 1.5 shows the changes in simulated FRET efficiency with

distance (solid black line) when the R_0 is 53Å, a commonly used value for the Cy3-Cy5

dye pair.[18] The dashed lines represent the FRET efficiency of 50% and the corresponding

R_0 value of 53Å.[20]
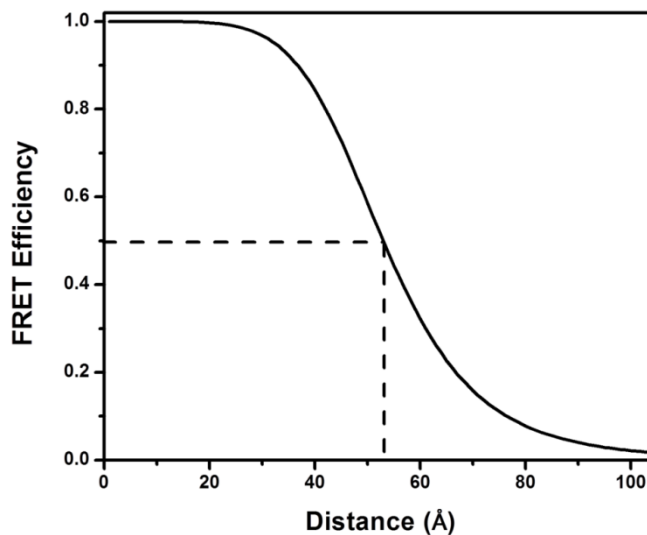
Figure 1.5. Plot of simulated FRET efficiency against distance (solid, black) when the value of R_0 is 53Å. The dashed lines show that the Förster's distance R_0 corresponds to 50% FRET efficiency.

Förster's distance can be mathematically described as,

$$R_0 = 0.211 \cdot [\kappa^2 \cdot n^{-4} \cdot \phi_D \cdot J(\lambda)]^{1/6} \text{ Å} \tag{1.2}$$

In the above equation, *n* is the refractive index of the solution, ϕ_D is the quantum yield of the donor in absence of the acceptor, *J(λ)* is the overlap integral between the donor emission and acceptor absorption spectra (where *λ* is calculated in nm), and κ^2 is the orientation factor. The refractive index is usually approximated from the refractive index of the buffer.[16] Each of these terms is further explained in the following section.

1.3.1.1. Quantum yield. The quantum yield of the donor in the absence of acceptor is usually calculated from the quantum yield of a known standard. Briefly, the absorbances of the sample and the standard are measured at the excitation wavelength of the emission spectra. Then, the emission spectra of both the sample and the standard are

obtained by exciting at the same wavelength (λ_{Ex}) and identical instrumental conditions. The total intensities (I_{tot}) , i.e. the area under the curve of the two emission spectra, are then calculated. Finally, the quantum yield of the samples are obtained using the following relation,

$$\phi_{Sample} = \frac{I_{tot}^{Sample}/A_{\lambda_{Ex}}^{Sample}}{I_{tot}^{Standard}/A_{\lambda_{Ex}}^{Standard}} \times \phi_{Standard} \tag{1.3}$$

The absorbances were kept low in order to ensure linear relation between the fluorescence and the absorbance. Fluorescence standards were chosen based on the maximum overlap of their absorption and emission spectra with the corresponding spectra of the samples. This technique of calculation of quantum yield is used in chapter 2 for the calculation of the quantum yields Cy3 and Cy5 labeled samples. The quantum yield of Cy3 is then used for the calculation of Förster's radius in the same chapter.

1.3.1.2. Overlap Integral. The overlap integral ($J(\lambda)$) is defined as the spectral overlap between the donor emission spectra and the acceptor absorption spectra. This is depicted by the light blue shaded region in Figure 1.6. It is calculated from the emission spectra ($I_D(\lambda)$) of the donor only sample (blue, solid) and the absorption spectra ($\varepsilon(\lambda)$) of the acceptor only sample (green, dashed), using the following relationship,[16]

$$J(\lambda) = \frac{\int_0^\infty I_D(\lambda) \cdot \lambda^4 \cdot \varepsilon(\lambda) d\lambda}{\int_0^\infty I_D(\lambda) \cdot d\lambda} \tag{1.4}$$

This relationship is also used in the calculation of Förster's distance in chapter 2.
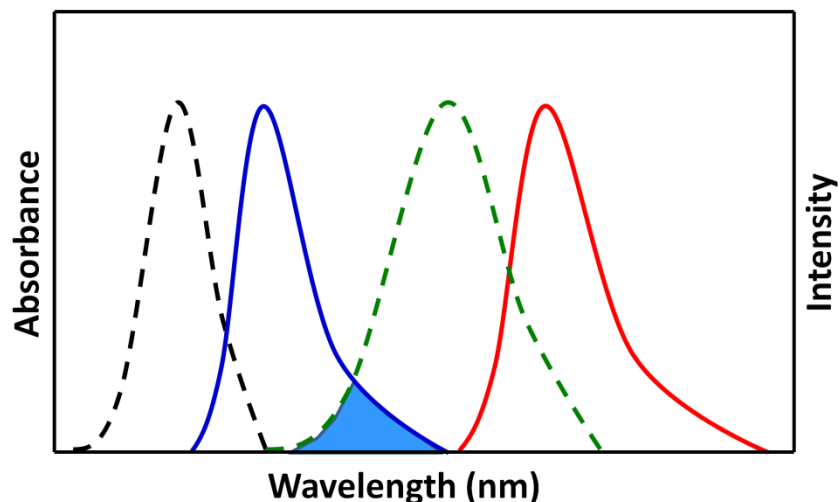
Figure 1.6. The overlap integral (light blue, shaded) of the donor emission spectra (blue solid) and the acceptor absorption spectra (green dashed). The donor absorption spectra and the acceptor emission spectra are depicted in black dashed and red solid, respectively.

1.3.1.3. Orientation factor (κ^2). The orientation factor (κ^2) is a measurement of the dependence of FRET efficiency on the angles of the donor and acceptor transition dipole moments. The orientation factor is defined as,[16]

$$\kappa^2 = [Cos(\theta_T) - 3 \cdot Cos(\theta_D) \cdot Cos(\theta_A)] \qquad (1.5)$$

Here, θ_T is the angle between the transition dipole moments of the donor and the acceptor. θ_D and θ_A are the angles between the transition dipole moments of the donor and acceptor, respectively, and the vector joining the two transition dipole moments, as described in Figure 1.7. The value of κ^2 can vary from zero to four. The collinear alignment of the donor and the acceptor transition dipole moments results in a κ^2 value of 4, and the perpendicular alignment of the transition dipole moments results in κ^2 value of

0. Therefore, if the two transition dipole moments are in perpendicular orientation, energy transfer does not take place, independent of how short the distance between FRET pairs is. The parallel alignment of the transition dipole moments results in a κ^2 value of 1. These scenarios are illustrated in Figure. 1.7. Often, during the measurement of FRET, the exact positions of the donor and the acceptor transition dipole moments are not known. In these cases a value of $\kappa^2 = 2/3$ is usually assumed and widely used for the translation of FRET measurements to calculated distances. This value of $\kappa^2 = 2/3$ is valid when both the donor and the acceptor molecules are rotating freely during the lifetime of fluorescence and the corresponding transition dipole moments occupy all the different rotational orientations during the timescale of energy transfer. This is seldom true when a fluorophore is bound to a biological molecule by a flexible linker. The chemical linkage and the close proximity of the biological molecule can lead to interaction of the fluorophore with the biomolecule and result in changes in the rotational mobility and photophysical properties.[27-37]
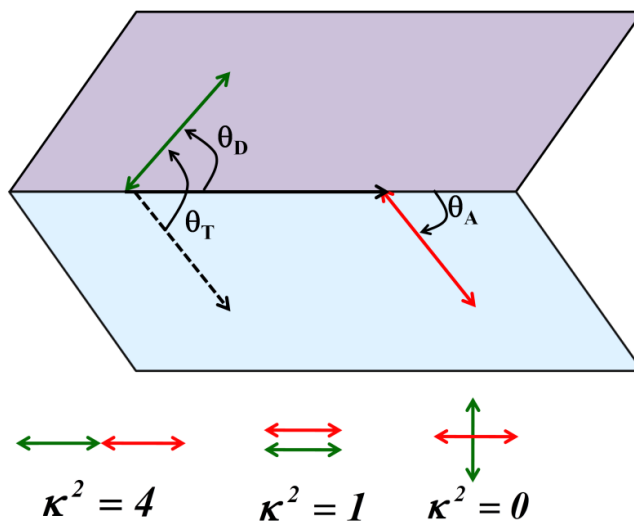
Figure 1.7. The angular dependence of FRET on κ^2. The green and red arrows represent the transitional dipole moments of the donor and the acceptor, respectively. θ_T is the angle between the transition dipole moments of the donor and acceptor moiety, θ_D and θ_A are the angles between the transitional dipole moments of the donor(D) or acceptor (A) and the vector joining the transition dipole moment of both.[16]

The value of $\kappa^2 = 2/3$ is only true for the case where both the donor and acceptor are rotating freely during the lifetime of fluorescence. This is the case for a small molecule like Cy3B (inset of Figure 1.8). Cy3B has a rotational correlation time of 380 ps and a lifetime of 2.4 ns.[35, 38] A comparison of the lifetime (red line) and the time resolved fluorescence anisotropy decay (blue line) of Cy3B is shown in Figure 1.8. Time resolved fluorescence anisotropy decay is a measurement of the rotational mobility of the fluorophore during the lifetime of fluorescence. The description of the time resolved fluorescence anisotropy decay is presented in section of 1.3.3.3. of this chapter. This comparison shows that Cy3B rotates much faster than the lifetime of fluorescence and can occupy all the possible rotational orientations. Under these circumstances $\kappa^2 = 2/3$

value is true. However, it has been shown that when fluorophores are attached to biomolecules, the rotational mobility of the dye decreases, and, thus, the value of κ^2 cannot be assumed to be 2/3.[24, 39-45] The idea of restricted rotation is further expanded in chapter 2. Chapter 2 describes the results from the FRET efficiency measurements of the fluorescent backbone modification of the double stranded DNA. These fluorescent modifications are rigidly attached to B-DNA and are expected to follow the structure and geometry of B-DNA. These modifications restrict the rotation of the dyes during the lifetime of fluorescence and prove the invalidity of the assumption that $\kappa^2 = 2/3$. The almost collinear alignment of these modifications results in measurement of FRET efficiency above 100 Å. The importance of these restricted rotations are also the rationale behind the work described in chapter 3, where the interaction between the fluorophores (Cy3B, TAMRA and Alexa 546) and the deoxynucleotide monophosphates (dAMP, dCMP, dGMP and dTMP) are investigated.[38] In this thesis, the interactions of the dNMPs with fluorophores in absence of quenching as well as interactions that lead to restriction rotations and thus can have affect on translating FRET efficiency to distance, have been investigated by various fluorescence methods (described in chapter 3). This work resembles the work by Harvey et al. where Cy3 was shown to interact with dNMPs and the single stranded DNA when attached to the 5' end.[46] Publications from Dr. David Lilley's lab at University of Dundee have shown that Cy3 also stacks on the end of the DNA as an extra base pair when attached to the 5' end of the double stranded DNA.[24, 40, 41, 44]
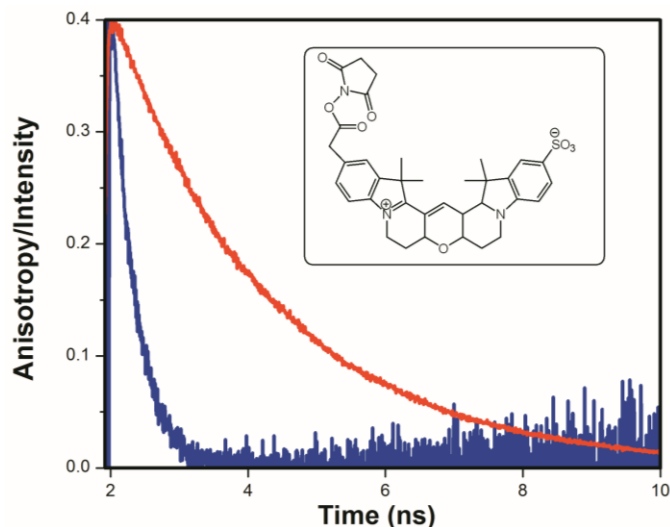
Figure 1.8. The comparison of the time resolve intensity decay (red) and the time resolved fluorescence anisotropy decay (blue) of a small fluorophore Cy3B (inset). The much faster decay of anisotropy proves that the dye rotates and occupies all of the possible rotational orientation during the lifetime of its fluorescence.

1.3.2. Quenching. The most common technique used to reveal interactions between fluorophores and biomolecules is the quenching of fluorescence.[47-50] Many organic dyes, rhodamines, oxazines, and coumarines are known to interact with biomolecules resulting in a decrease of fluorescence efficiency. This decrease in the efficiency of fluorescence is known as the quenching of fluorescence.[15] The quenching of fluorescence is usually represented by the Stern-Volmer equation. The origin of quenching usually comes from two different pathways: static and dynamic. The combination of both the static and dynamic quenching pathways can also be responsible for the observed quenching.

1.3.2.1. Static Quenching. Static quenching can be described as quenching of
fluorescence due to the formation of a non-fluorescent ground state complex between the
fluorophore and the quencher. This complex can be completely non-fluorescent or simply
have a much lower efficiency of fluorescence compared to the fluorophore. The
association constant between the fluorophore and the quencher is given by,[15]

$$k_S = \frac{[M-Q]}{[M]\cdot[Q]} \tag{1.6}$$

where k_S is the association constant or the static Stern-Volmer constant, and *[M-Q],[M]
and [Q]* are the concentration of the complex, fluorophore and the quencher,
respectively. Rearrangement of equation 1.6, assuming that the complex is a 1:1 complex
and is non-fluorescent, leads to the static Stern-Volmer equation:[15, 16]

$$F_0/F = 1 + K_s\,[Q] = 1 + k_s\tau_0[Q] \tag{1.7}$$

Here *F* and F_0 are the intensities of fluorescence in presence and absence of the quencher
molecule, respectively. K_s and τ_0 are the static Stern-Volmer constant and the lifetime of
the fluorophore in absence of the quencher, respectively.

  1.3.2.2. Dynamic quenching. Dynamic quenching can be defined as the decrease
in fluorescence due to processes happening in the excited state of the fluorophore. One of
the most common reasons for dynamic quenching is collision. The excited molecule can
undergo collisions with other molecules in the solution so that the excited state energy is
lost as heat. This results in a non-radiative transition of the fluorophore from the excited
state to the ground state and loss of fluorescence.[15, 16]

If k_m represents the sum of rate constants of all the de-excitation pathways from the excited state in absence of the quencher, then k_m is equal to the reciprocal of the lifetime of fluorescence (τ_0). So,

$$k_m = k_r + k_{nr} = 1/\tau_0 \tag{1.8}$$

where k_r and k_{nr} are the rate constants of the radiative and the non radiative pathways, respectively.

If the concentration of the excited state species (M*) is given by $[M*]$, then the time evolution of the species M* following an excitation pulse in presence of the quencher can be explained by,

$$\frac{d[M^*]}{dt} = -\left(k_m + k_q \cdot [Q]\right) \cdot [M^*] = -\left(1/\tau_0 + k_q \cdot [Q]\right) \cdot [M^*] \tag{1.9}$$

Rearrangement of the answer to this differential equation, assuming that the intensity of fluorescence is proportional to $[M*]$, results in the dynamic Stern-Volmer equation, i.e.

$$\tau_0/\tau = 1 + K_q\,[Q] = 1 + k_q\tau_0[Q] \tag{1.10}$$

Here, τ_0 and τ represent the lifetimes of the fluorophore in absence and presence of the quencher, respectively. K_q and k_q are the dynamic Stern-Volmer constant and the dynamic bimolecular association constant, respectively.

In absence of static quenching, the quantum yield of fluorescence is proportional to the lifetime of the fluorescence. Hence, the intensity of the fluorescence is proportional to the lifetime of fluorescence and under such circumstances,

$$\tau_0/\tau = F_0/F = 1 + K_q [Q] = 1 + k_q\tau_0[Q] \tag{1.11}$$

Equation 1.11 is only true in absence of static quenching.[49]

1.3.2.3. Combination of static and dynamic quenching. If both the static and the dynamic quenching are involved in the quenching process, the remaining fluorescence (F/F_0) can be given by the products of the ratio of fluorescence from the dynamic quenching and the fraction of fluorescent molecules present:[15]

$$\frac{F}{F_0} = \left[\frac{F}{F_0}\right]_{dyn} \times \frac{[M]}{[M_0]} \tag{1.12}$$

Here, *[M]* and *[M₀]* represent the concentration of the fluorophore in presence and absence of static quenching, respectively. Rearrangement of equation 1.12 results in the combined quenching equation for both the static and dynamic pathways:

$$F_0/F = \left(1 + K_q [Q]\right) \times (1 + K_s [Q]) \tag{1.13}$$

Therefore, in the presence of both static and dynamic quenching, the association constant of the ground state complex formation can be calculated from the following equation:

$$\left.(F_0/F)\middle/(\tau_0/\tau) = 1 + K_s [Q] \right. \tag{1.14}$$

This method of calculating the dissociation constant was originally used by Heinlein et al.[49] Similar calculations were carried out in chapter 3 of this thesis to separate the dynamic and static components of the quenching of the three dyes (TAMRA, Cy3B and Alexa 546) by various dNMPs. To obtain the lifetime of the dyes in presence of dNMPs, the intensity decays were fitted with bi-exponentials. Time resolved

23

fluorescence intensity decays are explained later in this chapter. Suffice it to say here that the lifetimes, or the average lifetime, of the dyes can be obtained from the time resolved intensity decay by fitting the decay to a sum of exponentials. The bi-exponential fits resulted in a very short and another longer lifetime. The short lifetime was independent of the quencher concentration and the long lifetime was dependent on the quencher concentration. Heinlein et al.[49] argued that the very short lifetime is due to the presence of a slightly fluorescent stable ground state dye-quencher complex and only the longer timescales should be used for the calculation of dynamic Stern-Volmer complex. The same argument is used in chapter 3 to calculate the dynamic Stern-Volmer constant.

      1.3.2.4. Photoinduced electron transfer. Dynamic quenching influences the lifetime and the quantum yield of the fluorophore. Static quenching often decreases the fluorescence by forming π-stacked non-fluorescent conformations.[51] One of the most important pathways for forming a non-fluorescent complex is photoinduced electron transfer, or PET.[15] The oxidative and reductive properties of a fluorophore can become enhanced in the excited state. Electron transfer to or from the first excited state of the fluorophore from the quencher results in the formation of a radical anion or cation, respectively. This process is described in Figure 1.9. In this figure both (a) the reductive electron transfer and (b) the oxidative electron transfer are shown. The red arrow represents the direction of the electron transfer in both the cases. Transfer of the electron by PET changes the energy state of the molecule resulting in quenching of fluorescence.

Reductive electron transfer

Oxidative electron transfer
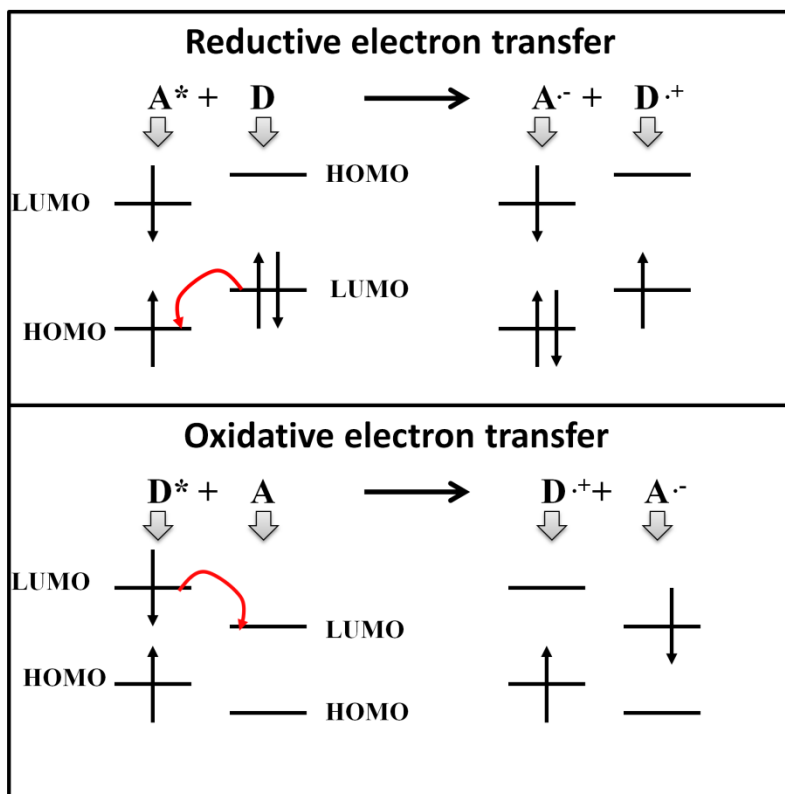
Figure 1.9. Reductive and oxidative electron transfer. The red arrow indicates the direction of the electron transfer. Electron transfer to (reductive) or from (oxidative) the fluorophore results in loss of fluorescence. This figure is modified from the Figure 4.3 of the book Molecular Fluorescence by Dr. Bernard Valeur.[15]

The quenching of the dyes by the nucleotides through PET is described in detail in chapter 3. In the presence of a nucleotide, the most common pathway for PET to occur is by the transfer of an electron to the first excited state of the fluorophore from the nucleotide.[47-49, 52, 53] The feasibility of quenching by PET is given by the Rehm-Weller theory, which is basically a comparison between the oxidation potential of the nucleotide and the excited state reduction potential of the fluorophore. The excited state reduction potential ($^*E_{red}^A$) of the fluorophore can be calculated from the ground state reduction potential (E_{red}^A) and the zero-zero transition energy ($E_{0,0}$) using the following equation,

$$^{*}E_{red}^{A} = E_{red}^{A} + E_{0,0} \tag{1.15}$$

The ground state reduction potentials of the fluorophores are calculated from the first reduction peak of the voltammograms.

The zero-zero transition energies ($E_{0,0}$) are calculated using the following equation:

$$E_{0,0} = \frac{1}{2}\, hc\, \left(\frac{1}{\lambda_{abs}} + \frac{1}{\lambda_{em}}\right) \tag{1.16}$$

where, λ_{abs} and λ_{em} are the wavelengths for the maxima of the absorption and the emission spectra, respectively.

The feasibility of the quenching by PET is then calculated by the Rehm-Weller equation,

$$\Delta G = E_{OX}^{D} - {}^{*}E_{red}^{A} + C = E_{OX}^{D} - E_{red}^{A} - E_{0,0} + C \tag{1.17}$$

C is a Coulombic term which is often neglected in polar solvents and $E^{D}{}_{OX}$ is the oxidation potential of the nucleotide.

Comparison of the $^{*}E_{red}^{A}$ with the E_{OX}^{D} determines the feasibility of electron transfer. To calculate the $^{*}E_{red}^{A}$ values, the cyclic voltammograms of the three dyes under study were obtained and their fluorescence and absorption spectra were taken. The detailed procedure and the calculations are shown in chapter 3.

1.3.2.5. Quenching by H-dimer formation. Fluorescence can also be quenched by a different pathway. The presence of two fluorophores at a close vicinity can lead to self association and quenching of fluorescence. Rhodamine dyes, including tetramethylrhodamine and iodoacetamidotetramethylrhodamine, are known to self-associate.[54] The stacking interaction of the π orbitals from the two dyes results in the formation of H-dimer and a change in the fluorescent properties of the dye. H-dimer formation results in the quenching of the fluorescence and a blue shifted absorption spectra with a very distinguishable separation from the original absorption spectra of the free dye.[53] Figure 1.10 shows the molecular structure and position of the two TAMRA dyes bound by a short linker in different solvents. The increase in the solvent polarity causes the two TAMRA dyes to interact more and the resulting absorption spectra show a more pronounced secondary peak at a blue shifted position compared to the absorption spectra of the free dye.[53] This type of self-quenching of TAMRA is used in the chapter 4 of this thesis where the sliding clamps are labeled in a way that in the closed structures of the clamps the two dyes are in a close proximity and mostly quenched. The opening of the clamp or monomerization of the clamp results in the increased distance between the dyes and increase in fluorescence.
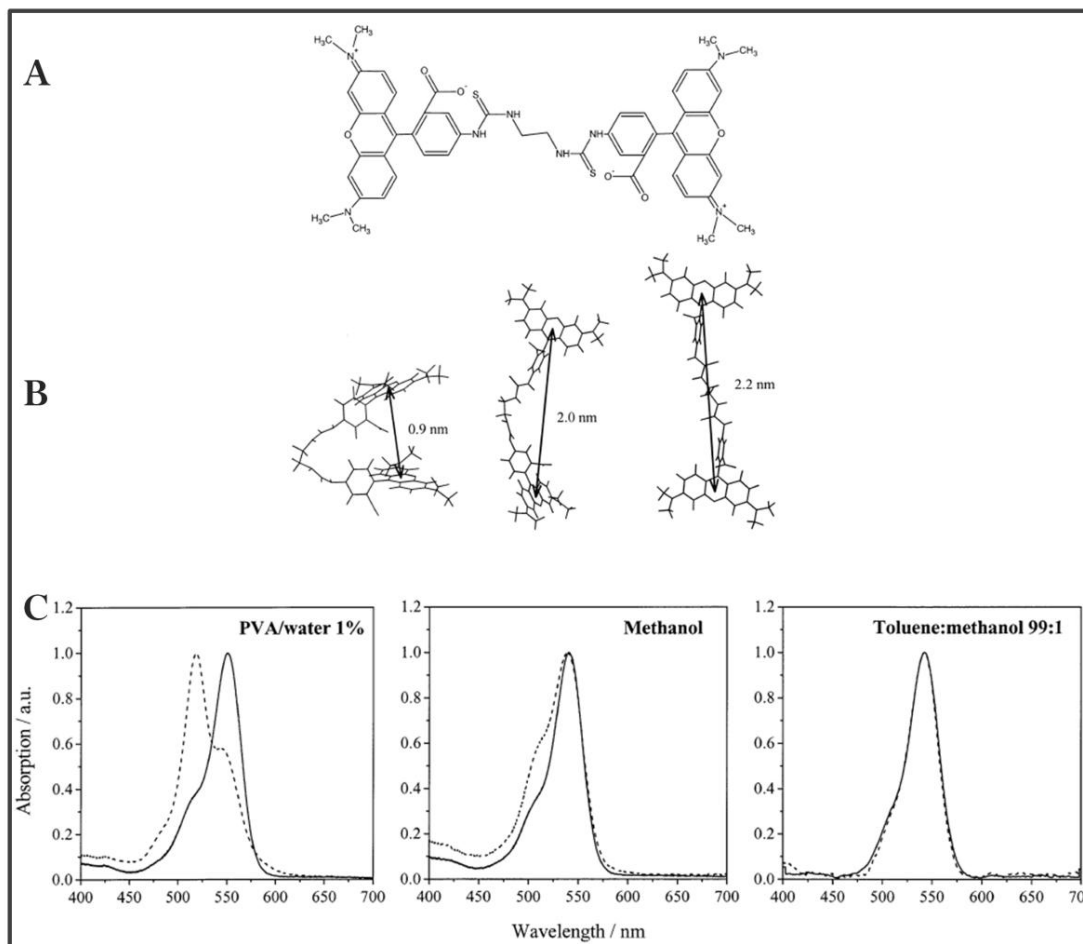
Figure 1.10. Formation of H-dimer of TAMRA. (A) - The structure of the two TAMRA dyes covalently linked to each other. (B) - Optimal geometric configurations calculated for the dimer - folded, gauche, and extended (from left to right). (C) - The absorption spectra of the dimer shown in (A) (dotted line) and the free dye (solid nine) with decreasing solvent polarity. In polar solvent the spectra corresponding to H-dimer is very evident. Adapted with permission from Hernando et al. *J. Phys. Chem. A*, 2003, 107 (1), pp 43–52. Copyright 2003 American Chemical Society.[50]

1.3.3. Time resolved fluorescence. Time resolved fluorescence measurements have been used extensively in fluorescence spectroscopy. Time resolved fluorescence measurements contain more information compared to steady state results. The lifetime of a fluorophore can be obtained from the time resolved intensity decay.[15, 16] These lifetimes

28

can be used to separate the dynamic and static quenching (as described in chapter 3) and

to calculate the efficiency of FRET (in chapter 2). Similarly, time resolved fluorescence

anisotropy decays contain information about the rotation of the fluorophores during the

lifetime of fluorescence. Excited with a polarized light, the fluorophores, having their

excitation transition dipole moment parallel or closely parallel to the polarization axis of

the light get preferentially excited and have the major contribution to the fluorescence

emission. The free rotation of the molecules results in fast depolarization of the emitted

light and the time resolved anisotropy decays are the perfect way to visualize the

quickness of this depolarization. The time resolved fluorescence anisotropy decays of the

fluorophores in presence and absence of dNMPs were used to uncover evidence of

interactions between the dyes and the dNMPs (chapter 3). This technique has also been

used to show evidence of interaction between DNA and an internally-attached Cy3 via a

six carbon linker (chapter 2).

The technique used to obtain the time resolved intensity and anisotropy decays in

these experiments is called time correlated single photon counting (TCSPC). The

principle of the TCSPC can be described the following way. The laser pulse from a

pulsed laser is used to excite the fluorophores. The condition of the TCSPC is set in a

way that at most only one emitted photon by the fluorophores can be detected at a time.

The laser pulse exciting the fluorophores starts a clock and the emitted photon (when it

reaches the detector) stops the clock. If the photon from the fluorescence does not stop

the clock within a certain set time then the next pulse from the laser stops the clock. This

process is repeated numerous times and a histogram of the number of photons against the

time required for the photon to arrive at the detector is plotted. After the deconvolution of

the obtained histogram with the shape of the laser pulse the intensity decays are obtained. This is pictorially described in Figure 1.11.[16]
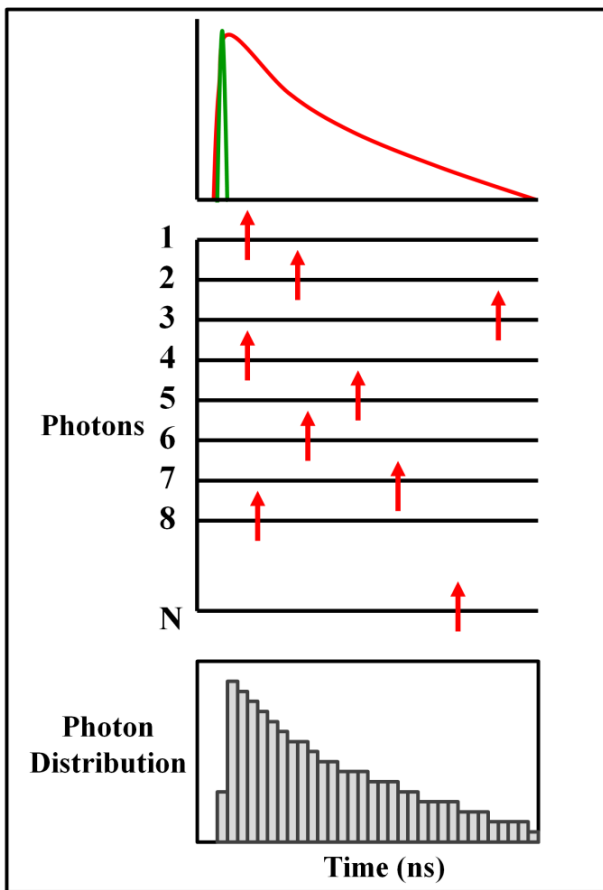
Figure 1.11. Principle of TCSPC. The red arrows represent the arrival of a photon originated from fluorescence to stop the timer started by the pulse of the laser (green). The bottom shows the histogram of the photon distribution with the arrival time (grey bars). The top part represents the obtained intensity decay (red) and the shape of the laser pulse. Modified from Figure 4.7 form Principles of Fluorescence Spectroscopy by Joseph R Lakowicz.[16]

1.3.3.1. Instrumentation. The TCSPC instrument used in these works had two different excitation sources: (1) Ti-Sapphire (2) a super continuum Fianium (Southampton, UK) laser. Briefly, for the excitation using Ti-Sapphire as the laser source,

a high power 532 nm solid state laser (Milennia) was used to excite a Ti-Sapphire laser (Tsunami). This produced a pulsed laser excitation of 80 MHz. The output light was then passed through a frequency doubler and a pulse picker to obtain a pulse of 4 MHz at 450/460 nm. Vertical pulses from the excitation laser were selected using an excitation polarizer to excite the samples. The fluorescence was collected at 575 nm, with the emission polarizer being kept at different angles (for different decays) compared to the vertical excitation. In the experiments using the white laser source, the samples were excited with a super continuum Fianium laser (Southampton, UK). The excitation wavelength of 530 nm was selected using an acousto-optic tunable filter (AOTF) and then further corrected with an interference filter of 5nm bandwidth before passing through a polarizer to select vertical excitation. The laser was operated with a 10 MHz frequency and the fluorescence was collected at 575 nm after passing through an polarizer kept at different angles with respect to the vertical position of the excitation polarizer. The detection part of the instrumentation for both excitations were mostly same. The only difference was the presence of a long-pass filter that was placed in the emission path for the Fianium excitation to block the scattered excitation light, due to the fact the excitation and the emission wavelengths were very close. The emission wavelength was is selected by passing the fluorescence through a Gemini-180 double grating monochromator and the data were is measured using a R3809U-50 microchannel plate detector. A SPC-830 single photon card from Becker-Hickl was is used for the data acquisition. The other difference between the two excitations was that the Ti-Sapphire excitation required an external trigger diode to send the start signal to the photon counting card while the Fianium uses an internal trigger that can be connected to the card.

A diagram of the TCSPC instrument is presented in Figure 1.12. The top part of the picture shows the excitation by Ti-Sapphire and the bottom part shows the Fianium excitation.
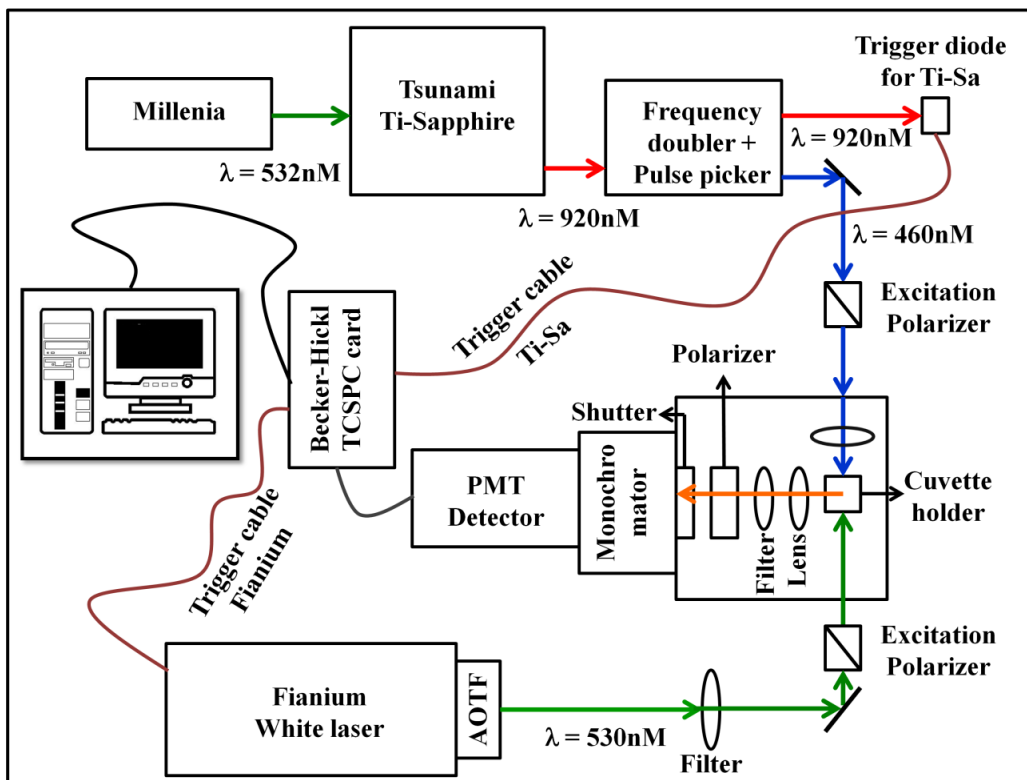
Figure 1.12. Diagram of the TCSPC set up used. The top part describes the Ti-Sapphire excitation and the bottom part describes the excitation by Fianium. Either one of these excitation was used for the experiments.

1.3.3.2. Time resolved intensity decay. Fluorescence lifetimes can be obtained from the fluorescence intensity decays. To achieve this, the fluorescence intensity decays were obtained with the emission polarizer being kept at the magic angle (54.7°) compared to the excitation polarizer (0°). The magic angle position of the emission polarizer ensures that there are no polarization artifacts in the obtained intensity decay. The

instrument response function (IRF) was measured by using 2-3% Ludox (Sigma-Aldrich, St. Louis, MO) scattering solution with the emission monochromator being kept at the same wavelength as that of the excitation laser line. The time resolved intensity decay was then obtained after iterative deconvolution of the measured decay with the IRF. The decays were fitted assuming that the decays can be described by sum of exponentials i.e.

$$I(t) = \sum \alpha_i \cdot Exp\left(-\frac{t}{\tau_i}\right) \tag{1.18}$$

The fitting and the deconvolution were carried out using the ASUFIT software. The goodness of the fit was determined from the χ^2 and the randomness of the residuals. The average lifetime was then calculated from the measured lifetimes using the following relation:[15]

$$\langle \tau \rangle = \frac{\sum \alpha_i \cdot \tau_i}{\sum \alpha_i} \tag{1.19}$$

The obtained average lifetimes of the donor-only and the donor-acceptor sample have been used to calculate the efficiency of FRET of the backbone modified DNA samples in chapter 2. The lifetimes were also used to distinguish between the dynamic quenching and the static quenching of the fluorophores by dNMPs in chapter 3.

1.3.3.3. Time resolved fluorescence anisotropy decay. Time resolved fluorescence anisotropy decay provides an experimental technique through which the rotational motion of a fluorophore during the lifetime of fluorescence can be observed.[55] The origin of fluorescent anisotropy is the photoselection of the fluorophores by linearly polarized light.[16] The fluorophores having their absorption transition moment aligned mostly or fully parallel to the orientation of polarized excitation light are preferentially

excited and will then emit. Following a flash of excitation, some of the fluorophores are preferentially excited and they are the major contributors towards the emitted fluorescence. The rotation of these preferentially excited fluorophores during the lifetime of fluorescence causes the emission of light from different angles relative to the excitation light and depolarization of fluorescence. This depolarization causes a decrease in fluorescence anisotropy.

Time resolved fluorescence anisotropy is defined as:[16]

$$r(t) = \frac{I_{VV}(t) - I_{VH}(t) * G}{I_{VV}(t) + 2 * I_{VH}(t) * G} \tag{1.20}$$

In the above equation, *VV* and *VH* represent the vertical and horizontal positions of the emission polarizer relative to the vertical position of the excitation polarizer, respectively. *G* is a correction factor that corrects for the difference in the sensitivity of the detector for the two components. The *G* factor is experimentally calculated using rhodamine 6G in methanol by the tail matching method. Rhodamine 6G in methanol has a very fast anisotropy decay. Hence, at long times, the I_{VH} and I_{VV} of rhodamine 6G should overlap. The tail matching method uses this idea to match the two intensities and calculate the calibration factor. The anisotropy decays in our experiments were calculated without deconvolution. They were fitted with either mono-exponential or bi-exponential functions. The goodness of the fits were determined from the χ^2 and the randomness of the residuals.

Time resolved fluorescence anisotropy decays were used to find evidence of interaction of organic dyes with dNMPs (chapter 3). These decays were also used to determine that the attachment of the fluorophore to the DNA via a long linker does not

essentially prohibit the fluorophore to interact with the DNA. The difference in rotational mobility of the fluorophores during the lifetime of the fluorescence for different types of attachment to the DNA have also been studied using this technique (chapter 2).

      1.3.4. Fluorescence correlation spectroscopy (FCS). Fluorescence correlation spectroscopy (FCS) is a quantitative technique where fluctuations in the fluorescence intensity arising from a optically restricted volume are analyzed. The rates of various processes, including diffusion, conformation dynamics and photophysics are measured in this technique. FCS involves a very small (3-6 fL) optically restricted volume created either by a high numerical aperture objective and a pinhole or by two photon excitation. The excitation laser intensity in this optically restricted confocal volume is non-homogeneous, with the center having the most intense excitation and the intensity continually decreasing towards the edge. The diffusion of the fluorophores in and out of the observation volume and the movements of the fluorophores inside this non-homogeneously illuminated confocal volume create fluctuations in the intensity of fluorescence. FCS can also measure the rates of any secondary processes, including photophysics, FRET, and quenching capable of creating fluctuations in the fluorescence intensity prior to the diffusion of the molecule out of the confocal volume.[56-59] The theory and first experiments of FCS were originally described by Magde et al.[60, 61] The stability of the laser sources and the advent of detectors with single molecule detection capability have increased the use of FCS considerably. FCS is unique in its ability to measure rates of processes that occur in the sub microsecond to second timescales, limited only by the diffusion time of the fluorophore. The other speciality of FCS is that it can operate at very low concentrations. In fact, the lower concentration results in

smoother decays provided that enough photons are detected. This method has been used

to investigate the interactions between the fluorophores (Cy3B, TAMRA and Alexa 546)

and the dNMPs and these results are described in chapter 3. This method has also been

used to find evidence of rapid spontaneous fluctuations between the closed and open

structures of β-clamp (from *E. coli*) and PCNA (from *S. cerevisiae*) as well as these two

proteins' solution stability and dissociation constants. These results are discussed in

chapter 4.

1.3.4.1. Instrumentation of FCS: Fluorescence correlation decays were collected

in a fluorescence microscope assembled in house, as depicted in Figure 1.13. Briefly, a

532 nm laser, either Coherent Compass 215-M10 (Santa Clara, CA) or Crystalaser (Reno,

NV) was attenuated to a power of 100 μW after a beam expansion to 4 mm, and focused

onto the sample (on top of a coverslip) using a high numerical aperture (1.4 NA)

objective (Olympus plan-Apo, 1.4 NA, 100X, Oil). The samples were kept in a chamber

created by sticking a perfusion chamber (Grace Biolabs, Bend, OR) on a coverslip.

Measurements were carried out after passivating the chamber with BSA. The

fluorescence was collected using the same objective used for excitation. The fluorescence

was then passed through a dichroic filter (Semrock) placed after the objective, focused

onto a 50 μM pinhole, split into two channels, passed through optical filters (Omega

3RD560-620), and then collected by two independent avalanche photodiodes (Perkin-

Elmer, SPCM-AQR14). The signal from the two detectors was fed to a ALV5000/60X0

correlator (ALV, Germany). The signals were either autocorrelated or cross-correlated

with each other. The autocorrelation gives a better signal to noise ratio, whereas cross-

correlation does not have the contribution from the after pulse effect. The inset on the

right side of Figure 1.13 depicts the optically restricted confocal volume.
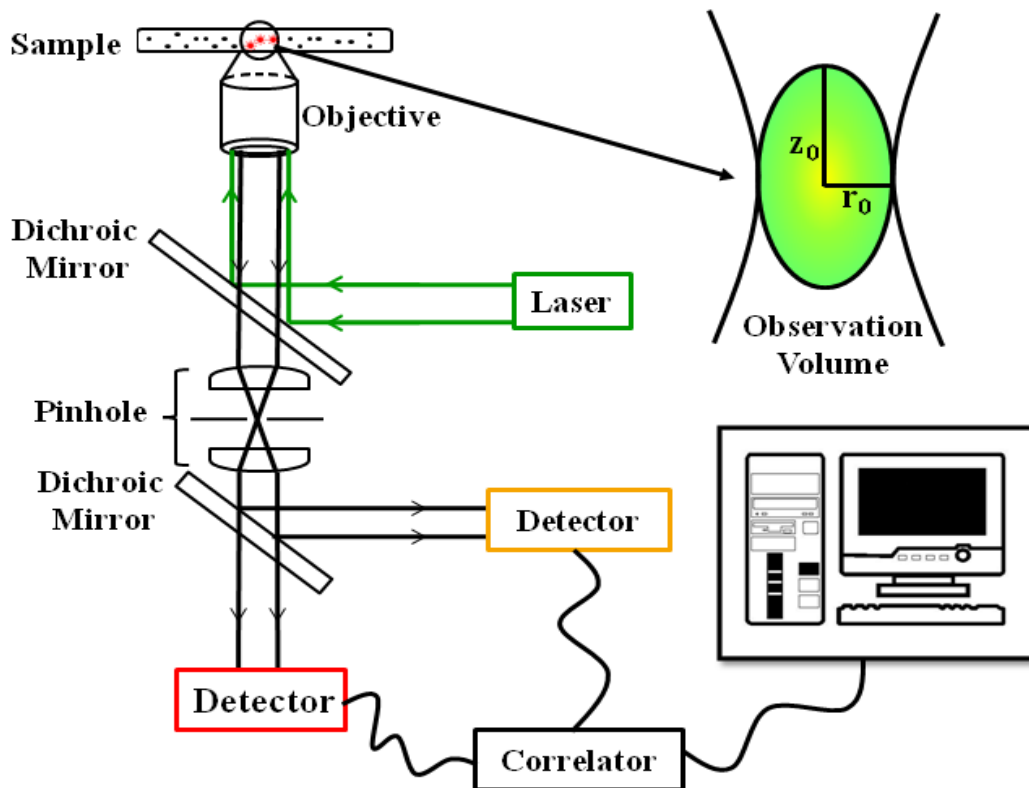
Figure 1.13. The fluorescence microscope set up for FCS. The high NA objective and the pinhole create a small confocal observation volume of inhomogeneous excitation (shown in the right side of the picture). As fluorophores translate through this illuminated volume, they are excited and emit fluorescence. The inhomogeneous nature of the confocal volume results in position dependent excitation of the fluorophore: the closer it is to the center, the higher the laser power and brighter the molecule fluoresces.

1.3.4.2. Theory of FCS. The diffusion of the molecule in and out of the

observation volume and through the non-homogeneous confocal volume results in the

fluctuation of fluorescence. FCS is a technique where the fluctuations in the fluorescent

intensity are analyzed to obtain rate of various biophysical processes, including diffusion. The correlation function is mathematically defined as:[16, 62]

$$G'(\tau) = \frac{\langle \delta I(t)_x \cdot \delta I(t+\tau)_y \rangle}{\langle I(t)_x \rangle \cdot \langle I(t)_y \rangle} \qquad (1.21)$$

In this equation $\delta I(t)$ is the fluctuation of the intensity $I(t)$ from the mean $\langle I(t) \rangle$ at time t and is equal to,

$$\delta I(t) = I(t) - \langle I(t) \rangle. \qquad (1.22)$$

τ is defined as the lag time. In equation 1.21, if x and y correspond to the same APD, then the correlation is called autocorrelation and if they belong to the signal from two different APDs, then the correlation is called cross-correlation. In the left panel of Figure 1.14. the intensity $I(t)$ (black) is plotted as a function of time and the intensity fluctuates around a mean value $\langle I(t) \rangle$ (green). In the right panel the fluctuation of the intensity $\delta I(t)$ (red) is plotted against the time and here the fluctuation of the intensities fluctuates around zero (green). The plot on the right panel (red) is derived from the measured intensities of the left panel.
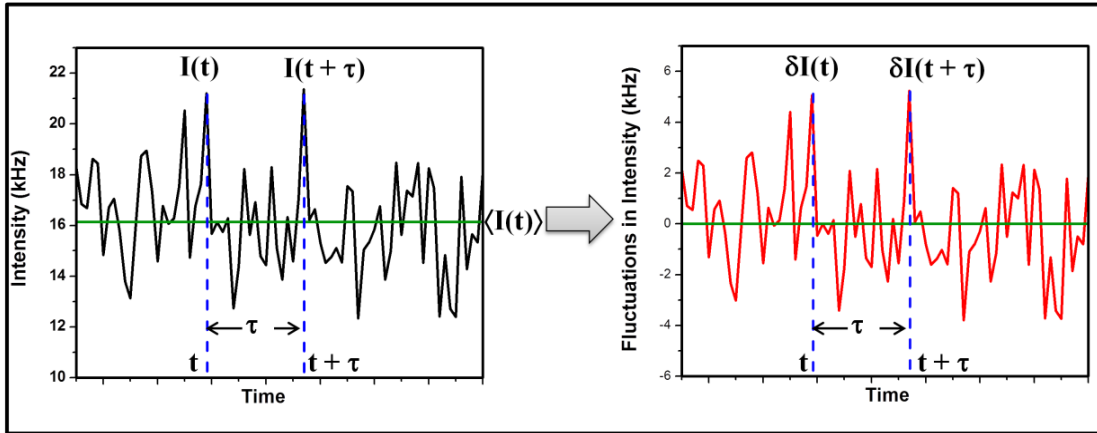
Figure 1.14. Plot of intensity (black, left panel) and fluctuations in the intensity (red, right panel) against time. The green lines represent the average intensity (left panel) and zero (right panel). The correlation of the intensities at time (*t*) and time (*t+τ*) results in the autocorrelation curve (figure 1.15.).

The correlation of the fluctuation in the intensity at time *t, δI(t)*, with the fluctuation at the time *t+τ, δI(t+τ)*, results in the obtained correlation decay. This decay is usually plotted against the lag time (τ) in a semi-log fashion. The correlation decay (black circles) obtained from the fluctuations shown in Figure 1.14 (red line) is plotted in figure 1.15.
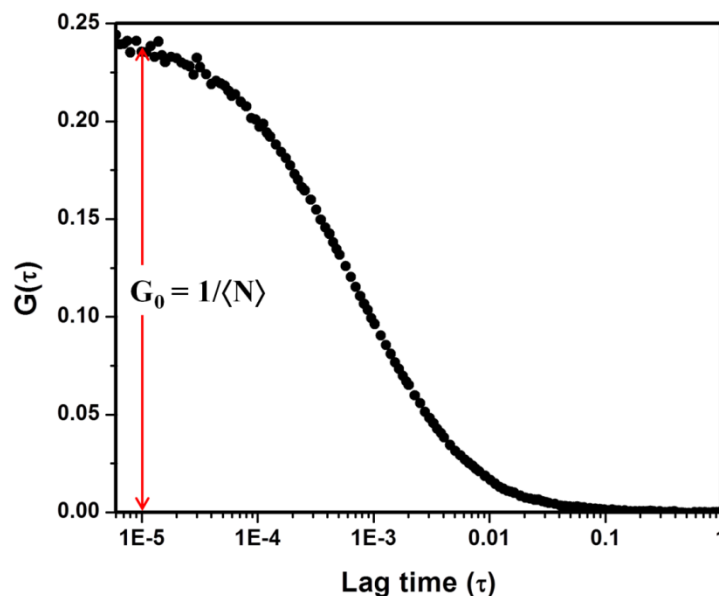
Figure 1.15. The autocorrelation decay obtained from the fluctuations shown in Figure 1.14. The plot is semi-log in fashion for the investigation of the fast processes. Here, the amplitude is the inverse of the average number of molecules, which is why a lower concentration in FCS is so beneficial.

1.3.4.3. Contributions to the FCS decays.

1.3.4.3.1. Diffusion. The main application of FCS is to calculate hydrodynamic properties. FCS has been historically employed to calculate the diffusion constant of the fluorophores. If the confocal volume can be approximated as a three dimensional Gaussian function, then the volume can be described as $V = \pi^{3/2} \cdot r^2 \cdot z$, where r and z are the radial and axial radii, respectively. In absence of any secondary processes, diffusion of the fluorophores in and out of the non-homogeneously illuminated confocal volume is the sole reason behind the fluctuations. Under these circumstances, for single photon excitation, the correlation decay can be described by,[16]

40

$$G(\tau) = \frac{1}{\langle N \rangle} \left(1 + \frac{4D\tau}{r^2}\right)^{-1} \left(1 + \frac{4D\tau}{z^2}\right)^{-\frac{1}{2}} \tag{1.23}$$

In the above equation, $\langle N \rangle$ is the average number of molecules present in the confocal volume (see Figure 1.15), and D is the diffusion constant of the fluorophore.

Thus, for a diffusion-only species the diffusion constant can be calculated by fitting the autocorrelation decay provided the optical parameters r and z are known. The optical parameters can be obtained by fitting the autocorrelation decay of either a dye or a protein with known diffusion constants. For the results described in chapter 3, the optical parameters were calculated using 5/6 carboxytetramethylrhodamine (TAMRA) in water as the standard. The diffusion constant of TAMRA is 420 μm^2/s.[63-66] The fitting of the autocorrelation decay of TAMRA in water results in the estimation of the r and z, and use of these values results in the calculation of the diffusion constants of other samples.

1.3.4.3.2. FRET and quenching. FCS can also be used to investigate conformational dynamics in biological molecules. To use FCS as an investigating tool for the conformational dynamics of a biomolecule, the intensity of fluorescence has to fluctuate with the conformational change. In other words, if the intensity of fluorescence fluctuates due to the rapid spontaneous fluctuation between different conformations of a biomolecule, then FCS can be used to investigate the conformational dynamics. FRET and quenching are two different pathways that these intensity fluctuations can be achieved. Although sensitive to very different length scales, the intensity of fluorescence, for both FRET and quenching, is dependent on the distance between the donor-acceptor or the fluorophore-quencher, respectively. The conformational dynamics in a

biomolecule can change the distance between two different parts of the biomolecule, and if properly labeled with fluorophores or quenchers, this dynamics can be reflected at the fluctuations in florescence and hence be reflected in the FCS decay.

If conformational change does not affect the fluorescence intensity (e.g. a donor only sample when FRET is used as the probe) the resulting FCS decay is representative of the diffusion only decay $(T(\tau))$.

$$G_1(\tau) = T(\tau) \qquad\qquad (1.24)$$

When the conformational equilibrium affects the intensity of fluorescence (e.g. donor-acceptor sample), the corresponding FCS curve has the contribution from both the kinetics of the equilibrium $(X(t))$ and the diffusion $(T(t))$,[67, 68] and the correlation function is given by,

$$G_2(\tau) = T(\tau) \cdot X(\tau) \qquad\qquad (1.25)$$

The ratio of the FCS curve obtained for the sample with FRET, or quenching, to the FCS curve obtained for the diffusion only sample is then representative of the kinetic part of the FCS decay. Fitting this ratio to the appropriate kinetic equation can result in the calculation of the kinetic rates and parameters.

$$G_2(\tau)/G_1(\tau) = X(\tau) \qquad\qquad (1.26)$$

To study the ring opening and closing of DNA sliding clamps self-quenching of TAMRA was employed as the fluorescent probe. Two different fluorescent modifications of the same clamp were used in this study. In one sample, the dyes are in very close

proximity in the closed conformation of the clamp and are self-quenched. The opening of

this clamp results in the separation between the dyes and the recovery of fluorescence and

hence the FCS decay obtained using this sample has contribution from both diffusion and

kinetic term. In the other sample, opening and closing of the clamp does not affect the

intensity of fluorescence and the FCS decay of this sample is representative of only the

diffusion of the clamp. The ratio of these two samples was then used to find the kinetic

parameters. This work is described in detail in chapter 4.

1.3.5. Single molecule fluorescence: Single molecule techniques can distinguish

bulk behavior from the individual behavior of the molecules.[69] The bulk properties can

have multiple sources of origin. It can come from the same behavior of every molecule in

the solution. It can also originate from an average of different populations of molecules

showing drastically different properties. Single molecule techniques can distinguish

between these different populations that are undistinguishable in bulk measurements.

Single molecule fluorescence has the same characteristics as that of other single molecule

measurements: it can differentiate populations of molecules that have different

fluorescence properties. Advancements in the various fields, including (a) reduction of

the background by either creating a shallow depth of field using TIRF or a very small

illumination volume using confocal microscopy, (b) brighter more stable fluorophores,

(c) better detectors (both CCDs and APDs), (d) high NA, high magnification objectives,

and (e) improved lasers, have resulted in the very low signal-to-noise ratios required for

the detection of single molecule fluorescence.[25] Among the various common single

molecule fluorescence techniques, single molecule fluorescence in a freely diffusing

solution is one of the more prominent techniques. In this case, the molecules freely

diffuse in and out of the small observation volume created by the confocal microscope, and the fluorescence signal arising due to the presence of the molecules in the confocal volume is collected and analyzed.[70]

1.3.5.1. Experimental setup and single molecule condition. Single molecule fluorescence measurements were carried out in the confocal microscope set up described in section 1.3.4.1. and Figure 1.13. The difference was that the fluorescence signal was separated based on the color using a dichroic mirror (Omega XF2012). The donor and the acceptor signals were then corrected for the further unwanted light using two bandpass filters, Omega 3RD 560-620 and Chroma BP 670/40, respectively. Then, fluorescence was collected with 1 ms resolution using two independent avalanche photodiodes (SPCM-AQR14) and a National Instruments measurement card. The NI card saved intensity traces with one ms resolution. The data were separated into the intensities arising from two detectors and analyzed using labview, matlab and origin. The confocal set up creates a very small volume (~ 1 fL) and the use of a low concentration of the sample (~10 pM) creates a very small average number of molecules (0.006). This means the probability of having one molecule is just 0.596% and probability of having 2 molecules is almost non-existent (0.002%). This ensures the signal originates from only a single molecule. In contrast, on an average of 1 molecule in the confocal volume instead of 0.006 molecule results in the fact that 2 molecules are present 18.4% of the time.

1.3.5.2. Single molecule FRET. Single molecule FRET (smFRET) was first used to demonstrate DNA templates.[71] Since then smFRET have been used to investigate the conformational dynamics in DNA, proteins, RNA, and interaction of DNA or RNA with

the protein.[17, 21, 26, 69, 72, 73] In dual color smFRET, the anti-correlated fluorescence bursts are selected and analyzed. If the efficiency of the energy transfer is very high then the acceptor intensity is high and donor intensity is low. In absence of FRET, the reverse is true. The intensity bursts were selected based on the fact that either the donor or the acceptor intensity was above a certain threshold value. This selection criteria is different from the criteria where both the acceptor and the donor fluorescence intensities have to be above certain threshold values to be considered as bursts. The selection criteria used for our experiments ensures that both very low FRET and very high FRET states are not ignored. The signals collected in the two channels were corrected for background contributions and crosstalk (Cy3 intensity leaking to Cy5 channel). The FRET efficiency from the single molecule measurements are given by,

$$E_{FRET} = \frac{I_A}{I_A + \gamma \cdot I_D} \tag{1.27}$$

where I_A and I_D are the intensity in the acceptor channel and donor channel, respectively, and γ is a correction term that corrects for differences in the efficiency of the two detectors and quantum yield of the dyes. The value of γ can be calculated from the bulk FRET efficiency of a molecule by matching the smFRET histogram to the measured bulk FRET efficiency.[70] FRET histograms are calculated from the plot of fraction of molecules against FRET efficiency.

smFRET histograms are used in chapter 2 to distinguish the bulk and the single molecule behavior of the double stranded DNA sample labeled with both Cy3 and Cy5 fluorescent backbone modified dyes. smFRET results were used to prove the absence of

higher order structure formation by the single stranded DNA. Single molecule

fluorescence results were also used to follow the monomerization of both β-clamp and

PCNA qualitatively. These results are discussed in chapter 4.

1.4. References

1.   Yao, N.; Turner, J.; Kelman, Z.; Stukenberg, P. T.; Dean, F.; Shechter, D.; Pan, Z. Q.; Hurwitz, J.; O'Donnell, M., Clamp loading, unloading and intrinsic stability of the PCNA, beta and gp45 sliding clamps of human, E. coli and T4 replicases. *Genes Cells* **1996,** 1, (1), 101-13.

2.   Kornberg, A., DNA-Replication. *J Biol Chem* **1988,** 263, (1), 1-4.

3.   Kuriyan, J.; Odonnell, M., Sliding Clamps of DNA-Polymerases. *J Mol Biol* **1993,** 234, (4), 915-925.

4.   Johnson, A.; O'Donnell, M., Cellular DNA replicases: Components and dynamics at the replication fork. *Annu. Rev. Biochem.* **2005,** 74, 283-315.

5.   Lehninger, A.; Nelson, D.; Cox, M., *Lehninger Principles of Biochemistry*. W. H. Freeman: 2008.

6.   Watson, J. D.; Crick, F. H. C., The Structure of DNA. *Cold Spring Harbor Symp. Quant. Biol.* **1953,** 18, 123-131.

7.   Froimowitz, M., HyperChem: a software package for computational chemistry and molecular modeling. *BioTechniques* **1993,** 14, (6), 1010-1013.

8.   Georgescu, R. E.; Kim, S. S.; Yurieva, O.; Kuriyan, J.; Kong, X. P.; O'Donnell, M., Structure of a sliding clamp on DNA. *Cell* **2008,** 132, (1), 43-54.

9.   Krishna, T. S.; Kong, X. P.; Gary, S.; Burgers, P. M.; Kuriyan, J., Crystal structure of the eukaryotic DNA polymerase processivity factor PCNA. *Cell* **1994,** 79, (7), 1233-43.

10.   McNally, R.; Bowman, G. D.; Goedken, E. R.; O'Donnell, M.; Kuriyan, J., Analysis of the role of PCNA-DNA contacts during clamp loading. *BMC Struct Biol* **2010,** 10, 3.

11.   Oakley, A. J.; Prosselkov, P.; Wijffels, G.; Beck, J. L.; Wilce, M. C.; Dixon, N. E., Flexibility revealed by the 1.85 A crystal structure of the beta sliding-clamp subunit

of Escherichia coli DNA polymerase III. *Acta Crystallogr D Biol Crystallogr* **2003,** 59, (Pt 7), 1192-9.

12.   Argiriadi, M. A.; Goedken, E. R.; Bruck, I.; O'Donnell, M.; Kuriyan, J., Crystal structure of a DNA polymerase sliding clamp from a Gram-positive bacterium. *BMC Struct Biol* **2006,** 6, 2.

13.   Pettersen, E. F.; Goddard, T. D.; Huang, C. C.; Couch, G. S.; Greenblatt, D. M.; Meng, E. C.; Ferrin, T. E., UCSF chimera - A visualization system for exploratory research and analysis. *J Comput Chem* **2004,** 25, (13), 1605-1612.

14.   McNally, R.; Bowman, G. D.; Goedken, E. R.; O'Donnell, M.; Kuriyan, J., Analysis of the role of PCNA-DNA contacts during clamp loading. *BMC Struct Biol* **2010,** 10.

15.   Valeur, B., *Molecular Fluorescence: Principles and Applications*. Wiley-VCH: Weinheim, Germany, 2001.

16.   Lakowicz, J. R., *Principles of fluorescence spectroscopy*. Springer: 2006; Vol. 1.

17.   Rothenberg, E.; Ha, T., Single-molecule FRET analysis of helicase functions. *Methods Mol Biol* **2010,** 587, 29-43.

18.   Parkhurst, K. M.; Parkhurst, L. J., Fret Studies of Oligo-DNA Interactions. *Biophys J* **1994,** 66, (2), A154-A154.

19.   Koopmans, W. J. A.; Buning, R.; Schmidt, T.; van Noort, J., spFRET Using Alternating Excitation and FCS Reveals Progressive DNA Unwrapping in Nucleosomes. *Biophys J* **2009,** 97, (1), 195-204.

20.   Ishii, Y.; Yoshida, T.; Funatsu, T.; Wazawa, T.; Yanagida, T., Fluorescence resonance energy transfer between single fluorophores attached to a coiled-coil protein in aqueous solution. *Chem. Phys.* **1999,** 247, (1), 163-173.

21.   Ha, T., Single-molecule fluorescence resonance energy transfer. *Methods* **2001,** 25, (1), 78-86.

22.   Stryer, L.; Haugland, R. P., Energy Transfer - a Spectroscopic Ruler. *Proc. Natl. Acad. Sci. U. S. A.* **1967,** 58, (2), 719-&.

23.   Vogelsang, J.; Doose, S.; Sauer, M.; Tinnefeld, P., Single-molecule fluorescence resonance energy transfer in nanopipets: Improving distance resolution and concentration range. *Anal Chem* **2007,** 79, (19), 7367-7375.

24.   Iqbal, A.; Arslan, S.; Okumus, B.; Wilson, T. J.; Giraud, G.; Norman, D. G.; Ha, T.; Lilley, D. M. J., Orientation dependence in fluorescent energy transfer between Cy3 and Cy5 terminally attached to double-stranded nuclelic acids. *Proc. Natl. Acad. Sci. U. S. A.* **2008,** 105, (32), 11176-11181.

25.   Chakraborty, M.; Kuriata, A. M.; Henderson, J. N.; Salvucci, M. E.; Wachter, R. M.; Levitus, M., Protein Oligomerization Monitored by Fluorescence Fluctuation Spectroscopy: Self-Assembly of Rubisco Activase. *Biophys J* **2012,** 103, (5), 949-958.

26.   Choi, U. B.; Strop, P.; Vrljic, M.; Chu, S.; Brunger, A. T.; Weninger, K. R., Single-molecule FRET-derived model of the synaptotagmin 1-SNARE fusion complex. *Nat Struct Mol Biol* **2010,** 17, (3), 318-U84.

27.   Brismar, H.; Trepte, O.; Ulfhake, B., Spectra and Fluorescence Lifetimes of Lissamine Rhodamine, Tetramethylrhodamine Isothiocyanate, Texas Red, and Cyanine-3.18 Fluorophores - Influences of Some Environmental-Factors Recorded with a Confocal Laser-Scanning Microscope. *J. Histochem. Cytochem.* **1995,** 43, (7), 699-707.

28.   Buschmann, V.; Weston, K. D.; Sauer, M., Spectroscopic study and evaluation of red-absorbing fluorescent dyes. *Bioconjugate Chem* **2003,** 14, (1), 195-204.

29.   Meller, A.; Di Fiori, N., The Effect of Dye-Dye Interactions on the Spatial Resolution of Single-Molecule FRET Measurements in Nucleic Acids. *Biophys J* **2010,** 98, (10), 2265-2272.

30.   Gruber, H. J.; Hahn, C. D.; Kada, G.; Riener, C. K.; Harms, G. S.; Ahrer, W.; Dax, T. G.; Knaus, H. G., Anomalous fluorescence enhancement of Cy3 and Cy3.5 versus anomalous fluorescence loss of Cy5 and Cy7 upon covalent linking to IgG and noncovalent binding to avidin. *Bioconjugate Chem* **2000,** 11, (5), 696-704.

31.   Harvey, B. J.; Levitus, M., Nucleobase-Specific Enhancement of Cy3 Fluorescence. *J Fluoresc* **2009,** 19, (3), 443-448.

32.   Massey, M.; Algar, W. R.; Krull, U. J., Fluorescence resonance energy transfer (FRET) for DNA biosensors: FRET pairs and Forster distances for various dye-DNA conjugates. *Anal Chim Acta* **2006,** 568, (1-2), 181-189.

33.   Rasnik, I.; Myong, S.; Cheng, W.; Lohman, T. M.; Ha, T., DNA-binding orientation and domain conformation of the E-coli Rep helicase monomer bound to a partial duplex junction: Single-molecule studies of fluorescently labeled enzymes. *J Mol Biol* **2004,** 336, (2), 395-408.

34.   Sabanayagam, C. R.; Eid, J. S.; Meller, A., Using fluorescence resonance energy transfer to measure distances along individual DNA molecules: Corrections due to nonideal transfer. *J. Chem. Phys.* **2005,** 122, (6), -.

35.   Sanborn, M. E.; Connolly, B. K.; Gurunathan, K.; Levitus, M., Fluorescence properties and photophysics of the sulfoindocyanine Cy3 linked covalently to DNA. *J. Phys. Chem. B* **2007,** 111, (37), 11064-11074.

36.   Schobel, U.; Egelhaaf, H. J.; Brecht, A.; Oelkrug, D.; Gauglitz, G., New-donor-acceptor pair for fluorescent immunoassays by energy transfer. *Bioconjugate Chem* **1999,** 10, (6), 1107-1114.

37.   Tolosa, L.; Malak, H.; Raob, G.; Lakowicz, J. R., Optical assay for glucose based on the luminescence decay time of the long wavelength dye Cy5 (TM). *Sensor Actuat B-Chem* **1997,** 45, (2), 93-99.

38.   Ranjit, S.; Levitus, M., Probing the Interaction Between Fluorophores and DNA Nucleotides by Fluorescence Correlation Spectroscopy and Fluorescence Quenching. *Photochem Photobiol* **2012,** 88, (4), 782-791.

39.   Dolghih, E.; Roitberg, A. E.; Krause, J. L., Fluorescence resonance energy transfer in dye-labeled DNA. *J Photoch Photobio A* **2007,** 190, (2-3), 321-327.

40.   Iqbal, A.; Wang, L.; Thompson, K. C.; Lilley, D. M. J.; Norman, D. G., The structure of cyanine 5 terminally attached to double-stranded DNA: Implications for FRET studies. *Biochemistry* **2008,** 47, (30), 7857-7862.

41.   Ouellet, J.; Schorr, S.; Iqbal, A.; Wilson, T. J.; Lilley, D. M. J., Orientation of Cyanine Fluorophores Terminally Attached to DNA via Long, Flexible Tethers. *Biophys J* **2011,** 101, (5), 1148-1154.

42.   Unruh, J. R.; Gokulrangan, G.; Lushington, G. H.; Johnson, C. K.; Wilson, G. S., Orientational dynamics and dye-DNA interactions in a dye-labeled DNA aptamer. *Biophys J* **2005,** 88, (5), 3455-3465.

43.   Unruh, J. R.; Gokulrangan, G.; Wilson, G. S.; Johnson, C. K., Fluorescence properties of fluorescein, tetramethylrhodamine and Texas Red linked to a DNA aptamer. *Photochem Photobiol* **2005,** 81, (3), 682-690.

44.   Urnavicius, L.; McPhee, S. A.; Lilley, D. M. J.; Norman, D. G., The Structure of Sulfoindocarbocyanine 3 Terminally Attached to dsDNA via a Long, Flexible Tether. *Biophys J* **2012,** 102, (3), 561-568.

45.   Vamosi, G.; Gohlke, C.; Clegg, R. M., Fluorescence characteristics of 5-carboxytetramethylrhodamine linked covalently to the 5' end of oligonucleotides: Multiple conformers of single-stranded and double-stranded dye-DNA complexes. *Biophys J* **1996,** 71, (2), 972-994.

46.   Harvey, B. J.; Perez, C.; Levitus, M., DNA sequence-dependent enhancement of Cy3 fluorescence. *Photoch Photobio Sci* **2009,** 8, (8), 1105-1110.

47.   Doose, S.; Neuweiler, H.; Sauer, M., Fluorescence Quenching by Photoinduced Electron Transfer: A Reporter for Conformational Dynamics of Macromolecules. *Chemphyschem* **2009,** 10, (9-10), 1389-1398.

48.   Dunn, D. A.; Lin, V. H.; Kochevar, I. E., The Role of Ground-State Complexation in the Electron-Transfer Quenching of Methylene-Blue Fluorescence by Purine Nucleotides. *Photochem Photobiol* **1991,** 53, (1), 47-56.

49.   Heinlein, T.; Knemeyer, J. P.; Piestert, O.; Sauer, M., Photoinduced electron transfer between fluorescent dyes and guanosine residues in DNA-hairpins. *J. Phys. Chem. B* **2003,** 107, (31), 7957-7964.

50.   Seidel, C. A. M.; Schulz, A.; Sauer, M. H. M., Nucleobase-specific quenching of fluorescent dyes .1. Nucleobase one-electron redox potentials and their correlation with static and dynamic quenching efficiencies. *J Phys Chem-Us* **1996,** 100, (13), 5541-5553.

51.   Doose, S.; Neuweiler, H.; Sauer, M., A close look at fluorescence quenching of organic dyes by tryptophan. *Chemphyschem* **2005,** 6, (11), 2277-2285.

52.   Vaiana, A. C.; Neuweiler, H.; Schulz, A.; Wolfrum, J.; Sauer, M.; Smith, J. C., Fluorescence quenching of dyes by tryptophan: Interactions at atomic detail from combination of experiment and computer simulation. *J Am Chem Soc* **2003,** 125, (47), 14564-14572.

53.   Hernando, J.; van der Schaaf, M.; van Dijk, E. M. H. P.; Sauer, M.; GarcÃ-a-ParajÃ³, M. a. F.; van Hulst, N. F., Excitonic Behavior of Rhodamine Dimers:â€‰ A Single-Molecule Study. *The Journal of Physical Chemistry A* **2002,** 107, (1), 43-52.

54.   Kunzelmann, S.; Webb, M. R., A Fluorescent, Reagentless Biosensor for ADP Based on Tetramethylrhodamine-Labeled ParM. *Acs Chem Biol* **2010,** 5, (4), 415-425.

55.   Jameson, D. M.; Ross, J. A., Fluorescence Polarization/Anisotropy in Diagnostics and Imaging. *Chemical Reviews* **2010,** 110, (5), 2685-2708.

56.   Jares-Erijman, E. A.; Jovin, T. M., Imaging molecular interactions in living cells by FRET microscopy. *Curr. Opin. Chem. Biol.* **2006,** 10, (5), 409-416.

57.   Müller, J. D.; Chen, Y.; Gratton, E., Fluorescence correlation spectroscopy. In *Methods Enzymol.*, Academic Press: 2003; Vol. 361, pp 69-92.

58.   Schwille, P.; Korlach, J.; Webb, W. W., Fluorescence correlation spectroscopy with single-molecule sensitivity on cell and model membranes. *Cytometry* **1999,** 36, (3), 176-82.

59.   Thompson, N. L., FLuorescence Correlation Spectroscopy. In *Topics in Fluorescence Spectroscopy*, Lakowicz, J. R., Ed. Plenum Press: New York, 1991; Vol. 1, pp 337-355.

60.   Magde, D.; Elson, E. L.; Webb, W. W., Fluorescence correlation spectroscopy. II. An experimental realization. *Biopolymers* **1974,** 13, (1), 29-61.

61.   Magde, D.; Webb, W. W.; Elson, E., Thermodynamic Fluctuations in a Reacting System - Measurement by Fluorescence Correlation Spectroscopy. *Phys Rev Lett* **1972,** 29, (11), 705-708.

62.   Gurunathan, K.; Levitus, M., FRET Fluctuation Spectroscopy of Diffusing Biopolymers: Contributions of Conformational Dynamics and Translational Diffusion. *J. Phys. Chem. B* **2010,** 114, (2), 980-986.

63.   Culbertson, M. J.; Williams, J. T. B.; Cheng, W. W. L.; Stults, D. A.; Wiebracht, E. R.; Kasianowicz, J. J.; Burden, D. L., Numerical fluorescence correlation spectroscopy for the analysis of molecular dynamics under nonstandard conditions. *Anal Chem* **2007,** 79, (11), 4031-4039.

64.   Gendron, P. O.; Avaltroni, F.; Wilkinson, K. J., Diffusion Coefficients of Several Rhodamine Derivatives as Determined by Pulsed Field Gradient-Nuclear Magnetic Resonance and Fluorescence Correlation Spectroscopy. *J Fluoresc* **2008,** 18, (6), 1093-1101.

65.   Muller, C. B.; Loman, A.; Pacheco, V.; Koberling, F.; Willbold, D.; Richtering, W.; Enderlein, J., Precise measurement of diffusion by multi-color dual-focus fluorescence correlation spectroscopy. *Europhys. Lett.* **2008,** 83, (4), 46001.

66.   Petrasek, Z.; Schwille, P., Precise measurement of diffusion coefficients using scanning fluorescence correlation spectroscopy. *Biophys J* **2008,** 94, (4), 1437-1448.

67.   Li, G.; Levitus, M.; Bustamante, C.; Widom, J., Rapid spontaneous accessibility of nucleosomal DNA. *Nat Struct Mol Biol* **2005,** 12, (1), 46-53.

68.   Chattopadhyay, K.; Elson, E. L.; Frieden, C., The kinetics of conformational fluctuations in an unfolded protein measured by fluorescence methods. *Proc. Natl. Acad. Sci. U. S. A.* **2005,** 102, (7), 2385-9.

69.   Deniz, A. A.; Mukhopadhyay, S.; Lemke, E. A., Single-molecule biophysics: at the interface of biology, physics and chemistry. *J R Soc Interface* **2008,** 5, (18), 15-45.

70.   Deniz, A. A.; Laurence, T. A.; Dahan, M.; Chemla, D. S.; Schultz, P. G.; Weiss, S., Ratiometric single-molecule studies of freely diffusing biomolecules. *Annu Rev Phys Chem* **2001,** 52, 233-253.

71.   Deniz, A. A.; Dahan, M.; Grunwell, J. R.; Ha, T. J.; Faulhaber, A. E.; Chemla, D. S.; Weiss, S.; Schultz, P. G., Single-pair fluorescence resonance energy transfer on freely diffusing molecules: Observation of Forster distance dependence and subpopulations. *Proc. Natl. Acad. Sci. U. S. A.* **1999,** 96, (7), 3670-3675.

72.   Michalet, X.; Weiss, S.; Jager, M., Single-molecule fluorescence studies of protein folding and conformational dynamics. *Chem. Rev. (Washington, DC, U. S.)* **2006,** 106, (5), 1785-813.

73.   Ferreon, A. C.; Moran, C. R.; Gambin, Y.; Deniz, A. A., Single-molecule fluorescence studies of intrinsically disordered proteins. *Methods Enzymol.* **2010,** 472, 179-204.

Chapter 2

Photophysics of fluorescent backbone modifications of DNA: reducing uncertainties in FRET

2.1. Introduction

The photophysics of the DNA backbone modified Cy3 and Cy5 (known as iCy3 and iCy5, respectively) dyes were studied in this chapter with the goal of reducing uncertainties associated with the translation of the Förster resonance energy transfer (FRET) efficiency to distances. FRET is a process through which the energy from the excited state of one molecule (called the donor) can be non-radiatively transferred to the ground state of another molecule (known as the acceptor). The efficiency of energy transfer depends on the distance between the donor and the acceptor dyes (R_{DA}), which is why FRET is often used to measure distances in biological molecules.[1-5] Since its discovery, FRET has become one of the most widely used techniques to study structural and functional properties of various biological systems. Stryer first introduced this technique as a tool for distance measurement in biological systems and termed this technique "spectroscopic ruler".[6] The orientation factor (κ^2) is one of the uncertainties which precludes FRET from being a truly quantitative technique. In this work, the backbone DNA modified fluorophores are shown to have constrained rotational flexibility. As a result, the relative orientation of the fluorophores during FRET can be predicted based on the geometry of the DNA, resulting in control of orientation and measurement of FRET at distances which would have been impossible for the freely rotating fluorophores.

FRET has been extensively used over the years in biological systems. Lately, the advancements in the fields of optical detection, newer brighter light sources, and the development of bright organic fluorophores have resulted in the detection of FRET at the single molecule level and increased the use of this technique considerably.[2, 7-9] A detailed description of FRET is given in section 1.3.1. As mentioned, there are multiple sources of uncertainties that contribute towards the calculation of the distance between the donor and the acceptor (R_{DA}) from the efficiency of FRET, of which the orientation factor is one of the most important and widely discussed one.

The carbocyanine dyes, Cy3 and Cy5, have been widely used in the field of biochemistry and biophysics. The high photostability and brightness of Cy3 (when bound to a biomolecule) have led to the widespread use of Cy3 in single molecule fluorescence techniques.[8, 10, 11] Cy3 and Cy5 have been one of the most used dye pairs in FRET, especially in single molecule FRET (smFRET), due to (a) their high photo stability in oxygen free environments, (b) comparable quantum yields (useful for clearly anti-correlated intensity changes of donor and acceptor during a FRET event), (c) the large spectral separation (~100 nm, resulting in reduction of direct excitation of acceptor and reduction of crosstalk due to the leakage of donor emission to the acceptor channel), and (d) commercial availability in amino, thiol and carbonyl reactive forms.[12] These dyes, either independently or in combination with each other, have also been used in the evolving field of super resolution microscopy.[13-18] It has been shown that Cy3, when bound to the double stranded DNA by a six carbon flexible linker, is neither rigid nor rotates freely during the lifetime of fluorescence.[19] It has also been shown that Cy3 and Cy5, when bound to the 5' end of the double stranded DNA, can interact with the

terminal base pairs, resulting in primarily stacked conformation.[8, 20-22] The angular

positions of the 5'Cy3 or 5'Cy5 relative to the terminal base pairs are dependent on the

length of the linkers, but the stacking behavior is independent of it. This has been proved

using both FRET measurements[8, 21] and NMR methods.[20, 22] Theoretical simulations show

that Cy5 attached to the double stranded DNA via a long flexible linker can bind to the

major groove of the DNA in two very different conformations, resulting in a change of up

to 8 Å in the donor acceptor distances.[23] Similarly, some rhodamine dyes, Texas red[24]

and tetramethylrhodamine,[24, 25] can also interact with the biomolecule under study. The

use of long linkers when attaching a fluorophore to the biomolecule was based on the

assumption that the long linkers would prohibit the interactions and the fluorophore could

rotate freely. The interactions described earlier show that the presence of a long flexible

linker does not necessarily inhibit the interaction of the fluorophore with the biological

systems and can actually facilitate interactions by allowing too much flexibility. These

interactions not only create uncertainties in the relative orientation of the donor and

acceptor transition dipole moments, but also create uncertainties in the relative donor

acceptor distances.[23] Dye-biomolecule interactions can also change the photophysical

properties of the fluorophores, affecting any FRET efficiency measurement. For example,

the quantum yield of Cy3 changes from 0.03 in its free form in water to 0.39 when bound

to the 5' end of the ss DNA.[26] Also, fluorophores are also often quenched when bound to

the biomolecule.[27, 28] The interactions can also lead to the changes in the absorption or

emission spectra.[27, 29-31] These factors introduce further uncertainties in the calculation of

the distance from the measured FRET efficiency.

In this chapter, a different approach and synthetic strategy compared to the flexible linkers has been employed to reduce the uncertainties associated with FRET. Most of the aforementioned drawbacks are result of the flexibility of the linkers. Thus the rationale used in this work was to eliminate the contributions to FRET from flexibility. To achieve this the rigid fluorescent backbone modifications of the double stranded DNA have been selected as the fluorescent donor and acceptor pairs. In these modifications, both iCy3 and iCy5 dyes are attached to the phosphate backbone between two phosphate groups in place of the deoxyribose sugar. The complementary strand has an unpaired base opposite to the position of the dye. These fluorescent modifications are expected to follow the helical backbone structure in double stranded DNA. The angles and the distance between the donor and the acceptor dyes can therefore be predicted from the B-DNA geometry. The structures of the backbone modification and the commonly used Cy3/Cy5 with 6 carbon linker attachment are depicted in Figure 2.1. The cartoon represents the expected position of backbone modified dyes in the DNA strands (Figure 2.1.C). The data shows that during the lifetime of fluorescence, there is no considerable rotational motion of the dyes. Hence, the relative orientation between the two fluorophores, measured by κ^2, does not change during the relevant timescales of the energy transfer. The rigid position of the dyes in the backbone of the DNA means that the distance between the donor and the acceptor is fixed and does not fluctuate.
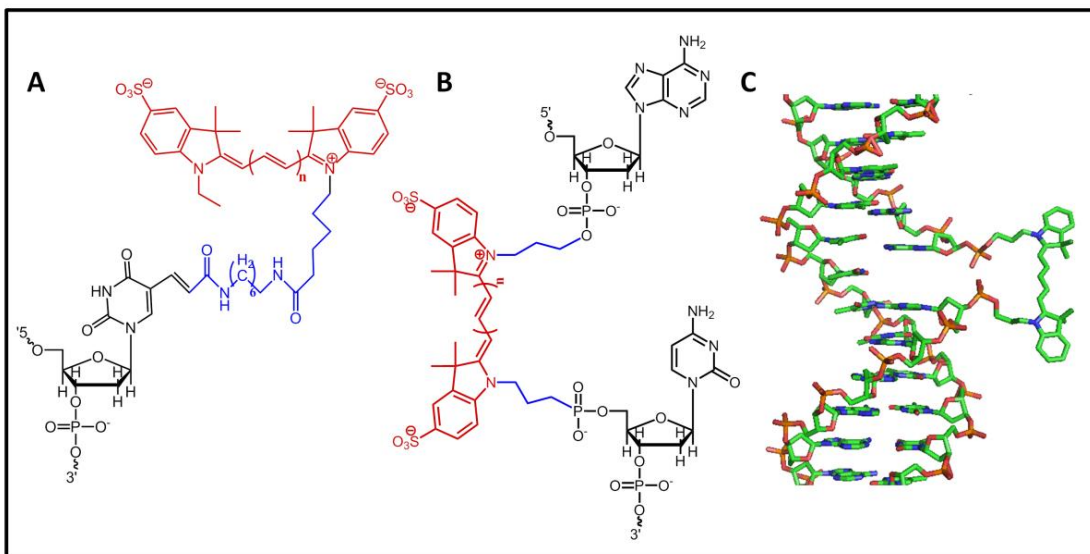
Figure 2.1. Structure of the cyanine dyes used in these experiments. (A) The structure of the commonly used Cy3 (n=1) and Cy5 (n=2) dyes (shown in red) when connected to to a thymine (shown in black) on the DNA via a six carbon linker.. The total length of the linker is typically much longer (shown in blue) (B) The backbone modified cyanine moiety: iCy3 (n=1) and iCy5 (n=2) (shown in red) dyes are bound to two phosphates by a 3-carbon linker (shown in blue). (C) A cartoon representation of the backbone modification of Cy5 dye (iCy5). This figure is representative of the expected position of the dye and should only be used as a visual aid as no energy minimization calculation was performed in this structure.

2.2 Materials and Methods

2.2.1. DNA Samples. The oligonucleotides used in these experiments are shown in chart 1. These nucleotides were purchased from Integrated DNA Technologies (Coralville, IA).

A	5' GAT GAT GTC ATC GAC /iCy3/ GCG CGA TAT TAG CT 3'
B	5' CTC TAG CAG GGT AGC /iCy5/ CAG GTG CGA GGC TG 3'
C	5' GAT GAT GTC ATC GAC AGC /iCY3/ CGA TAT TAG CTC TCT AGC AGG GTA GCA CAG GTG CGA GGC 3'
D	5' GAT GAT GTC ATC GAC /iCy3/ GCG CGA TAT TAG CTC TCT AGC AGG GTA GCA CAG GTG CGA GGC TG 3'
E	5' CAG CCT CGC ACC TGT GC /iCy5/ A CCC TGC TAG AGA GCT AAT ATC GCG CTG TCG ATG ACA TCA TC 3'
F	5' CAG CCT CGC ACC TGT GCT ACC CTG CTA GAG AGC TAA TAT CGC GCT GTC GAT GAC ATC ATC 3'
G	5' GAT GAT GTC ATC GAC /iAmMC6T/ GCG CGA TAT TAG CTC TCT AGC AGG GTA GCA CAG GTG CGA GGC TG 3'
H	5' CAG CCT CGC ACC TGT GCT ACC CTG CTA GAG AGC TAA TAT CGC GCA GTC GAT GAC ATC ATC 3'
I	5' GAT GAT GTC ATC GAC AGC GCG ATA TTA GCT CTC TAG CAG GGT AGC ACA GGT GCG AGG CTG 3'

Chart .2.1. The sequence of the oligonucleotides used in these experiments.

Here, /iAmMC6T/ represents the internal amino modified C_6 dT. The methyl group at position 4 of the thymine ring is extended to a six carbon chain ending with a primary amine group that can react with the succinimidyl ester of Cy3/Cy5 to produce the structure shown in Figure 2.1.A. The /iCy3/ and /iCy5/ represent the DNA backbone modified fluorophore, where a base and the corresponding sugar from the DNA backbone have been replaced by the fluorophores Cy3 and Cy5, respectively. The samples where the fluorophores are bound to the thymine by the linker are termed as the internal modifications. All the strands from chart 1 were HPLC purified and their mass spectra contained a single peak, demonstrating the high purity of the samples.

Sample 1 was prepared by ligating strand A and strand B and then annealing it with strand F. A kination step preceded the ligation procedure. First, sample B was treated with T4 polynucleotide kinase (NEB, Ipswich, MA), and then the product was ligated with strand A in presence of T4 DNA ligase (NEB, Ipswich, MO), strand F and ATP using the protocol supplied by the manufacturer. The ligated product was purified from a 12% denaturing gel, and then annealed with strand F to produce sample 1.

Strand G was reacted with monofunctionalized N-hydroxysuccinimidyl (NHS) ester of the dye Cy3 (GE Healthcare, Piscataway, NJ) in borate buffer (pH=9). The labeled DNA strand was separated from the unreacted dye by using a micro Bio-Spin p6 size exclusion column (Bio-Rad, Hercules, CA). Then, the fluorescently labeled G strand was annealed with strand H to produce the internally modified Cy3 labeled DS DNA, sample 4.

61

Samples 2, 3, 5, 6 and 7 were prepared by annealing the following strands:

Sample 2 ⟶ Strand D + Strand E,

Sample 3 ⟶ Strand C + Strand E,

Sample 5 ⟶ Strand D + Strand F,

Sample 6 ⟶ Strand I + Strand F,

Sample 7 ⟶ Strand I + Strand E,

The purity of the all the double stranded DNA were checked and confirmed by gel electrophoresis and fluorescent gel scanning (Typhoon FLA 7000, Pittsburg, PA).

The experiments described in this chapter were carried out in 10 mM TRIS buffer at pH 7.4, unless mentioned otherwise. The long DNA strands can have significantly stable secondary structures. Hence, the double stranded DNA structures were prepared by heating up the annealing solutions to 90°C and then slowly cool to room temperature (~25°C) over hours. This slow cooling means that the most stable thermodynamic product, the complete double stranded DNA, is the only product and there are no single stranded secondary structures present. The absorbance and the fluorescence intensity of the dyes pre- and post-heating remained unchanged, indicating that the dyes are chemically insensitive to the temperature change in the experiments.

2.2.2. Absorbance measurements. The absorption spectra for the calculation of the concentrations of the DNA samples were measured in a Shimadzu UV-1700 spectrophotometer. Three consecutive runs at a medium scan rate were performed for

each sample. Average absorption spectrum for each sample was calculated from the three

runs after a background correction. The concentrations of the unlabeled DNA samples

were calculated from the absorbances at 260 nm using the extinction coefficient (at 260

nm) provided by the manufacturer. The concentration of the labeled DNA samples were

calculated using the extinction coefficient of the corresponding fluorophore at the

maxima of the absorption spectra ($\varepsilon_\lambda^{max}$) of the dye. The extinction coefficient at the

maxima of the absorption spectra used for the Cy3 and the Cy5 labeled DNA samples

were 150,000 $M^{-1}cm^{-1}$ and 250,0000 $M^{-1}cm^{-1}$, respectively. During the annealing

procedure, the unlabeled DNA was added in slight excess (1.2 times), to ensure that all

the labeled samples were double stranded. The maximum absorption of the band under

consideration for the concentration measurement was kept under 1 to ensure a linear

relation between the concentration and absorbance.

The temperature-dependent absorption measurements and the melting temperature

experiments were carried out in a Cary 300 Bio UV-Vis spectrophotometer (Agilent,

Santa Clara, CA), equipped with a Peltier heating system. Four cuvettes containing the

buffer used in this experiment (10mM TRIS, 100mM NaCl, 25 mM $MgCl_2$, pH = 7.4)

and samples 2, 5 and 6 were kept in the cuvette holder attached with the peltier system

and the absorbances were measured simultaneously. The initial and final temperature of

the heating cycle were 10°C and 100°C, respectively, with a heating rate of 1°C/min. The

absorbances were recorded at 260 nm with a 0.5°C temperature intervals. The absorbance

data were corrected for the background using the buffer solution and the melting

temperatures were determined using the program provided by the instrument

manufacturer.

2.2.3. Steady state fluorescence. Excitation and emission fluorescence spectra were collected using a QuantaMaster-4/2005SE spectrofluorometer (PTI, NJ). Excitation spectra of the samples were collected by scanning the excitation wavelength while the emission monochromator was kept fixed at 700 nm. The excitation spectra were corrected for the fluctuations in the lamp intensity and wavelength dependence of lamp excitation by using a built in quantum counter. Emission spectra were collected by exciting the samples at 510 nm and scanning the emission monochromator. The emission spectra were corrected for the fluctuations of the lamp intensity and the wavelength dependent detection capability of the detector. The temperature dependent experiments were carried out using an attached temperature controlled water circulator. The temperatures of the samples were measured inside the cuvette using a thermocouple.

2.2.4. Quantum yield and overlap integral. Quantum yields of the Cy3 labeled samples were calculated relative to the quantum yield of carboxytetramethylrhodamine in methanol $(0.68)^{32}$ using the method described in the section 1.3.1.1. The excitation wavelength was 510 nm. Similarly Cy5 quantum yield was calculated using 3, 3' diethyldithiacarbocyanine iodide in methanol (ϕ_D=0.29).[33] The excitation wavelength for Cy5 excitation was 600 nm. The overlap integral ($J(\lambda)$) was calculated using the procedure described in section 1.3.1.2.

2.2.5. FRET from steady state excitation spectra. The corrected excitation spectra of the FRET samples were fitted with the following equation,[34]

$$I(\lambda_{Ex}) = K[\varepsilon^D(\lambda_{Ex}) \cdot E_{FRET} + \varepsilon^A(\lambda_{Ex})] \tag{2.1}$$

In the above equation E_{FRET} is the efficiency of the FRET, $\varepsilon^D(\lambda_{Ex})$ and $\varepsilon^A(\lambda_{Ex})$ are the wavelength dependent extinction coefficients of the donor and the acceptor only double stranded DNA, respectively. The maxima of the extinction spectra were fixed at 150,000 and 250,000 for Cy3 and Cy5, respectively. K is a normalization constant.

The advantages of this technique over a more traditional donor only based technique is twofold. First, it does not require a donor only sample, and second, there is no need to measure very low absorbances required for calculation of FRET efficiency from emission spectra. Precise measurements of these low absorbances in a microcuvette, required for the scarcity of the samples, are very challenging.

The presence of an excess of donor only samples does not contribute towards the calculation of FRET efficiency in this method as the donor only samples cannot transfer energy to the acceptor molecules and, at the wavelength of the collection of the data (700 nm), they are dark. Thus, during the preparation of the samples for these experiments, sample 2 and 3 were annealed in the presence of excess donor only samples to ensure absence of any acceptor only single stranded DNA. Sample 1, containing both the donor and the acceptor in the same strand, was annealed with its complementary DNA strand in excess to ensure absence of single stranded labeled strand.

2.2.6. Steady state anisotropy. Steady state anisotropies of the samples were calculated from the polarized intensities obtained by placing polarizers in the excitation and the emission paths of the fluorometer. The steady state fluorescent anisotropy was calculated using the following relation,[35]

$$\langle r \rangle = \frac{I_{VV} - I_{VH} \cdot G}{I_{VV} + 2 \cdot I_{VH} \cdot G} \tag{2.2}$$

In the above equation, G is the correction factor, and is given by I_{HV}/I_{HH}. Here, the subscript represents the measured intensity at the position of the excitation polarizer (first letter) and the emission polarizer (last letter). H and V correspond to the horizontal and vertical orientations of the polarizer, respectively.

2.2.7. Time resolved fluorescence intensity and anisotropy decay. The time resolved fluorescence decays were obtained by exciting the samples at 450 nm using a Ti-Sapphire laser as described in section 1.3.3.

2.2.7.1. Determination of FRET from the time resolved fluorescence intensity decay.[34] The average lifetime of the donor only ($\langle \tau_D^0 \rangle$) and the donor-acceptor ($\langle \tau_D \rangle$) sample was obtained from the time resolved intensity decays as described earlier in section 1.3.3.2. FRET efficiency was then calculated using the following equation,

$$E_{FRET} = 1 - \frac{\langle \tau_D \rangle}{\langle \tau_D^0 \rangle} \tag{2.3}$$

The measurement of FRET efficiency using this method is independent of presence of the acceptor only molecules as they are not directly excited by the excitation wavelength and do not emit at the wavelength of the measurement. Hence, the samples for this experiment were prepared with slight excess of acceptor only single stranded DNA to ensure absence of donor only single stranded DNA.

2.2.8. Single molecule fluorescence. Sample 1 contains both the donor and the acceptor in the same strand of DNA. Thus, the calculated FRET efficiency from the bulk

66

measurements can be representative of either of the two following scenarios. The first is where all of the DNA samples are double stranded and have the calculated FRET efficiency. The second scenario is one where a combination of two conformations of the single stranded DNA are present : one having a high FRET efficiency and the other having a very low FRET efficiency. The average behavior of these two structures can lead to the observed average FRET efficiency. To distinguish between these two scenarios, single molecule FRET measurements in freely diffusing solution were performed in a confocal microscope with a single molecule sensitivity following the procedure described in section 1.3.5. If there is a mixture of conformations, then the FRET efficiency histogram should contain two distinctive peaks at a low and high FRET. Absence of the peak at high FRET in the histogram will prove the homogeneity of the sample 1 and the absence of secondary structures. These experiments were carried out in presence of 140 mM β-mercaptoethanol to reduce Cy5 blinking. The signals were further corrected for background contributions (~1.5 counts/ms for the donor and ~3 counts/ms for the acceptor) and the crosstalk (5% of the Cy3 intensity leaking to Cy5 channel). The FRET efficiency was calculated from the method described in section 1.3.5.2. The value of γ was calculated using the sample 3, where the single molecule FRET histogram was matched to the measured bulk FRET efficiency. A threshold of >14 counts/ms was used in both channels to ensure that the contribution from the background and the unwanted signals were completely excluded.

2.3. Results

2.3.1. FRET measurements. The efficiency of FRET for each sample was measured using two independent techniques. One method was through the steady state FRET efficiencies from the excitation spectra of the donor-acceptor samples. The calculated FRET efficiency for samples 1, 2 and 3 were 16%, 15% and 40%, respectively. Figure 2.2 shows the measured excitation spectra for sample 1 (black, solid), sample 2 (green, solid) and sample 3 (red, solid) along with the simulated excitation spectra for 0% (blue, dashed) and 100% FRET (brown, dashed). These two simulated spectra give the lower and upper limit of FRET and the extent of contribution from the energy transfer from Cy3 that can be expected in the excitation spectra of the iCy3-iCy5 fluorophores.
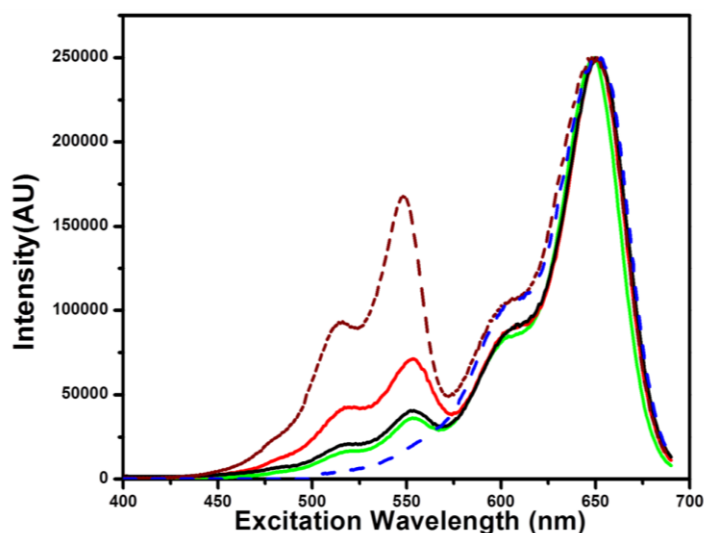
Figure 2.2. Calculation of FRET efficiency from the excitation spectra. The black, green and red solid lines represent the excitation spectra of sample 1, 2 and 3, respectively. The fits of these excitation spectra using equation 2.1 give the FRET efficiency of 16%, 15% and 40% for the sample 1, 2, and 3, respectively. The blue and brown dashed lines represent the calculated spectra for 0% and 100% FRET efficiency, respectively.

The FRET efficiencies of sample 2 and sample 3 were also measured using time resolved fluorescence intensity decays. The lifetime of Cy3 is often dependent on the microenvironment the dye is in. It has been shown that for Cy3 attached to the 5' end of the single stranded DNA, the average lifetime of Cy3 is a function of the sequence of the DNA.[26] It is also known that the quantum yield of Cy3 can change when it is attached to different areas of the same protein molecule.[11] Thus, to measure FRET of each of the donor acceptor sample, the lifetime of Cy3 was measured in the corresponding donor only sample. This ensures that any change in lifetime of the Cy3, which is position-dependent, does not introduce any artifact in the FRET efficiency calculation. Table 2.1 shows the lifetimes of both the donor only and donor acceptor samples. The Cy3 lifetimes in the two donor only samples were not equal, demonstrating the need for measuring the donor only samples for each FRET measurement. The intensity decays of sample 2, 3 and 5 (iCy3 only DS sample) are plotted in blue, red and black, respectively, in Figure 2.3.

Sample	Lifetime (ns)	Amplitude (%)	$\langle \tau \rangle$ ns
Sample 2 donor only	1.62	49.5	1.09
	0.56	50.5	
Sample 2	2.00	17.8	0.93
	0.92	58.6	
	0.13	23.6	
Sample 3 donor only	2.14	31.8	1.28
	0.87	68.2	
Sample 3	2.10	17.4	0.70
	0.76	40.0	
	0.08	42.6	

Table. 2.1. The measured lifetimes after fitting the donor intensity decays in the donor only and donor acceptor versions of sample 2 and sample 3. $\langle \tau \rangle$ represents the average lifetime of the donor iCy3 in the sample.
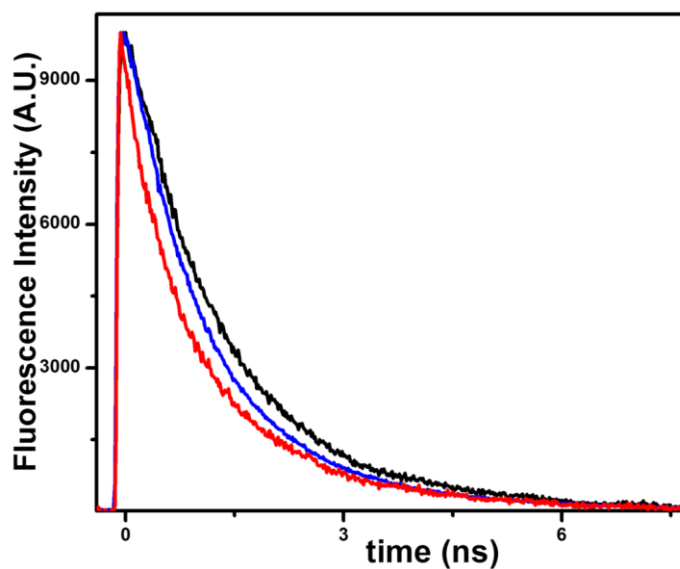
Figure. 2.3. The intensity decays of Sample 2, 3 and 5 (the donor only sample) in TRIS buffer. The faster decay indicates shorter lifetimes. The decay of the donor only sample of sample 3 (strand C + strand F) is very similar in appearance to that of the sample 5 and was not plotted. The decays were fitted with a model assuming that the decays can be explained by the sum of exponentials. The least number of terms required for very low χ^2 and complete randomness of the residuals were used as the lifetime parameters.

2.3.2. Calculation of the distances between the iCy3 and iCy5. Models of double stranded DNA having the exact sequence as that of the experimental samples were constructed using Hyperchem (Gainsville, FL) using a standard B DNA structure.[36] Then, iCy3 and iCy5 dyes were joined to the double stranded DNA after deleting the corresponding sugar moiety and attaching the 3 carbon linkers on both sides of the dye to the phosphate backbone. Distance was measured from the middle carbon of the polymethine chain of iCy3 to the middle carbon of the polymethine chain of the iCy5 using the software Chimera (UCSF, CA).[37] An error of $\pm$ 3 Å was estimated based on the flexibility of the linker carbon atoms. No energy minimization was carried during the preparation of the structures. Hence, the Figure 2.1.C does not represent the actual position of the dyes on the DNA. It is used only to illustrate the attachment and expected geometry. The distance between the FRET pairs in sample 1, 2 and 3 were calculated to be 102 Å, 90 Å and 83 Å, respectively.

2.3.3. Measurement of $J(\lambda)$. The overlap integral is shown by the yellow shaded region of the Figure 2.4. The $J(\lambda)$ was calculated from the absorption spectra of sample 5 and the emission spectra of sample 7 using equation 1.4. The value of the overlap integral was 7.456×10^8 M^{-1} nm^3. This value was used to create the κ^2 dependent FRET efficiency plot in Figure 2.6.
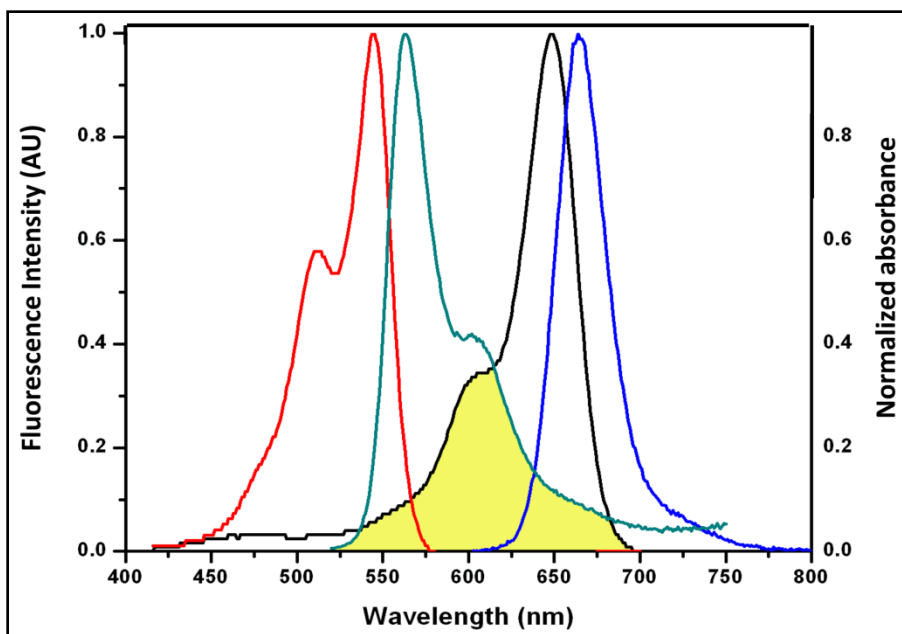
Figure 2.4. Overlap integral of iCy3-iCy5 FRET pairs. The yellow shaded region depicts the overlap of the donor iCy3 emission spectra (cyan) and the acceptor iCy5 absorption spectra (black). The iCy3 absorption spectra and the iCy5 emission spectra are shown in red and blue, respectively.

2.3.4. Quantum yield measurements. To measure the quantum yields of the donor and the acceptor, strand 5 (donor only double stranded DNA) and sample 7 (acceptor only double stranded DNA) were used. The average value of the quantum yields of the iCy3- and iCy5-only double stranded DNA samples were 0.31 ± 0.02 and 0.39 ± 0.03, respectively. This value of the iCy3-only double stranded DNA quantum yield was used for creating the plot of FRET efficiency dependence versus κ^2 in Figure 2.6. Figure 2.5 represents the five set of independent measurements done for the calculation of quantum yield of the iCy3 (black square) and iCy5 (red circle) only double stranded DNA.

72
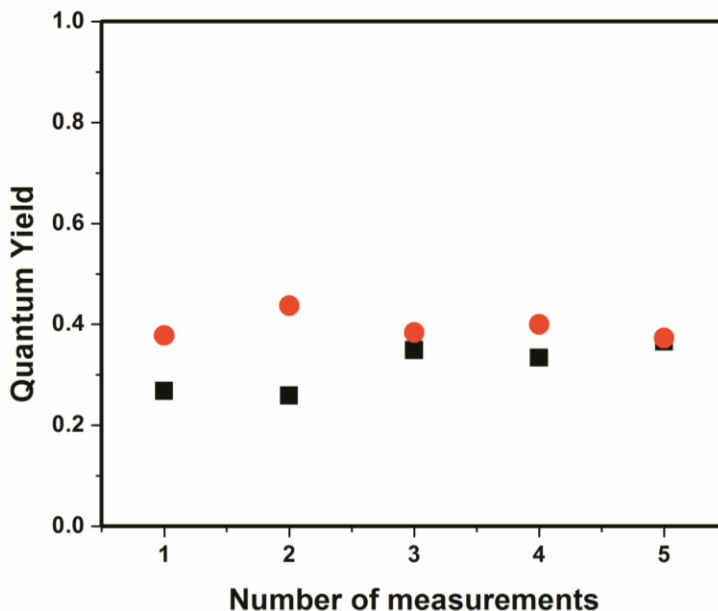
Figure 2.5. Quantum yields of iCy3 (black squares) and iCy5 (red circles) only DS DNA samples. The average quantum yields of these five measurements were 0.31 ± 0.02 (iCy3) and 0.39 ± 0.03 for the iCy3 only and iCy5 only DS DNA, respectively.

2.3.5. FRET against distance. FRET as a function of distance is dependent on

the value of κ^2. Förster's distance is given by,

$$R_0 = 0.211 \cdot [\kappa^2 \cdot n^{-4} \cdot \phi_D \cdot J(\lambda)]^{1/6} \text{ Å, when } \lambda \text{ is in the unit of nm.}$$

Using the value of $\phi_D = 0.31$, $J(\lambda) = 7.456 \times 10^8$ M^{-1} nm^3, and the refractive index of the

water (n) = 1.33, Förster's radius for the iCy3-iCy5 DS DNA system was calculated as,

$$R_0 = 63.4 \times (\kappa^2)^{1/6} \text{ Å} \qquad (2.4)$$

From this, a plot of the efficiency of FRET against distance was calculated, where the R_0

value was changed from the commonly used 53 Å (black dotted line) for the Cy3-Cy5

pair[3] to different R_0 values calculated for the iCy3-iCy5 pair using the κ^2 values of 2/3

73

(red solid line), 1 (blue solid line), 2 (green solid line), 3 (violet solid line) and 4 (orange

solid line). This is represented in Figure 2.6. The measured FRET efficiency of sample 1

(black circle), 2 (red circle) and 3 (blue circle) are also plotted in Figure 2.6.
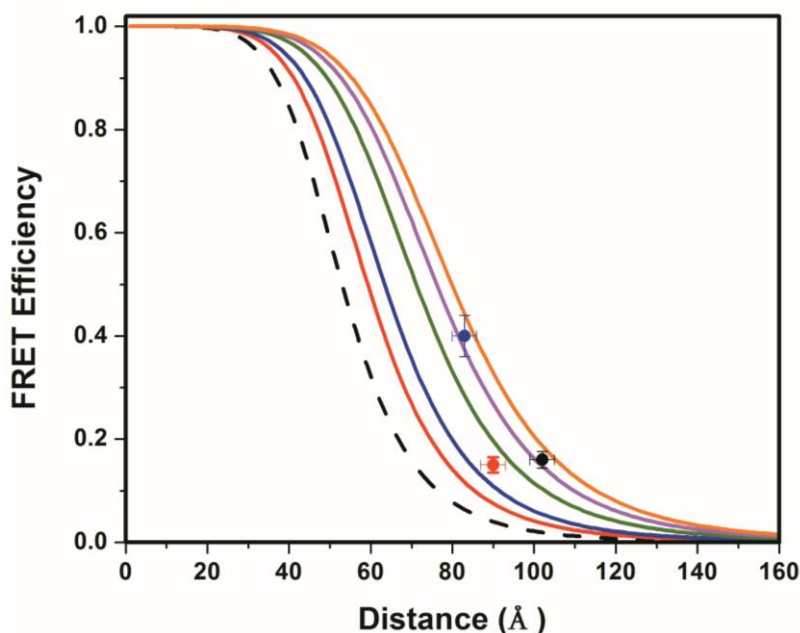
Figure 2.6. Plot of FRET efficiency against donor-acceptor distances. The black dotted line represents the simulated efficiency of energy transfer with a R_0 value of 53 Å, the most commonly used value for the Cy3-Cy5 FRET pair. The simulated FRET efficiency plots for the iCy3-iCy5 FRET pairs, where R_0 values were calculated using $\kappa^2 = 2/3$ (red solid line), 1 (blue solid line), 2 (green solid line), 3 (violet solid line) and 4 (orange solid line). The FRET efficiency of sample 1 (black circle), 2 (red circle) and 3 (blue circle) are also plotted in the same plot with their corresponding estimated distances.

2.3.6. Steady state anisotropy. The steady state anisotropy of the iCy3 only

double stranded DNA (sample 5) was measured in the fluorometer using the procedure

described before. The excitation transition dipole moment and the emission transition

dipole moment of cyanines like Cy3 are approximately collinear. In this situation the

steady state anisotropy can have a value of 0 to 0.4.[35] A value of fluorescence anisotropy

equaling zero represents complete rotational randomization during the lifetime of fluorescence and a value of 0.4 represents no rotational motion during the relevant timescales of fluorescence. The higher the fluorescence anisotropy, the less the rotation. Five independent fluorescence anisotropy measurements of iCy3 DS DNA (sample 5) were carried out and the average anisotropy was 0.28 ± 0.01. This high value of anisotropy represents that the iCy3 moiety does not rotate and depolarize light during the lifetime of fluorescence. Figure 2.7 shows five separate anisotropy results used for the calculation of the average steady state fluorescence anisotropy of iCy3 only DS DNA (sample 5).
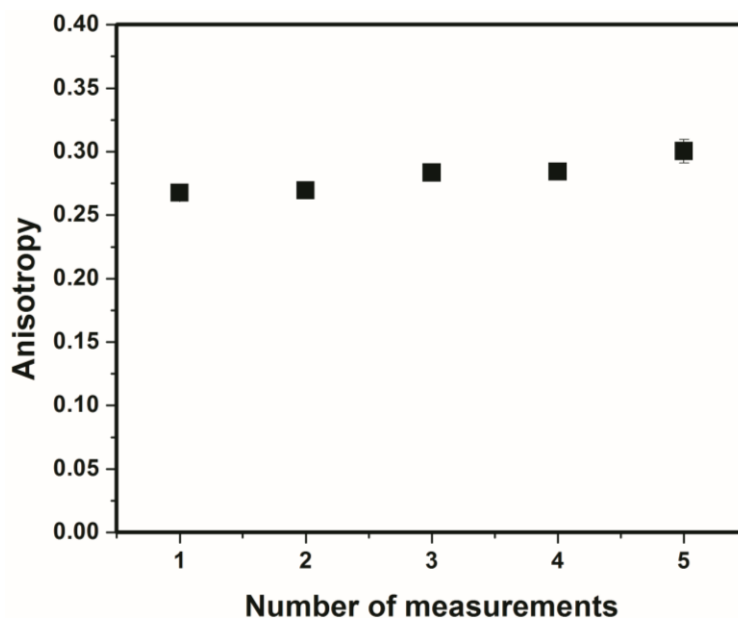
Figure. 2.7. The steady anisotropy of the iCy3 only DS DNA. Five independent measurement were carried out. The value of the average steady state anisotropy was calculated to be 0.28 ± 0.01.

2.3.7. Time resolved fluorescence anisotropy. Time resolved anisotropy gives a direct way to observe the rotational motion of the fluorophores during the lifetime of fluorescence. For a fast rotating molecule, the fluorescence anisotropy decay decreases to zero much faster than the lifetime of the fluorescence. Such a decay is represented in Figure 1.8. where the dye Cy3b has a rotational correlation time of 380 ps (blue decay), much less than its lifetime of 2.4 ns.[19, 38] A fluorophore, when attached to a biomolecule, can have restricted rotational mobility compared to the free dye and therefore the fluorophore, under restricted rotation, may not be able to occupy all the rotational orientations possible during the lifetime of fluorescence. Under these circumstances, the emitted light is not completely depolarized and the anisotropy decay becomes slower or comparable to the intensity decay. Figure 2.8 shows the anisotropy decay of Cy3 attached to a 60 base pair DS DNA (sample 4) in red. It is clear that the anisotropy does not go to zero during the fluorescence lifetime. The iCy3 modification in the DS DNA (sample 5) shows even less rotational depolarization (black decay) in the 5 ns window in Figure 2.8. In these cases, the fluorophores do not occupy all the possible orientations during the relevant timescales of energy transfer. Thus, the isotropic situation of FRET, where κ^2 can be assumed to be 2/3, does not arise and the use of $\kappa^2 = 2/3$ during the translation of the FRET efficiency to the distance measurement can give rise to erroneous results.
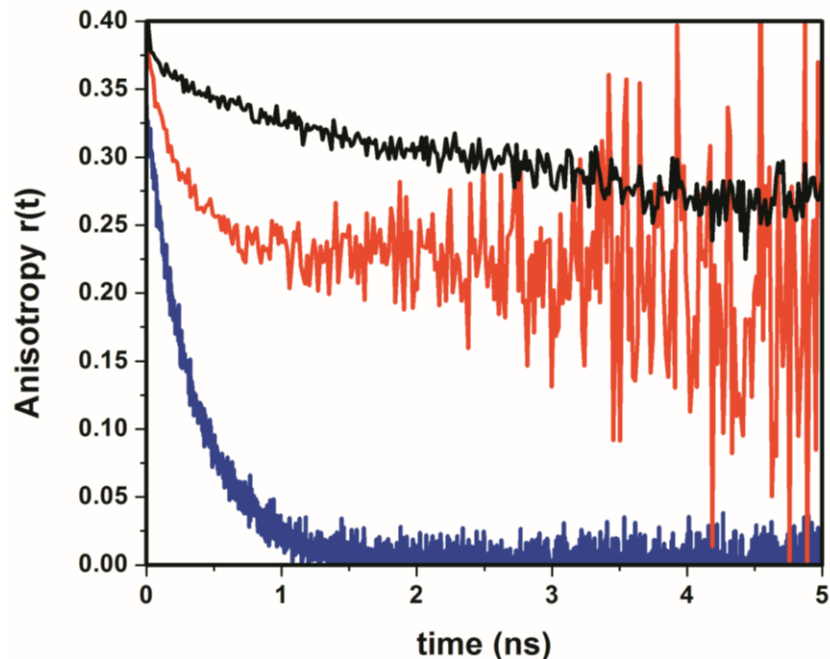
Figure 2.8. Time resolved fluorescence anisotropy decay of Cy3B (blue), internal Cy3 bound to a 60 base pair DS DNA by a six carbon linker (sample 4, red), and the iCy3 DS DNA (sample 5, black) in buffer. The rotation of the free dye is much faster, resulting in a fast anisotropy decay. In contrast, the iCy3 and internal Cy3 modifications show restricted rotation.

The iCy3 and internally modified Cy3 anisotropy decays were fitted with a bi-exponential function. The fits and the residuals are plotted in Figure 2.8. Figure 2.9 clearly illustrates that internal Cy3 bound to the double stranded DNA does not rotate freely during the lifetime of fluorescence. Only 34% of the decay is represented by the fast motion ($\tau_R = 0.21 \pm 0.08$ ns). The other 66% decay has a long rotational correlation time of 23 ± 6 ns. The local motion of the iCy3 sample (Figure 2.9) is far more suppressed (15% with $\tau_R = 0.8 \pm 0.6$ ns) and the rest of the decay has a 26 ± 4 ns rotational correlation time. In both of these cases, the long correlation time is representative of the tumbling motion of the DNA, and the short correlation times are

77

representative of depolarization due to the motions of the dye made possible due to attachment of the linkers. The absence of a prevalent local motion in the backbone modified DNA sample shows that the fluorophore does not rotate during the lifetime of fluorescence and the relative orientation of the donor and acceptor transition dipole moments does not change in the relevant timescale of FRET.
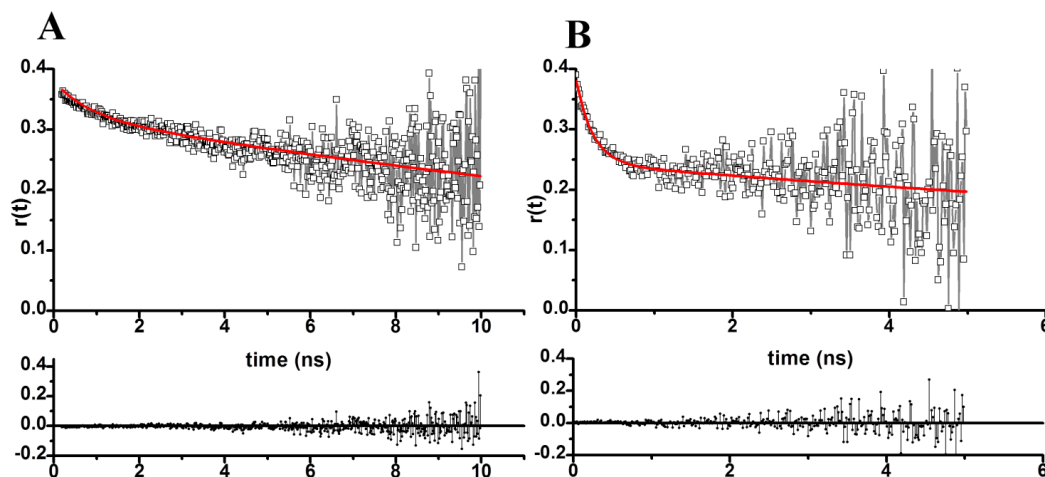
Figure 2.9. The anisotropy decays (grey squares), the fits to bi-exponential model (red line) and the randomness of residuals (black squares) of the backbone modified sample 5 (panel A) and the internal Cy3 bound by a six carbon linker to the DS DNA in sample 4 (panel B). The fluorophore in sample 4 obviously shows more local motion compared to sample 5.

2.3.8. Single molecule FRET. The single molecule FRET histogram of sample 1, presented in Figure 2.10., shows only one peak at a low FRET value. The absence of a peak at a high FRET efficiency proves that sample 1 is homogeneous and there is no secondary structure present. The width of the histogram in the smFRET measurements does not indicate presence of more than one FRET efficiency. The origin of the broadening lies in the shot noise resulting because of the low counts measured in these

experiments and other experimental artifacts arising out of various photophysical

processes of the donor and the acceptor.[39]
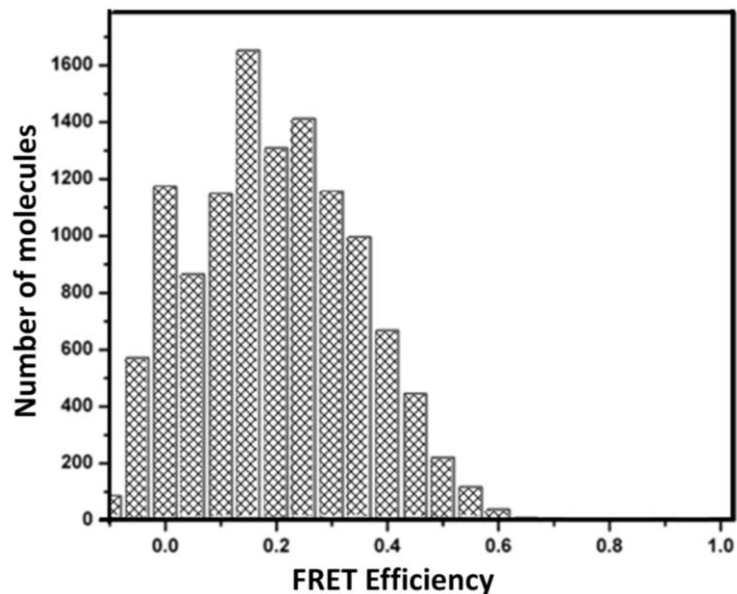
Figure 2.10. Single molecule FRET histogram of sample 1. The absence of a peak at
high FRET demonstrates the homogeneity of the sample 1.

2.3.9. Temperature dependent FRET and the quantum yield. The

homogeneity of sample 1 was also tested using a different experiment. The melting

temperature of any secondary structures of the single stranded version of sample 1

predicted by "mfold" server[40] was much lower compared to the melting temperature of

the double stranded structure. If the FRET efficiency is measured as a function of

increasing temperature and if the sample contained only the double stranded DNA, then

the changes in FRET efficiency will only be due to the decrease in the quantum yield of

the donor with the increasing temperature. On the contrary, if the sample had some

secondary structure of the single stranded version of DNA, then the change in FRET

efficiency of the sample will be very abrupt on heating, due to the secondary structure being denatured. FRET efficiency of sample 1 was measured as a function of temperature from 23˚C to 63˚C. The FRET decreased from 0.16 at 23 ˚C to 0.10 at 63˚C. This change in the FRET efficiency can be quantitatively accounted for by the change in the quantum yield in these two temperatures ($\phi_D^{23˚C}/\phi_D^{63˚C} = 2.4$). Thus, from the temperature dependent FRET experiment it can be concluded that there is no presence of secondary structure in sample 1,as was also shown in the single molecule FRET experiments. The changes in excitation spectra of sample 1 as a function of temperature are shown in the Figure 2.13 (top panel). The inset of the top panel shows the extent of decrease in donor excitation which is transferred to the acceptor with increasing temperature. The temperatures measured include 23˚C (black), 33˚C (red), 43˚C (blue), 53˚C (cyan) and 63˚C (purple). The bottom panel represents the change in the quantum yield of the iCy3 only double stranded DNA (sample 5) as a function of temperature.
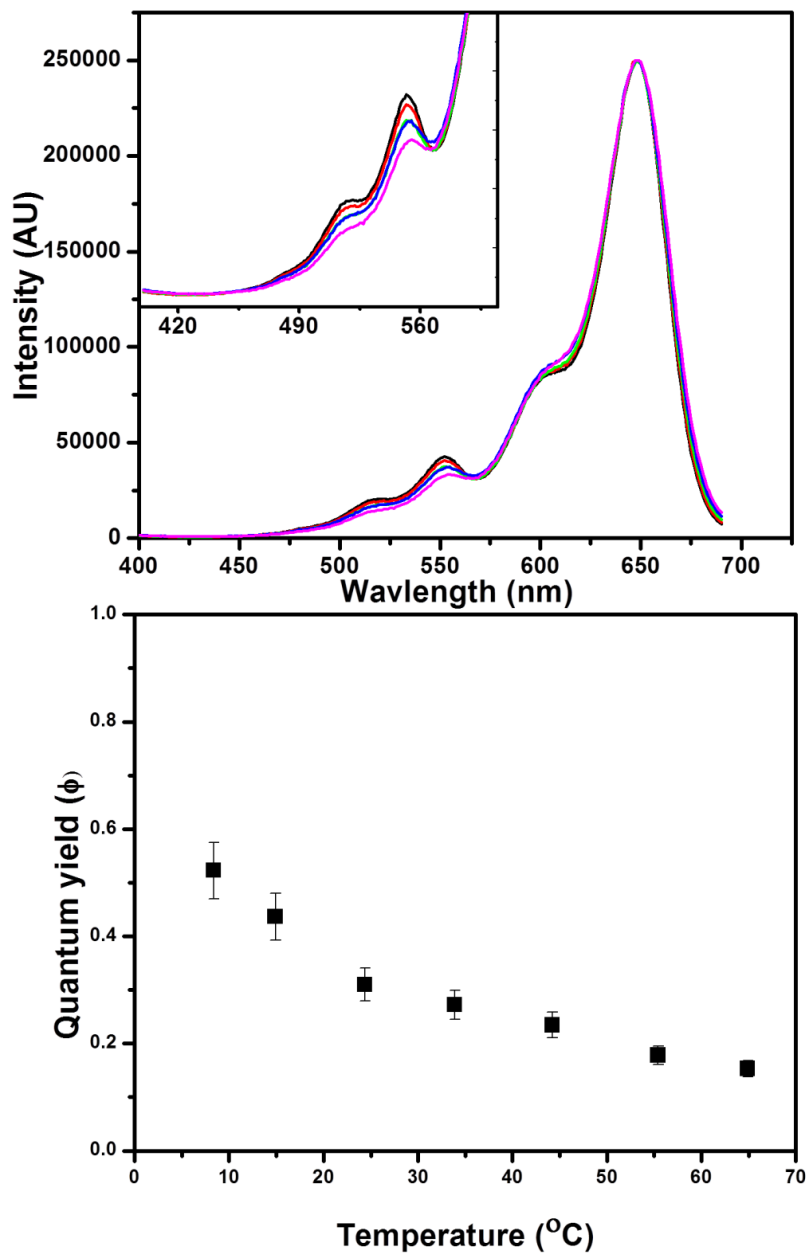
Figure 2.11. The FRET efficiency of sample 1 (top panel) and the quantum yield of sample 5 (bottom panel) as a function of temperature. The different colors represent the excitation spectra measured at 23˚C (black), 33˚C (red), 43˚C (blue), 53˚C (cyan) and 63˚C (purple). The changes in FRET of sample 1 can be quantitatively explained by the changes in quantum yield of the donor iCy3.

2.3.10. Measurement of melting temperature. To measure the effect of the

backbone modification on the stability of the DNA, the melting temperature of the

following three samples were measured: sample 2 (which has both iCy3 and iCy5

modifications), sample 5 (which has just the iCy3 modification), and sample 6 (which has

the same sequence but no modification). The absorbances as a function of temperature

(filled triangles) and the derivatives of the absorbances (solid lines) of sample 2 (red),

sample 5 (black) and sample 6 (blue) are plotted in Figure 2.12. The melting temperature

of sample 6 was 88.07 ˚C. The incorporation of one backbone modification (iCy3)

decreases the melting temperature to 87.02 ˚C. The incorporation of both the donor and

the acceptor modifications decreases the melting temperature to 85.02 ˚C. These minor

decreases in the melting temperature of the DNA suggest that the incorporation of the

backbone modification do not decrease the stability of the DNA significantly.[41]
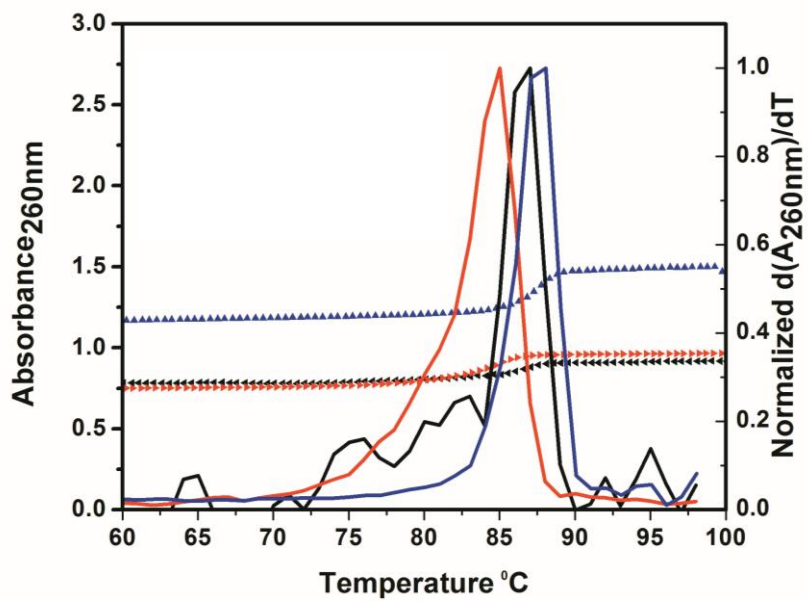
Figure 2.12. The plot of the absorbances (solid triangles) and the derivatives of the absorbances (solid lines) as a function of temperature for sample 2 (red), sample 5 (black) and sample 6 (blue). The melting temperature (the maxima of the derivative plot) decreases as the number of modifications increases.

2.4. Discussion

Among the various uncertainties associated with the translation of measured FRET efficiency to calculated distance, the orientation factor is probably the most discussed one.[2, 42-44] The uncertainties associated with the orientation factor have led to the widespread use of long flexible linkers as the means of attaching fluorescent dyes to DNA. It was assumed that the presence of these long linkers would enable the fluorophores to maximize their rotational mobility and decrease the interaction with the DNA. The time resolved fluorescence anisotropy decays of internally labeled Cy3 (sample 4) in Figures 2.8 and 2.9 suggest that the mobility of the dye is essentially restricted during the lifetime of both fluorescence and energy transfer. The longer rotational correlation time (23 ± 6 ns) is consistent with the tumbling motion of the DNA. This value is similar to the value reported for the DNA tumbling motion by Ramereddy et.al, measured using 2 aminopurine,[45] and the value predicted by hydropro.[46] This long correlation time contributes 64% towards the fluorescent anisotropy decay of sample 4, where a long linker attaches the dye to the DNA. This high contribution of the tumbling motions towards the anisotropy decay suggests that a population of the dye is strongly interacting with the DNA double helix, and that flexible linkers are not capable of providing the fluorophores with the rotational mobility required to assume the isotropic situation of $\kappa^2 = 2/3$. These long linkers also create uncertainty in the distance between the donor and the acceptor, as the position of the dyes during the energy transfer is seldom known.

In contrast, the backbone modification is mostly rigid during the relevant timescales of the energy transfer. This can be easily seen from Figure 2.8 and Figure 2.9. The absence of local motion, depicted in Figure 2.9, means that the relative orientation of both the donor and the acceptor transition dipole moments does not change during the relevant timescales of the energy transfer. Thus, the κ^2 remains constant during FRET. The rigidity of the dyes also decreases the non-radiative de-excitation pathways competing with fluorescence. These non radiative processes include excited state photoisomerization, a very potent de-excitation pathway for Cy3.[19, 33] This results in the increased quantum yield of the backbone modified Cy3 ($\phi_D = 0.31$) compared to the Cy3 bound to the DNA by a flexible linker.[19]

The orientation of the donor and the acceptor in the backbone modified DNA is controlled by the architecture and structure of the B-DNA. Three different backbone modified FRET DNA samples were prepared to illustrate this point. Sample 1 contains both the donor iCy3 and the acceptor iCy5 in the same strand and was prepared by annealing the complementary non-labeled strand F with the ligated product of strand A and strand B. Sample 2 and sample 3 were prepared by annealing strand D and strand C, respectively, with strand E. In sample 1, there are 29 base pairs in between the donor and the acceptor and the dyes are present in the same strand. In sample 2 and sample 3 the dye pairs are present on opposite strands and there are 26 and 23 base pairs, respectively, in between the dye pairs. The lowest electronic transition dipole moment of the carbocyanine dyes reside along the principal axis of the molecule. Thus, when the dyes are on the same strand and separated by multiple of 10 base pairs (the helical turn of the B-DNA) they are supposed to be collinear. In sample 1, the dyes are in the same strand

and are separated by 3 turns (102 Å) and have a FRET efficiency of 16% corresponding

to a very high κ^2 value of 3.2. This is very close to the theoretical maximum of $\kappa^2 = 4$,

when the donor and the acceptor transition dipole moments are collinear to each other.

In sample 2, the distance between the donor and the acceptor decreases from the

102 Å in sample 1 to 90 Å. In contrast, the FRET efficiency actually decreases from 16%

in sample 1 to 15% in sample 2, in spite of the smaller distance in sample 2. The absence

of collinear orientation between the donor and the acceptor transition dipole moments in

sample 2 overcomes the effect of decreasing the distance between the dye pairs. Sample 3

has a distance of 83 Å between the donor and the acceptor molecules. The two

fluorophores, being 23 base pair apart and in complementary strands, are 2 and 1/2 turns

apart and should be in collinear arrangement. This is reflected in an increased FRET

efficiency to 40% and a value of $\kappa^2 = 3.5$. The commonly used R_0 value of 53 Å for the

Cy3-Cy5 FRET pair[3] results in a distance of 56 Å for 40% FRET, which is almost one

complete turn shorter than the distances measured here. The measurements of these high

FRET efficiencies at these long distances are due to the near collinear arrangement of the

donor and the acceptor transition dipole moments and are reflective of the fact that the

backbone modified dyes follow the geometry of the DNA.

This idea of using the rigid fluorophores has also been exploited by Lewis et al.,[47]

Iqbal et al.,[8, 20] Ouellet et al.,[21] and Urnavicius et al.[22] In these cases the dyes are stacked

at the end of the DNA. The κ^2 can vary from 0 (perpendicular alignment of the two

transition dipole moments) to 1 (parallel alignment) as the fluorophores are stacked on

the end of the double stranded DNA. The value of $\kappa^2 = 4$ (collinear alignment of the two

transition dipole moments) cannot be achieved using this geometry. Lewis et. al.[47] used stilbene dicarboxamide, covalently bound to both of the DNA strands, as a rigid donor fluorophore. However, stilbene dicarboxamide absorbs in UV and hence is not very conductive for biophysical work. Most of the difficulties for the fluoroscence measurement in biological systems arise due to Raman scattering and sample autofluorescence, so fluorophores that absorb in visible wavelength are required. Iqbal et al.[8, 20] Ouellet et al.[21] and Urnavicius et al.[22] used Cy3 and Cy5 dyes attached to the 5'end of the double stranded DNA for this reason. NMR studies have shown that these dyes, when bound to the 5'end of double stranded DNA stack on top of the terminal base pairs. The stacking behavior is independent of the length of the linker and is present when the length of the linker is increased from three carbons to thirteen carbons.[8, 20-22, 48] These stacking interactions are what introduce rigidity of the dyes to the double stranded DNA. In these cases, a modulation of FRET efficiency with the length of the DNA as the κ^2 varies from 0 to 1 is observed. The orientation of the stacked fluorophores relative to the terminal base pairs is dependent on the length of the linker. Hence, the modulation of the FRET efficiency with distances can vary with different linker lengths.[20, 21] However, this modulation is less pronounced than that predicted by the theoretical calculations considering the presence of only stacked conformation. This is consistent with the fact that 5'Cy3 and 5'Cy5 dyes are not completely rigid.[19] There is a fraction of population of these dyes which are not interacting and have more rotational freedom. The presence of this population of the fluorophores results in a less pronounced modulation of FRET with distances. The measurable distance using the 5'Cy3 and 5'Cy5 are rather short, as the

maximum value of κ^2 is 1 and not 4. The positions of the Cy3 (top) and Cy5 (bottom) when attached to the 5' ends of the double stranded DNA are represented in Figure 2.13.
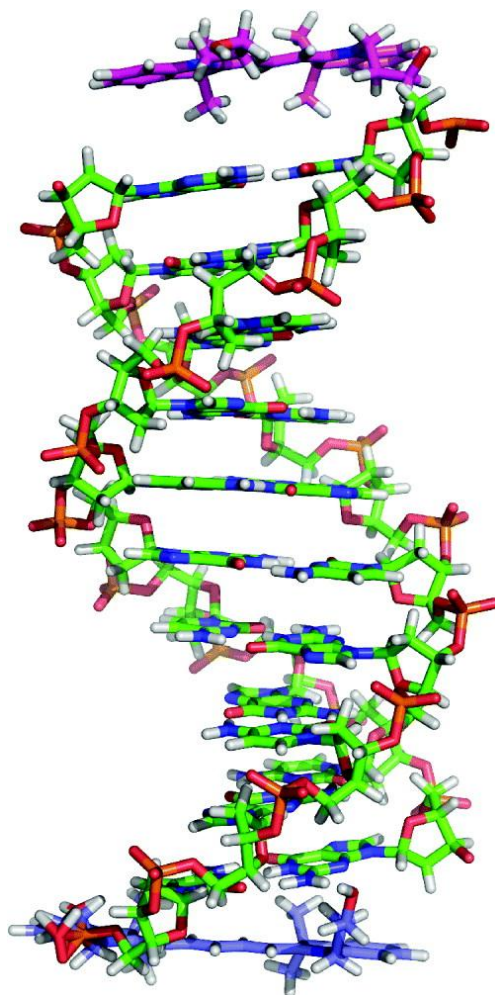
Figure 2.13. The molecular graphics model of Cy3 (top) and Cy5 (bottom) connected to5' end of a DNA double helix. The model represents the NMR data and shows the interaction of the dyes with the DNA. This figure was reproduced from reference 49.[49]

The backbone modifications used in the experiments described in this chapter are readily available commercially from the Integrated DNA Technologies (Coralville, IA) and are incorporated in the desired position of the DNA during the solid state synthesis of

the DNA. The solid state synthesis has a very high degree of incorporation and this decreases the amount of donor or acceptor only samples during the measurement of FRET. The absence of incorporation of the dye in the DNA results in the subsequent DNA strands that are smaller than the original and which can be easily separated by the various separation techniques, including HPLC and gel electrophoresis. In contrast, the fluorescent labeled amino modified DNA sample is of the same length as the unlabeled DNA and hence, more difficult to separate.

To conclude, an unusually high FRET efficiency was observed for sample 1 at a distance of more than 100 Å. The donor iCy3 and the acceptor iCy5 dyes in sample 1 are three DNA turns apart, yet still have a FRET efficiency of 16%. The almost collinear alignment of the donor and the acceptor transition dipole moments are responsible for this unusual high FRET efficiency. A decrease of 12 Å in the distance does not increase the FRET efficiency, as the orientation of the donor and the acceptor transition dipole moment changes to an unfavorable position compared to the original almost collinear position in sample 1. This shows the importance of the orientation dependence of FRET. Further decrease in the donor-acceptor distance, to 83 Å, results in an increase of FRET efficiency to 40%, corresponding to a value of $\kappa^2 = 3.5$ and almost collinear alignment of the donor and acceptor transition dipole moments. This rigidity also affects the photophysical properties of the dyes influencing the FRET measurements. The backbone modifications can be advantageous over other modifications as the contribution from the environmental factors are less and the variation of donor-acceptor distances due to the length of the linkers can be avoided.

2.5 References

1.   Koopmans, W. J. A.; Buning, R.; Schmidt, T.; van Noort, J., spFRET Using Alternating Excitation and FCS Reveals Progressive DNA Unwrapping in Nucleosomes. *Biophys J* **2009,** 97, (1), 195-204.

2.   Ha, T., Single-molecule fluorescence resonance energy transfer. *Methods* **2001,** 25, (1), 78-86.

3.   Ishii, Y.; Yoshida, T.; Funatsu, T.; Wazawa, T.; Yanagida, T., Fluorescence resonance energy transfer between single fluorophores attached to a coiled-coil protein in aqueous solution. *Chem. Phys.* **1999,** 247, (1), 163-173.

4.   Parkhurst, K. M.; Parkhurst, L. J., Fret Studies of Oligo-DNA Interactions. *Biophys J* **1994,** 66, (2), A154-A154.

5.   Rothenberg, E.; Ha, T., Single-molecule FRET analysis of helicase functions. *Methods Mol Biol* **2010,** 587, 29-43.

6.   Stryer, L.; Haugland, R. P., Energy Transfer - a Spectroscopic Ruler. *Proc. Natl. Acad. Sci. U. S. A.* **1967,** 58, (2), 719-&.

7.   Vogelsang, J.; Doose, S.; Sauer, M.; Tinnefeld, P., Single-molecule fluorescence resonance energy transfer in nanopipets: Improving distance resolution and concentration range. *Anal Chem* **2007,** 79, (19), 7367-7375.

8.   Iqbal, A.; Arslan, S.; Okumus, B.; Wilson, T. J.; Giraud, G.; Norman, D. G.; Ha, T.; Lilley, D. M. J., Orientation dependence in fluorescent energy transfer between Cy3 and Cy5 terminally attached to double-stranded nuclelic acids. *Proc. Natl. Acad. Sci. U. S. A.* **2008,** 105, (32), 11176-11181.

9.   Choi, U. B.; Strop, P.; Vrljic, M.; Chu, S.; Brunger, A. T.; Weninger, K. R., Single-molecule FRET-derived model of the synaptotagmin 1-SNARE fusion complex. *Nat Struct Mol Biol* **2010,** 17, (3), 318-U84.

10.   Meller, A.; Di Fiori, N., The Effect of Dye-Dye Interactions on the Spatial Resolution of Single-Molecule FRET Measurements in Nucleic Acids. *Biophys J* **2010,** 98, (10), 2265-2272.

11.   Rasnik, I.; Myong, S.; Cheng, W.; Lohman, T. M.; Ha, T., DNA-binding orientation and domain conformation of the E-coli Rep helicase monomer bound to a partial duplex junction: Single-molecule studies of fluorescently labeled enzymes. *J Mol Biol* **2004,** 336, (2), 395-408.

12.   Chakraborty, M.; Kuriata, A. M.; Henderson, J. N.; Salvucci, M. E.; Wachter, R. M.; Levitus, M., Protein Oligomerization Monitored by Fluorescence Fluctuation Spectroscopy: Self-Assembly of Rubisco Activase. *Biophys J* **2012,** 103, (5), 949-958.

13.   Bates, M.; Blosser, T. R.; Zhuang, X. W., Short-range spectroscopic ruler based on a single-molecule optical switch. *Phys Rev Lett* **2005,** 94, (10), -.

14.   Heilemann, M.; Margeat, E.; Kasper, R.; Sauer, M.; Tinnefeld, P., Carbocyanine dyes as efficient reversible single-molecule optical switch. *J Am Chem Soc* **2005,** 127, (11), 3801-3806.

15.   Huang, B.; Jones, S. A.; Brandenburg, B.; Zhuang, X. W., Whole-cell 3D STORM reveals interactions between cellular structures with nanometer-scale resolution. *Nat. Methods* **2008,** 5, (12), 1047-1052.

16.   Huang, B.; Wang, W. Q.; Bates, M.; Zhuang, X. W., Three-dimensional super-resolution imaging by stochastic optical reconstruction microscopy. *Science* **2008,** 319, (5864), 810-813.

17.   Rust, M. J.; Bates, M.; Zhuang, X. W., Sub-diffraction-limit imaging by stochastic optical reconstruction microscopy (STORM). *Nat. Methods* **2006,** 3, (10), 793-795.

18.   Sabanayagam, C. R.; Eid, J. S.; Meller, A., Using fluorescence resonance energy transfer to measure distances along individual DNA molecules: Corrections due to nonideal transfer. *J. Chem. Phys.* **2005,** 122, (6), -.

19.   Sanborn, M. E.; Connolly, B. K.; Gurunathan, K.; Levitus, M., Fluorescence properties and photophysics of the sulfoindocyanine Cy3 linked covalently to DNA. *J. Phys. Chem. B* **2007,** 111, (37), 11064-11074.

20.   Iqbal, A.; Wang, L.; Thompson, K. C.; Lilley, D. M. J.; Norman, D. G., The structure of cyanine 5 terminally attached to double-stranded DNA: Implications for FRET studies. *Biochemistry* **2008,** 47, (30), 7857-7862.

21.   Ouellet, J.; Schorr, S.; Iqbal, A.; Wilson, T. J.; Lilley, D. M. J., Orientation of Cyanine Fluorophores Terminally Attached to DNA via Long, Flexible Tethers. *Biophys J* **2011,** 101, (5), 1148-1154.

22.   Urnavicius, L.; McPhee, S. A.; Lilley, D. M. J.; Norman, D. G., The Structure of Sulfoindocarbocyanine 3 Terminally Attached to dsDNA via a Long, Flexible Tether. *Biophys J* **2012,** 102, (3), 561-568.

23.   Dolghih, E.; Roitberg, A. E.; Krause, J. L., Fluorescence resonance energy transfer in dye-labeled DNA. *J Photoch Photobio A* **2007,** 190, (2-3), 321-327.

24.   Unruh, J. R.; Gokulrangan, G.; Wilson, G. S.; Johnson, C. K., Fluorescence properties of fluorescein, tetramethylrhodamine and Texas Red linked to a DNA aptamer. *Photochem Photobiol* **2005,** 81, (3), 682-690.

25.   Vamosi, G.; Gohlke, C.; Clegg, R. M., Fluorescence characteristics of 5-carboxytetramethylrhodamine linked covalently to the 5' end of oligonucleotides: Multiple conformers of single-stranded and double-stranded dye-DNA complexes. *Biophys J* **1996,** 71, (2), 972-994.

26.   Harvey, B. J.; Levitus, M., Nucleobase-Specific Enhancement of Cy3 Fluorescence. *J Fluoresc* **2009,** 19, (3), 443-448.

27.   Heinlein, T.; Knemeyer, J. P.; Piestert, O.; Sauer, M., Photoinduced electron transfer between fluorescent dyes and guanosine residues in DNA-hairpins. *J. Phys. Chem. B* **2003,** 107, (31), 7957-7964.

28.   Seidel, C. A. M.; Schulz, A.; Sauer, M. H. M., Nucleobase-specific quenching of fluorescent dyes .1. Nucleobase one-electron redox potentials and their correlation with static and dynamic quenching efficiencies. *J Phys Chem-Us* **1996,** 100, (13), 5541-5553.

29.   Buschmann, V.; Weston, K. D.; Sauer, M., Spectroscopic study and evaluation of red-absorbing fluorescent dyes. *Bioconjugate Chem* **2003,** 14, (1), 195-204.

30.   Gruber, H. J.; Hahn, C. D.; Kada, G.; Riener, C. K.; Harms, G. S.; Ahrer, W.; Dax, T. G.; Knaus, H. G., Anomalous fluorescence enhancement of Cy3 and Cy3.5 versus anomalous fluorescence loss of Cy5 and Cy7 upon covalent linking to IgG and noncovalent binding to avidin. *Bioconjugate Chem* **2000,** 11, (5), 696-704.

31.   Schobel, U.; Egelhaaf, H. J.; Brecht, A.; Oelkrug, D.; Gauglitz, G., New-donor-acceptor pair for fluorescent immunoassays by energy transfer. *Bioconjugate Chem* **1999,** 10, (6), 1107-1114.

32.   Magde, D.; Brannon, J. H.; Cremers, T. L.; Olmsted, J., Absolute Luminescence Yield of Cresyl Violet - Standard for the Red. *J Phys Chem-Us* **1979,** 83, (6), 696-699.

33.   Aramendia, P. F.; Negri, R. M.; Sanroman, E., Temperature-Dependence of Fluorescence and Photoisomerization in Symmetrical Carbocyanines - Influence of Medium Viscosity and Molecular-Structure. *J Phys Chem-Us* **1994,** 98, (12), 3165-3173.

34.   Valeur, B., *Molecular Fluorescence: Principles and Applications*. Wiley-VCH: Weinheim, Germany, 2001.

35.   Lakowicz, J. R., *Principles of fluorescence spectroscopy*. Springer: 2006; Vol. 1.

36.   Froimowitz, M., HyperChem: a software package for computational chemistry and molecular modeling. *BioTechniques* **1993,** 14, (6), 1010-1013.

37.   Pettersen, E. F.; Goddard, T. D.; Huang, C. C.; Couch, G. S.; Greenblatt, D. M.; Meng, E. C.; Ferrin, T. E., UCSF chimera - A visualization system for exploratory research and analysis. *J Comput Chem* **2004,** 25, (13), 1605-1612.

38.   Ranjit, S.; Levitus, M., Probing the Interaction Between Fluorophores and DNA Nucleotides by Fluorescence Correlation Spectroscopy and Fluorescence Quenching. *Photochem Photobiol* **2012,** 88, (4), 782-791.

39.   Felekyan, S.; Kalinin, S.; Valeri, A.; Seidel, C. A. M., Filtered FCS and Species Cross Correlation Function. *Proc. of SPIE- Int. Soc. Opt. Eng* **2009,** 7183, 71830D

40.   Zuker, M., Mfold web server for nucleic acid folding and hybridization prediction. *Nucleic Acids Res.* **2003,** 31, (13), 3406-3415.

41.   Aboulela, F.; Koh, D.; Tinoco, I.; Martin, F. H., Base-Base Mismatches - Thermodynamics of Double Helix Formation for Dca3Xa3G + Dct3Yt3G (X, Y = a,C,G,T). *Nucleic Acids Research* **1985,** 13, (13), 4811-4824.

42.   Deniz, A. A.; Dahan, M.; Grunwell, J. R.; Ha, T. J.; Faulhaber, A. E.; Chemla, D. S.; Weiss, S.; Schultz, P. G., Single-pair fluorescence resonance energy transfer on freely diffusing molecules: Observation of Forster distance dependence and subpopulations. *Proc. Natl. Acad. Sci. U. S. A.* **1999,** 96, (7), 3670-3675.

43.   Deniz, A. A.; Laurence, T. A.; Dahan, M.; Chemla, D. S.; Schultz, P. G.; Weiss, S., Ratiometric single-molecule studies of freely diffusing biomolecules. *Annu Rev Phys Chem* **2001,** 52, 233-253.

44.   Parkhurst, L. J.; Parkhurst, K. M.; Powell, R.; Wu, J.; Williams, S., Time-resolved fluorescence resonance energy transfer studies of DNA bending in double-stranded oligonucleotides and in DNA-protein complexes. *Biopolymers* **2001,** 61, (3), 180-200.

45.   Ramreddy, T.; Rao, B. J.; Krishnamoorthy, G., Site-specific dynamics of strands in ss- and dsDNA as revealed by time-domain fluorescence of 2-aminopurine. *J. Phys. Chem. B* **2007,** 111, (20), 5757-5766.

46.   Ortega, A.; Amoros, D.; de la Torre, J. G., Prediction of Hydrodynamic and Other Solution Properties of Rigid Proteins from Atomic- and Residue-Level Models. *Biophys J* **2011,** 101, (4), 892-898.

47.   Lewis, F. D.; Zhang, L. G.; Zuo, X. B., Orientation control of fluorescence resonance energy transfer using DNA as a helical scaffold. *J Am Chem Soc* **2005,** 127, (28), 10002-10003.

48.   Weston, K. D.; Carson, P. J.; DeAro, J. A.; Buratto, S. K., Single-molecule detection fluorescence of surface-bound species in vacuum. *Chem Phys Lett* **1999,** 308, (1-2), 58-64.

49.   Levitus, M.; Ranjit, S., Cyanine dyes in biophysical research: the photophysics of polymethine fluorescent dyes in biomolecular environments. *Q Rev Biophys* **2011,** 44, (1), 123-151.

Chapter 3

Probing the interaction between fluorophores and DNA nucleotides by fluorescence correlation spectroscopy and fluorescence quenching

3.1 Introduction

The interactions between the three fluorescent dyes TAMRA, Cy3B and Alexa 546 and the deoxynucleotide monophosphates (dNMPs) are investigated in this chapter. Fluorescence correlation spectroscopy (FCS), a technique capable of distinguishing the change in the diffusion coefficient of a fluorophore, is employed to study these interactions. The changes in the apparent diffusion constants and a shift of the autocorrelation decay to slower timescales of TAMRA and Cy3B in the presence of dNMPs provide evidence of an interaction between these molecules. These interactions are absent for Alexa 546, a structurally similar dye to that of TAMRA. None of these dyes show any significant quenching in presence of dAMP, dCMP and dTMP, and only TAMRA shows significant quenching in presence of dGMP. These results suggest that the presence of bulky Cl and charged SO_3^- groups prohibit Alexa 546 to interact with dNMPs. This chapter illustrates an alternate method to study dye-biomolecule interactions by using FCS in absence of significant quenching. These interactions are very important as they can perturb the photophysical and rotational properties of the fluorophores and influence the efficiency of FRET as well as have the potential to alter and affect the structure of DNA.

Fluorescence has been widely used as a tool to distinguish structural[1-3] and functional[4-6] properties of various biological systems. Compared to other probe

properties, e.g. absorbance or radioactivity, fluorescence offers much improved sensitivity.[7] This extraordinary sensitivity of fluorescence has led to the widespread use of the technique as one of the primary detection methods for molecules in low abundance in the cell,[8] and with single molecule resolution.[9] Continuous evolution in the field of optical detection, along with the increasing number of synthetic dyes with high photostability, quantum yield and sensitivity to the environment, have led to the evolution of single molecule fluorescence spectroscopy[10, 11] and super resolution imaging.[1, 2, 12, 13] Despite the extensive use of fluorescence in illuminating biological systems, obtaining quantitative information from this method is still complicated and requires quite a few assumptions. There are various instances where when a biological molecule is tagged with a fluorophore, the photophysical properties of the tag fluorophore change. These changes include: changes in the extinction coefficient,[14, 15] changes in the quantum yields[5, 16, 17] or lifetimes,[16, 17] shifts in absorption and fluorescence spectra,[18, 19] or changes in the rotational flexibility of the fluorophore.[20-23] These changes can have very important effects on various types of measurements and if not corrected for, can result in erroneous interpretation of the obtained data.

One of the most common techniques used in the field of the biological fluorescence is Förster resonance energy transfer (FRET).[24, 25] In FRET, the energy from the donor molecule is non-radiatively transferred to the acceptor molecule and the donor fluorescence is quenched, as described in the first chapter. The rate or efficiency of the energy transfer is dependent on the distance between the donor and the acceptor molecules. Thus, by measuring the efficiency of energy transfer, the distance between the two probes can be calculated.[25] This is the reason FRET has been termed as a

'spectroscopic ruler'.[26] The detailed description of this process along with the drawbacks are described in section 1.3.1. As mentioned in the section 1.3.1, one of the major drawbacks of FRET as a distance measurement tool is the uncertainty regarding the orientation factor (κ^2). When attached to a biomolecule, fluorophores can interact with the biomolecule, and these interactions can lead to lower rotational mobility of the fluorophore,[22, 27, 28] as well as, changes in the photophysical properties, e.g. quantum yield.[5, 16, 17] These interactions can prevent the dyes from sampling all the possible orientations during the lifetime of fluorescence and consequently, the assumption of κ^2 =2/3 breaks down. This has been observed for the cyanine dye-pair Cy3 and Cy5 attached to the 5' end of double stranded DNA strands.[27, 29, 30] The most common technique used to reveal interactions between fluorophores and the biomolecules is the quenching of fluorescence.[31-35] Fluorescence intensity of many organic dyes, like rhodamines, oxazines and coumarines decreases when they are interacting with biomolecules. A most prominent example of this is the interaction of organic dyes with guanine or deoxyguanosine monophosphates (dGMP), one of the four constituent bases of DNA or RNA. Among the four nucleotides, dGMP, having the lowest oxidation potential, is the most potent candidate for quenching fluorescence by photoinduced electron transfer (PET).[32, 34, 36, 37] Other dNMPs,[34] as well as amino acids with aromatic side chains, e.g. tryptophan and tyrosine,[38, 39] are also known to be potent quenchers of fluorescence. The different types of quenching and the calculation of the equilibrium constants from these quenching phenomena are described in section 1.3.2.

However, if the interaction between the dye and the biological molecule results in little or no change in the photophysical properties of the fluorophore, then the evidence of

the association equilibrium is much harder to identify and quantify. A different way of identifying these interactions is to find a method which can look at the properties that reflect these interactions independent of changes in photophysical properties. Such a process, which should be dependent on the presence of interaction, is diffusion. In absence of interaction, the diffusing moiety is just the individual fluorophore. When the fluorophores are bound to biomolecules, the diffusing moiety is the complex of fluorophore with the biomolecule. A small molecule diffuses faster than a large molecule, and hence has a larger diffusion constant. Thus, a process which looks at the diffusion properties of the molecule can distinguish between the presence and absence of an association equilibrium. FCS is such a process that can distinguish between slow and fast diffusion of a fluorescent moiety. The detailed description of the theory, instrumentation and analysis of FCS are presented in section 1.3.4. The end result of this analysis is the calculation of the diffusion constant of the fluorescent species, which contains information about the interactions.

A similar technique that can also be employed to identify the interaction between the fluorophore and the biomolecules in the absence of photophysical changes is fluorescence anisotropy. Time resolved fluorescence anisotropy is a measure of the rotational flexibility of the fluorescent species during the lifetime of fluorescence.[24, 25] Fast rotation of the molecule, during the lifetime of fluorescence, results in emission from all possible orientations, and creates a very fast anisotropy decay due to the depolarization of the light. In contrast, restricted rotation of the molecule, during the lifetime of fluorescence, creates a slow anisotropy decay. A fluorophore interacting with a biomolecule is a much larger moiety compared to just the dye. Hence, the decay of the

time resolved fluorescence anisotropy is faster for the free dye than a fluorophore-biomolecule complex.[40] This process is discussed in detail in section 1.3.3.3.

In this chapter, the association equilibrium between three dyes: Cy3B, Alexa 546 and TAMRA, and DNA deoxynucleotide monophosphates (depicted in Figure 3.1) have been investigated by means of FCS and other photophysical methods. TAMRA and Alexa 546 are members of the rhodamine family, and Cy3B belongs to cyanine family. Cy3B is structurally very similar to the commercially available and widely used Cy3 dye. The only difference is the structural rigidity of Cy3B that arrests the cis-trans isomerization of Cy3 in the excited state. This results in a much higher quantum yield of Cy3B compared to Cy3, as the cis-trans isomerization in the excited state is a very potent de-excitation pathway.[17] FCS provides evidence of complex formation between the dyes and dNMPS, where traditional photophysical methods do not provide evidence of any substantial association equilibria.
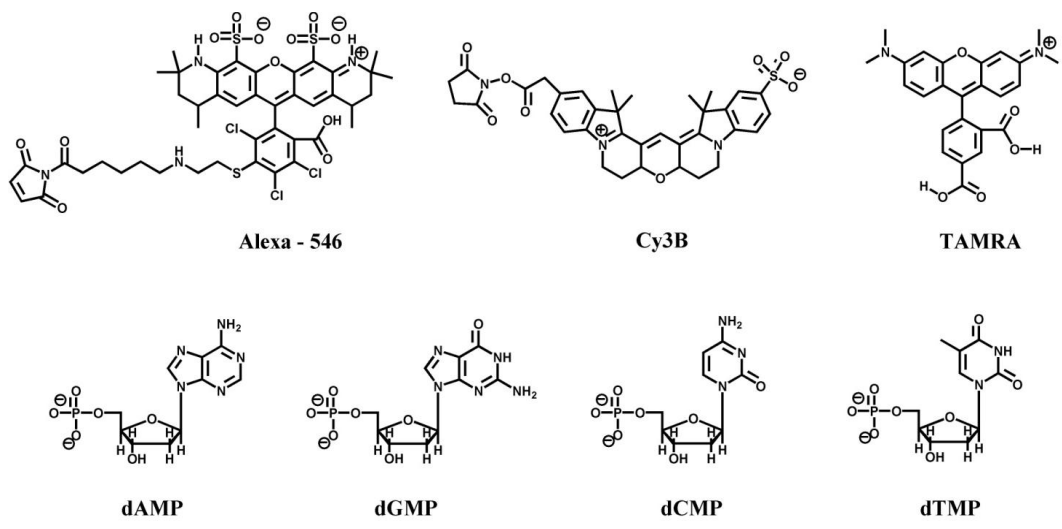
Figure 3.1. Structures of the dyes and dNMP samples under study. The structures of the three dyes are given in the top row and the deoxynucleotide monophosphates are shown in the bottom row. The first two dNMPs: dAMP and dGMP are purines and the next two: dCMP and dTMPs are pyrimidines.

3.2. Materials and methods

3.2.1. Materials. Alexa-546 maleimide and TAMRA were obtained from Molecular Probes (Eugene, OR), and Cy3B NHS ester was purchased from GE-Healthcare (Piscataway, NJ). The four dNMPs, 2′-deoxyadenosine 5′-monophosphate (dAMP), 2′-deoxycytidine 5′-monophosphate sodium salt (dCMP), 2′-deoxyguanosine 5′-monophosphate sodium salt hydrate (dGMP) and thymidine 5′-monophosphate disodium salt hydrate (dTMP), were purchased from Sigma-Aldrich (St. Louis, MO). Stock solutions of Cy3B, Alexa-546 and TAMRA were prepared in water and then diluted to desired concentration in TRIS buffer just before the experiments. The lifetime of the hydrolysis reaction of NHS esters at pH 7 is about 2 h, and therefore it is expected that the NHS ester of Cy3B hydrolyzed completely before the addition of the TRIS buffer.[41] In contrary, maleimides with similar hydrocarbon linker lengths as that of Alexa-546 are known to be stable over days in aqueous solution.[42] The short lifetimes of the hydrolysis reaction suggest that the dyes were in their hydrolyzed form during the various experiments described in this chapter.

3.2.2.Methods

3.3.2.1. Absorbance. The absorbance measurements were carried out using the exact same procedure described in section 2.2.2. The concentration of the dNMP solutions were measured using the following extinction coefficients at 260 nm: dGMP ($13700 \ M^{-1}cm^{-1}$), dCMP ($9300 \ M^{-1}cm^{-1}$), dTMP ($10200 \ M^{-1}cm^{-1}$), and dAMP($15300 \ M^{-1}cm^{-1}$).[43] Absorption comparison studies were carried out with the maximum absorbance of the main band in the range of 0.4 to 0.5. The extinction coefficient at the maxima for

TAMRA, Alexa 546 and Cy3B were 91000 $M^{-1}cm^{-1}$, 104000 $M^{-1}cm^{-1}$ and 130000 $M^{-1}cm^{-1}$, respectively.

3.2.2.2. Fluorescence. The fluorescence spectra were recorded in a PTI quantamaster-4/2005SE spectrofluorometer. The excitation wavelengths for the emission spectra were kept at 515 nm, 520 nm and 525 nm for Cy3B, TAMRA and Alexa 546, respectively. Quenching experiments were carried out by addition of increasing amount of concentrated dNMP solutions to 1 μM solution of the corresponding dye. The emission spectra were corrected for dilution and Stern-Volmer plots were constructed from the ratio of the maximum intensity of the emission spectra in absence and presence of the dNMPs, respectively.

3.2.2.3. Time resolved fluorescence. Time resolved fluorescence intensity decays were collected using a time correlated single photon counting (TCSPC) instrument. Intensity decays for the calculation of the lifetime were obtained by exciting the samples with a super continuum Fianium laser (Southampton, UK). Anisotropy decays were obtained using the Ti-Sapphire excitation. The detailed description of the experimental and analysis procedure is described in section 1.3.3. Time resolved anisotropy decays of Cy3B were obtained in presence of dNMP and in iso-viscous solutions.

3.2.2.4. Fluorescence Correlation Spectroscopy. Fluorescence correlation decays were collected in an epifluorescence microscope assembled in house, as depicted in Figure 1.13. The analysis of the autocorrelation decays results in the calculation of the apparent diffusion coefficients and is described in detail in section 1.3.4.

3.2.2.5. Viscosity. Viscosity of all the samples were measured using a calibrated Ostwald's viscometer (Cannon Instruments, PA) kept in a water bath at room temperature (25^oC). The time of elution between two marked positions on the viscometer was measured five times for each sample, with the average value being used for the calculation of the viscosity coefficient. The viscosity coefficient of the dyes of the solution was measured using the following equation,

Viscosity (in cP) = time of elution (s) × density of the solution × viscometer constant

The viscometer constant was supplied by the manufacturer (0.003576) and density of the solution was measured by measuring the weight of a known volume of solution. Iso-viscous solutions, having the same viscosity of that of the dNMP solutions, were produced by mixing varying amount of glycerol and water by trial and error methods, verifying the viscosity by the method outlined above.

3.2.2.6. Index of refraction. The index of refraction (η) of the prepared solutions were measured using a refractometer from Bausch and Lomb Optical Co.(Rochester, NY). The iso-refractive index solutions were prepared by mixing ethanol ($\eta = 1.36$) and water ($\eta = 1.33$) by trial and error method until they matched the refractive indices of the dNMP solutions.

3.2.2.7. Electrochemistry. Cyclic voltammograms were obtained from the CV measurements carried out with a Cypress CS-1090 electroanalytical instrument (Cypress systems Inc., Kansas City, Mo). A three electrode system, consisting of a platinum auxiliary electrode, an Ag/AgCl reference electrode and a screen printed carbon electrode (Zensor R&D Co. Ltd., Taichung County, Taiwan) was used for these measurements.

103

The screen printed electrode was used as it required much smaller amount of sample compared to that of a regular three electrode system. The ground state reduction potentials of the fluorophores were calculated from the first reduction peak of the voltammograms (Figure 3.11) after taking the derivative of the reduction peak of the scan.

3.3 Results

3.3.1. Quenching studies. Time resolved and steady state fluorescence intensity measurements were carried out to study the quenching of the three fluorophores: TAMRA, Alexa 546, and Cy3B, in the presence of the four DNA nucleotide monophosphates (dNMPs). Among the three dyes and four mononucleotides under study, only TAMRA in presence of dGMP showed strong quenching, as predicted by the redox potential of the TAMRA-dGMP complex. The detailed description and the calculation of different Stern-Volmer and bimolecular association and quenching constants are described in detail in section 1.3.2.

The plot of F_0/F of TAMRA against the quencher (dGMP) concentration resulted in a K_s value of $61M^{-1}$, which was very close to the value reported for TMR ($51M^{-1}$),[33] a structurally similar dye. The other three dNMPs: dAMP, dCMP, and dTMP, did not show any substantial quenching for TAMRA, and the K_s values were in the range of $0-0.7M^{-1}$. In complete contrast with the quenching of TAMRA, Alexa 546, another rhodamine derivative, did not show any substantial quenching in the presence of any of the mononucleotides. The K_s value obtained for the Alexa 546-dGMP combination was only $4.2M^{-1}$, which is approximately an order of magnitude lower than the value obtained for TAMRA. The other three oligonucleotides showed negligible quenching of Alexa 546, with K_s values in the range of $0.8{\sim}1.3M^{-1}$, almost equal within the experimental errors. Stern-Volmer plots of Cy3B showed a K_s value of $2.3M^{-1}$ for dGMP, and less than $1.5M^{-1}$ for the other three nucleotides, representing negligible quenching by all the dNMPs. These results are represented in Figure 3.2 below.
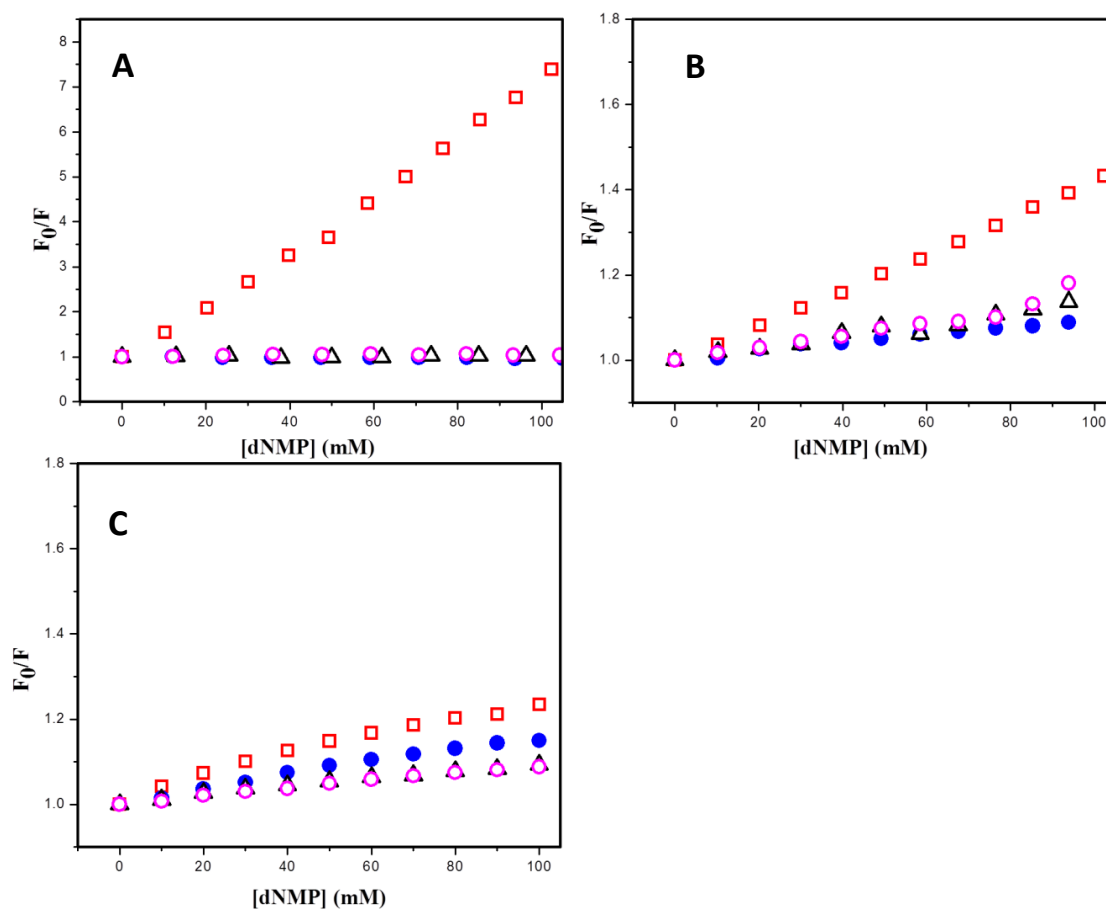
Figure 3.2. Stern-Volmer plots of (A) TAMRA, (B) Alexa 546 and (C) Cy3B with increasing concentrations of dNMPs. The ratio of the fluorescence intensity in the absence (F_0) and presence (F) of nucleotides is plotted as a function of increasing concentration of dGMP (red squares), dAMP (blue filled circles), dCMP (black empty triangles) and dTMP (open purple squares)

To distinguish between the dynamic and static quenching, time resolved intensity decays were also obtained for the three dyes in presence and absence of dGMP. The intensity decays of the fluorophores, in absence and presence of dNMPs, were fitted with a either a mono-exponential or a bi-exponential decay, after iterative deconvolution with

106

the instrument response factor. The equation used to fit the bi-exponential decay is given

by:

$$F(t) = F(0) \left[A_1\, Exp\left(-\frac{t}{\tau_1}\right) + (1 - A_1)\, Exp\left(-\frac{t}{\tau_2}\right) \right]$$ (3.1)

Where, $F(t)$ is the fluorescent intensity decay, and τ_1, τ_2 are the two lifetimes,

respectively. The parameters of the fits obtained are given in table 3.1.

Similar to the results obtained by Heinlein et. al.,[33] only the longer of the two

lifetimes for both TAMRA-dGMP and Alexa 546-dGMP pairs, were dependent on the

quencher concentration. The faster of the two lifetimes is indicative of the lifetime of the

ground state complex and is very small as this moiety is almost non-fluorescent. The

longer lifetime, which is dependent on quencher concentration, is indicative of dynamic

quenching. Therefore, just the longer lifetimes were used to calculate the dynamic

quenching in the Stern-Volmer plots.[33] The dynamic Stern-Volmer quenching constant,

K_q, were then calculated from the slope of τ_0/τ plotted against the quencher

concentration, as shown in the inset of the Figure 3.3.The plot of the time-resolved

intensity decays of the three dyes in buffer, 100mM and 250mM dGMP in Figure 3.3

shows that the dynamic quenching is much more prominent for TAMRA compared to

Alexa-546. Cy3B, on the other hand, does not show any evidence of dynamic quenching.

TAMRA in presence of dGMP had a K_q value of 2.3M^{-1}, an order of magnitude lower

that the K_s value obtained from steady state experiments. The large difference between

the K_s and the K_q value indicates that the main mechanism of quenching of TAMRA by

dGMP is by ground state complex formation. The bimolecular dynamic quenching

constant, k_q, for the TAMRA-dGMP pair was calculated to be 1.2×10^9 M^{-1} s^{-1}, and is comparable to 1.8×10^9 M^{-1} s^{-1} calculated for TMR.[33] The use of the average lifetime instead of the longer quencher dependent lifetime resulted in a higher value for K_q. This value of K_q is still much smaller than the K_s obtained for the same dye-dNMP combination. The K_q for Alexa 546 and dGMP was 1.1M^{-1}, resulting in a k_q of 3.2×10^8 M^{-1}s^{-1}. Cy3B, on the contrary, did not show any change in lifetime in the presence of dNMPS.
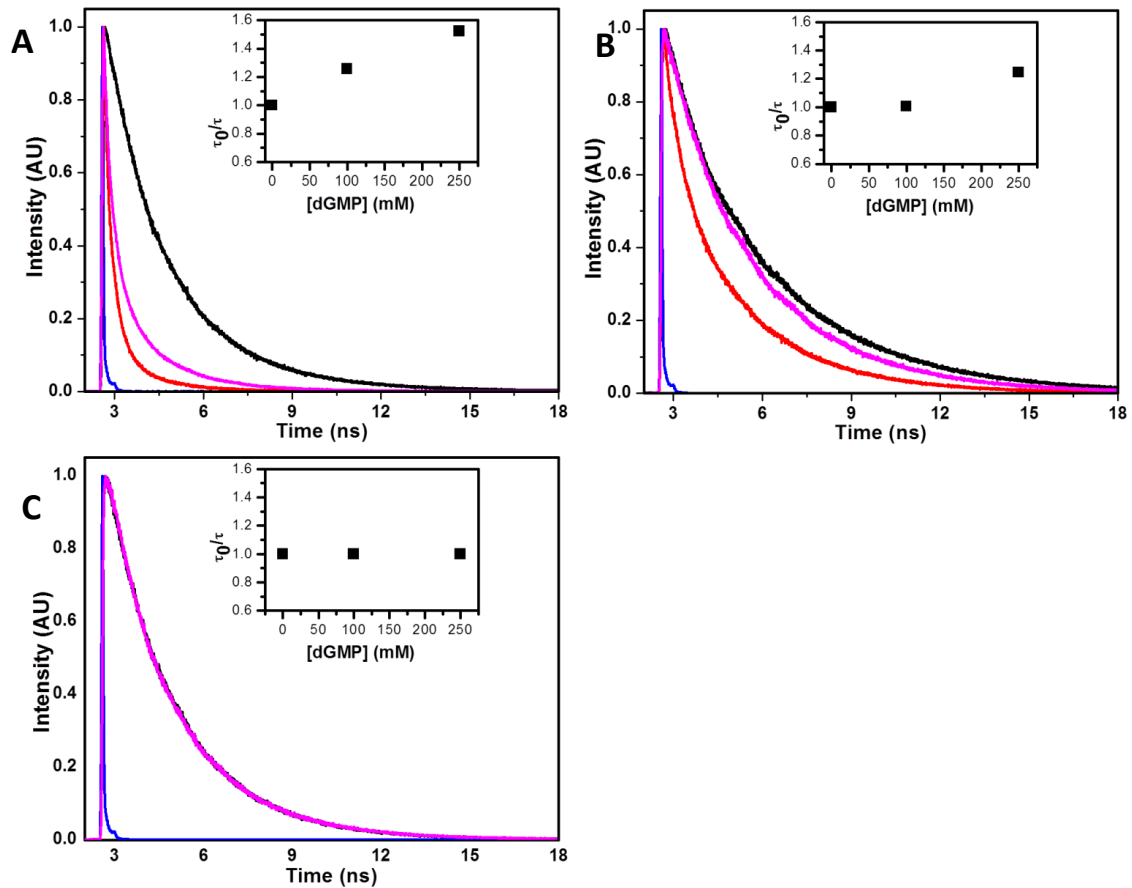
Figure 3.3. Time resolved fluorescence intensity decays of (A) TAMRA, (B) Alexa 546 and (C) Cy3B in presence of increasing dGMP concentration. Black – free dye, Purple – dye in 100mM dGMP solution, Red – dye in 250 mM dGMP solution, Blue – Instrument response function. *Insets*: Dynamic Stern–Volmer plot using the quencher-dependent lifetime of the dye as a function of increasing concentrations of dGMP. The results show that although the lifetime of Cy3B is independent of dGMP, the lifetime of TAMRA and Alexa 546 are dependent on the concentration of dGMP.

Sample	A_1	τ_1(ns)	τ_2 (ns)
Cy3B	1	2.48	
Cy3B + 100 mM dGMP	1	2.51	
Cy3B + 250 mM dGMP	1	2.43	
TAMRA	1	2.15	
TAMRA + 100 mM dGMP	0.33	1.66	0.34
TAMRA + 250 mM dGMP	0.16	1.27	0.29
Alexa 546	1	3.46	
Alexa 546 + 100 mM dGMP	1	2.95	
Alexa 546 + 250 mM dGMP	0.63	2.72	0.57

Table 3.1. Fluorescence lifetimes as a function of dGMP concentration.

3.3.2. Spectral Properties. Bathochromic shift in the absorption spectra of the

fluorophores in presence of the biomolecules has often been used as an indication of the

ground state complex formation between the fluorophore and the biomolecule.[32, 33, 44-48]

Fluorophores, for example rhodamines (Rh6G, TMR), oxazines (JA242, MR121), and

rosamine (JA51-DS), show a red shift in the absorbance maxima in the presence of

dNMPs. Cy3B showed a similar trend in the absorption spectra in presence of high

concentration of dNMPs. In presence of 250 mM dGMP, Cy3B showed a 3 nm red shift

at the maxima of the absorption spectra. This could be indicative of a ground state complex formation between Cy3B and dGMP. A second factor that can also be responsible for a bathochromic shift in the absorption spectra is the change of refractive index of the solution.[49, 50] To determine if the changes in the refractive index at least are partially responsible for the red shift, the refractive indices of the buffer and 250 mM dNMP solutions were measured. The buffer showed a refractive index of 1.334 and the 250 mM dNMP solutions showed refractive indices in the range of 1.351~1.354. An ethanol/water solution having the refractive index of 1.354 was prepared and the absorption spectrum of Cy3B was measured in this iso-refractive index solution. An overlap of the absorption spectra of Cy3B in buffer, 250mM dGMP, and the iso-refractive index solution is presented in Figure 3.4 and it shows that the bathochromic shift for the 250mM dGMP is identical to the bathochromic shift for the ethanol-water mixture. This indicates that, at least for Cy3B, the bathochromic shift obtained in the absorption spectra, can be explained by the change in the refractive index of the medium, and thus, there is no need to consider ground state complex formation is occurring between Cy3B and dGMP. The emission spectrum of Cy3B is also independent of the excitation wavelength in the excitation range of 500-600nm, and the excitation spectrum is independent of the emission wavelength. If there is an equilibrium between Cy3B and the dNMPs present, then, by choosing different wavelengths of excitation or emission, a certain population can be selectively probed. Absence of this population selectivity does not necessarily exclude the possibility of the complex formation. It only confers that, even if there is an equilibrium in existence between Cy3B and dNMPs, the equilibrium does not affect the absorption spectra. Rhodamines have a much more complicated

relationship with the solvent, involving hydrogen-bonding and solvation of the side groups,[51, 52] and hence an analogous comparisons of absorption spectra of TAMRA and Alexa-546 were not done.
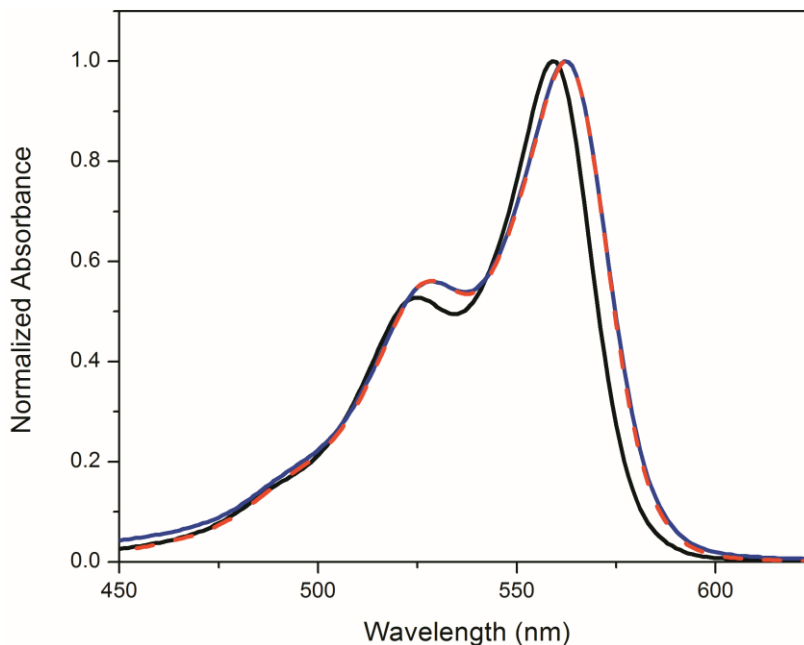
Figure 3.4. Absorbance of Cy3B in buffer (black), 250 mM dGMP (blue) and iso-refractive index ethanol-water (red dashed). The overlap of the absorption spectra in dGMP and iso-refractive index solution shows that, at least for Cy3B, the bathochromic shift can be explained by the change in the refractive index of the solution.

The interaction between the fluorophore and the dNMPs can also manifest its presence by causing a change in the fluorophore's extinction coefficient.[14, 34, 45] In Figure 3.5, the plot of the absorption of Cy3B in different concentrations of dNMPs shows that the absorbance of Cy3B is dependent on the concentration of dNMPs. This result shows that there is a small but measurable change in the extinction coefficient of Cy3B in the presence of dNMPs. The small amount of quenching observed for Cy3B in dNMP

solutions can thus at least be partly described by the changes in the extinction coefficient. Albeit the small amount of quenching of Cy3B in the presence of dGMP and dAMP cannot be ruled out, the changes in the extinction coefficients and the shifts in the absorption spectra, can at least partly be responsible for the apparent quenching of Cy3B fluorescence.
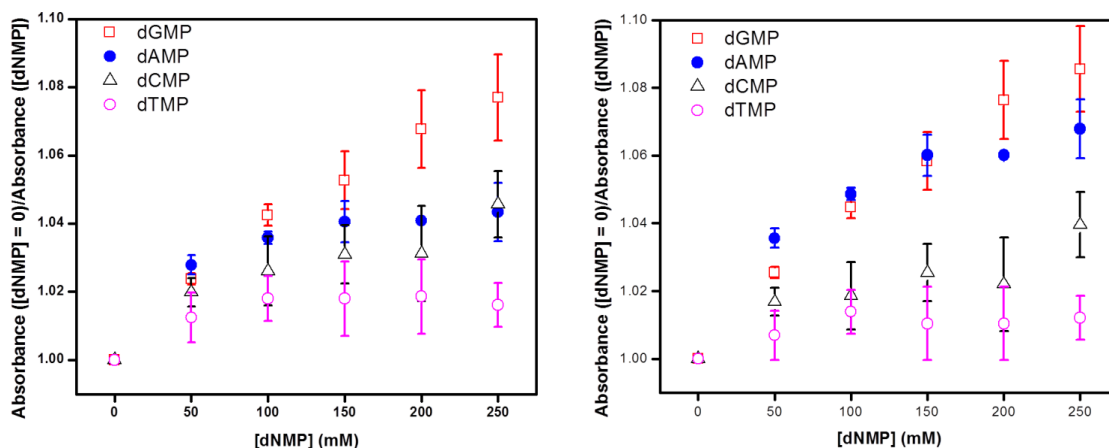
Figure 3.5. Plot of the ratio of absorbances against increasing concentrations of dNMPs at 525 nm (left panel) and at the maxima of the absorption spectra for Cy3B (right panel). The ratio of absorbances was calculated in the Stern-Volmer fashion by dividing the absorbance of Cy3B in buffer with the absorbance in the presence of dNMPs. These ratios are plotted in a Stern-Volmer fashion against increasing dNMP concentrations of dGMP (red square), dAMP (blue circle), dCMP(black triangle), dTMP (magenta open circles).

3.3.3. Fluorescence correlation spectroscopy. The complex formation equilibrium between the fluorophores and the dNMP solutions were further studied by FCS. The detailed description and analysis of the FCS is described in section 1.3.4. According to equation 1.23, the diffusion constant of a fluorophore can be calculated if the value of r and z are known. To estimate the value of r and z, the autocorrelation decay

113

of TAMRA in water was fitted and the optical parameters were determined. The diffusion constant of TAMRA used for this fitting was 420 μm^2/s.[53-56] All the other autocorrelation decays, including the decays for the three dyes in buffer, dNMP solutions, and the iso-viscous solutions, were fitted with the single diffusion constant model, using the optical parameters obtained in the fit for TAMRA. A single diffusion constant model was sufficient for the fits so a multiple diffusive species model was not used. In presence of a complex equilibrium between the fluorophore and the dNMPs, multiple species, e.g. free dye and complexes of the dye and dNMP at different proportions, can be present. Hence, the diffusion constant obtained from the single diffusing species fit of the autocorrelation decays of the dyes in presence of dNMPs are termed as apparent diffusion constants and denoted by D_{app}s.

The diffusion constant of Cy3B and Alexa 546 was measured to be 440 μm^2/s and 326 μm^2/s, respectively. The much smaller value for Alexa 546 is consistent with the bigger size of the molecule and very close to the measurement reported by Petraseck and Schwille et. al.[56] In the presence of dNMP solutions, the diffusion of the fluorophores becomes slower, the autocorrelation decays shift to longer timescales, and therefore result in smaller diffusion coefficients. The autocorrelation of Cy3B in buffer and in the 250mM dNMP solutions are represented in Figure 3.6. It is evident that in presence of the mononucleotides the decays shift to longer timescales than when in buffer (orange decay in Figure 3.6). Consequently, the diffusion constants measured in dNMPs are smaller than that measured in buffer, as shown in table 3.2.
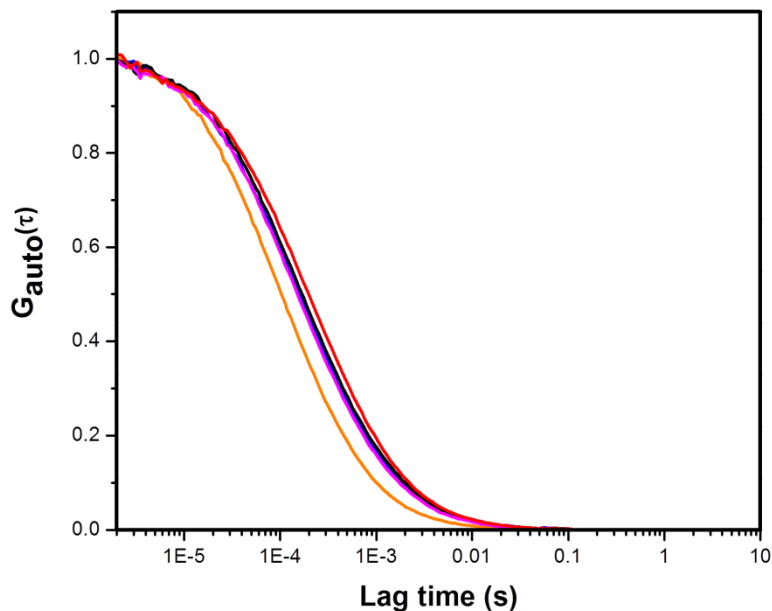
Figure 3.6. Autocorrelation decays of Cy3B in buffer (orange) and in the presence of 250 mM dAMP(blue), dCMP(black), dTMP(purple), and dGMP(red). The shift in the autocorrelation decays to a longer time is indicative of complex formation and a longer diffusion time of the Cy3B-dNMP complexes.

The origin of the slower diffusion in dNMP solutions can be of twofolds. One of the reasons can be the complex formation between the dNMPs and the dyes. These dye-dNMP complexes are much larger compared to the free dye, and hence have smaller diffusion constants. The other reason can be the increased viscosity of the solvents at high dNMP concentration. To determine the extent of the individual contributions from these two sources in slowing down the diffusion, the viscosity of the dNMP solutions was measured. The dNMP solutions are indeed more viscous than the buffer. However, the changes in viscosity are not enough to explain the extent of the decrease in diffusion constant of TAMRA and Cy3B in presence of dNMPs. To isolate the contribution towards the decrease in diffusion constant from the two different sources: viscosity and

complex formation, iso-viscous solutions having the same viscosities as that of the different dNMP solutions were prepared and the autocorrelation of the free dyes were obtained in these iso-viscous solutions. The overlap of the normalized auto correlation curves for free Cy3B in buffer (black), dNMP solutions (blue/orange) and the iso-viscous solutions (red) were plotted together in Figure 3.7. It is evident from the plots that although the iso-viscous solutions slow down the diffusion of the dyes, viscosity alone cannot be solely responsible for the extent of the slow movements.
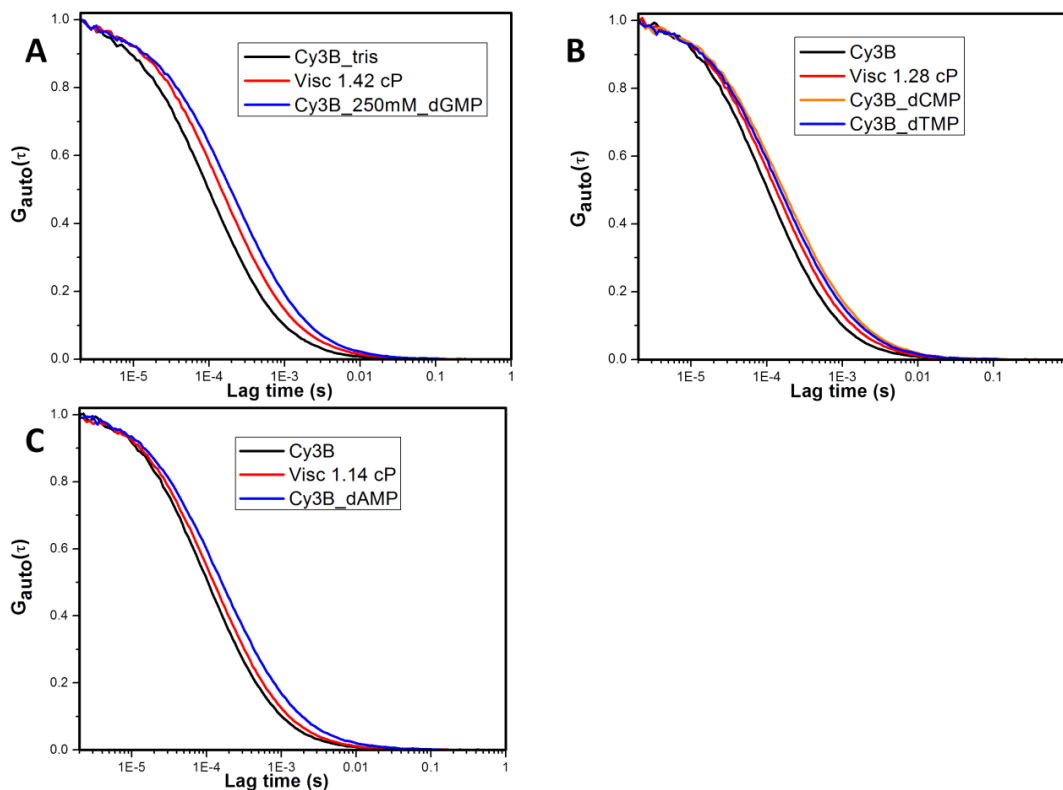
Figure 3.7. Overlap of the autocorrelation decays of Cy3B in buffer (black), 250 mM dNMP solutions (blue, orange) and the corresponding iso-viscous solution (red). The dNMP solutions are (A) dGMP, (B) dCMP and dTMP, and (C) dAMP. The overlap of the autocorrelation function shows that the change in the viscosity of the solution cannot be solely responsible in the observed decrease in diffusion constant of Cy3B in presence of dNMPs.

The overlapped autocorrelation decays of the three dyes in presence of 250mM dAMP (blue), in buffer (black), and in the iso-viscous solutions (red) are represented in Figure 3.8. The diffusion constants were calculated by fitting each autocorrelation decay individually. The ratio of the diffusion coefficients were calculated by dividing the apparent diffusion constant of the dye at a certain dNMP concentration (D_{app}) by the diffusion coefficient of the dye in the iso-viscous solution (D_η). A decrease in the ratio of diffusion coefficients indicates that the extent of decrease in diffusion coefficient is more in dNMP solutions than the iso-viscous solution. The insets in Figure 3.8 show the ratio of diffusion coefficients against increasing concentration of dAMP. The apparent diffusion coefficients (D_{app}) obtained from the fits of the autocorrelation decays and the ratio of the diffusion coefficients are shown in table 3.2.
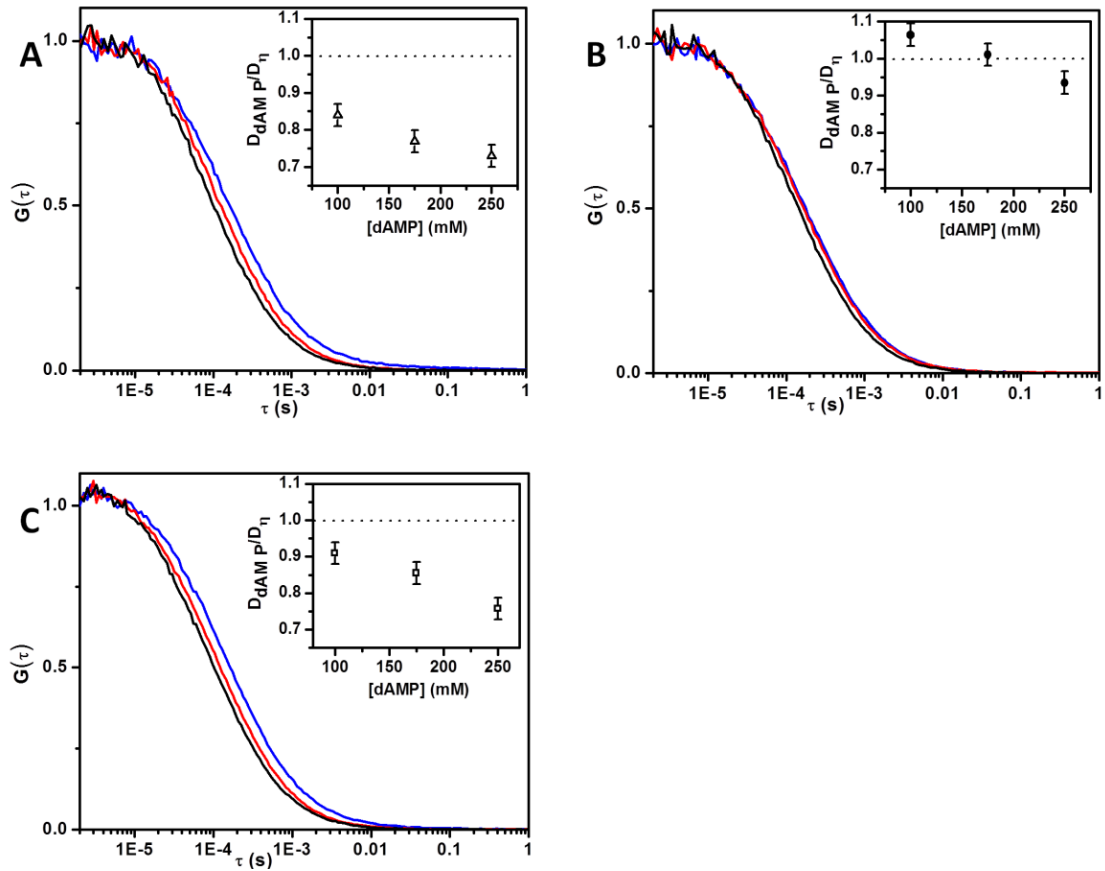
Figure 3.8. Autocorrelation decays of (A) Cy3B, (B) Alexa 546 and (C) TAMRA in buffer (black), 250 mM dAMP (blue), and iso-viscous solution of glycerol-water (red). *Insets*: Ratios of the apparent diffusion coefficients determined in dAMP (D_{dAMP}) and the diffusion coefficients determined in the control iso-viscous glycerol solutions ($D\eta$), as a function of increasing dAMP concentration.

	η (cp)	D_{app} (μm^2/s)	D_η (μm^2/s)	D_{app}/D_η	D_{app} (μm^2/s)	D_η (μm^2/s)	D_{app}/D_η	D_{app} (μm^2/s)	D_η (μm^2/s)	D_{app}/D_η
		Cy3B			**Alexa 546**			**TAMRA**		
buffer	0.98	440.0	440.0	1.00	325.3	325.3	1	420.0	420.0	1
0.10 M dAMP	1.06	333.5	369	0.90	304.5	284.5	1.07	290.7	345.0	0.84
0.175 M dAMP	1.12	300.2	353.2	0.85	269.7	267.0	1.01	254.1	330.3	0.77
0.25 M dAMP	1.14	266.0	353.2	0.75	250.8	267.0	0.94	241.4	330.3	0.73
0.25 M dGMP	1.42	218.7	305.3	0.72	235.0	238.1	0.99	--	260.5	--
0.25 M dTMP	1.28	281.4	335.0	0.84	249.6	260.0	0.96	225.4	289.0	0.78
0.25 M dCMP	1.28	290.4	335.0	0.87	236.6	260.0	0.91	222.5	289.0	0.77

Table 3.2. The apparent diffusion coefficients of the three dyes in dNMP and iso-viscous solutions. The ratio of the diffusion coefficients are calculated from D_{app} and D_{iso} using the following equation: $ratio = D_{app}/D_\eta$

It is evident from Figure 3.6, Figure 3.7, and Figure 3.8 that the extent of decrease of the diffusion constants for Cy3B and TAMRA in the presence of dNMPs cannot be fully explained by the changes in the viscosity, albeit the viscosity change definitely plays a certain role. The changes observed for Alexa 546, in contrast, can be explained solely by changes of the viscosity; no complex formation needs to be included. This is further supported by comparing the decrease in apparent diffusion constant of Alexa 546 in Figure 3.9. The smaller ratios of diffusion constant of TAMRA and Cy3B in dNMP

solutions compared to iso-viscous solutions suggest that there is definite complex formation between the dNMPs and these dyes. In contrast, Alexa 546 do not show any evidence of complex formation. For Cy3B, this interaction is much more evident for purine nucleotides than the pyrimidines. These results are similar to the results obtained by Harvey et al.,[44] where the authors saw stronger interaction between Cy3 and purines compared to Cy3 and pyrimidines.
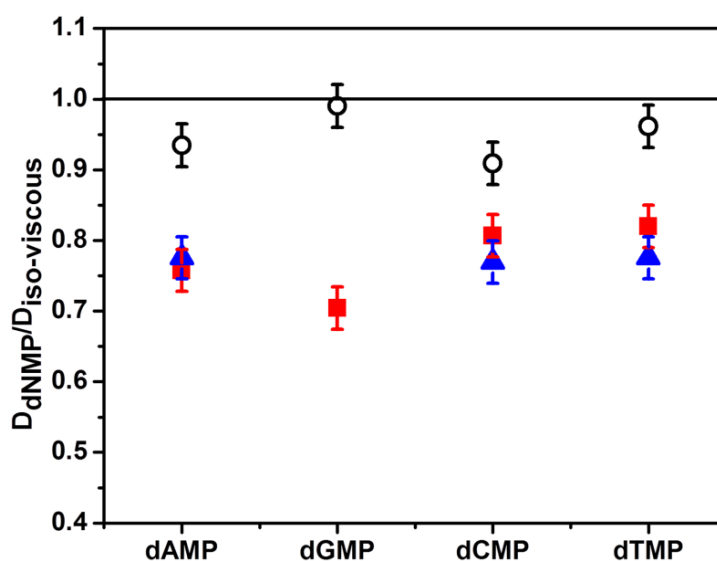
Figure 3.9. The ratio of the apparent diffusion constants in 250mM dNMPs and the corresponding iso-viscous solutions for Cy3B (red squares), TAMRA (Blue triangles) and Alexa 546 (Black circles). The ratio of 1 suggests the apparent slow diffusion in dNMP is a result of changes in viscosity only.

3.3.4. Time resolved fluorescence anisotropy. The dye-dNMP interactions were also studied by time resolved fluorescence anisotropy. The complexes between the fluorophores and the dNMPs are larger in size compared to the free fluorophores. The larger complexes thus take longer time to rotate, and hence have longer rotational correlation times compared to the free fluorophores.[24, 25] The effect of both viscosity and

complex formation on the anisotropy decay were distinguished from the time resolved anisotropy decays obtained for Cy3B in dNMP solution and iso-viscous solution. The overlap of the time resolved fluorescence anisotropy decays of Cy3B in dNMP solutions and corresponding iso-viscous solutions in Figure 3.10 show that viscosity changes of the solutions cannot solely be responsible for the observed change in rotational correlation time. The fluorescence anisotropy decays of Cy3B in dNMP solutions and the iso-viscous solutions can be fitted with a biexponential and monoexponential decays, respectively. The results of these fittings are shown in table 3.3. The smaller rotational correlation times of the biexponential fits for Cy3B in dNMP solutions are similar to that of the correlation times of the corresponding iso-viscous solutions. Considering that the shorter rotational correlation time belongs to the free dye, the longer correlation time might be indicative of a larger complex. These results corroborate the results obtained from the fluorescence correlation decays.
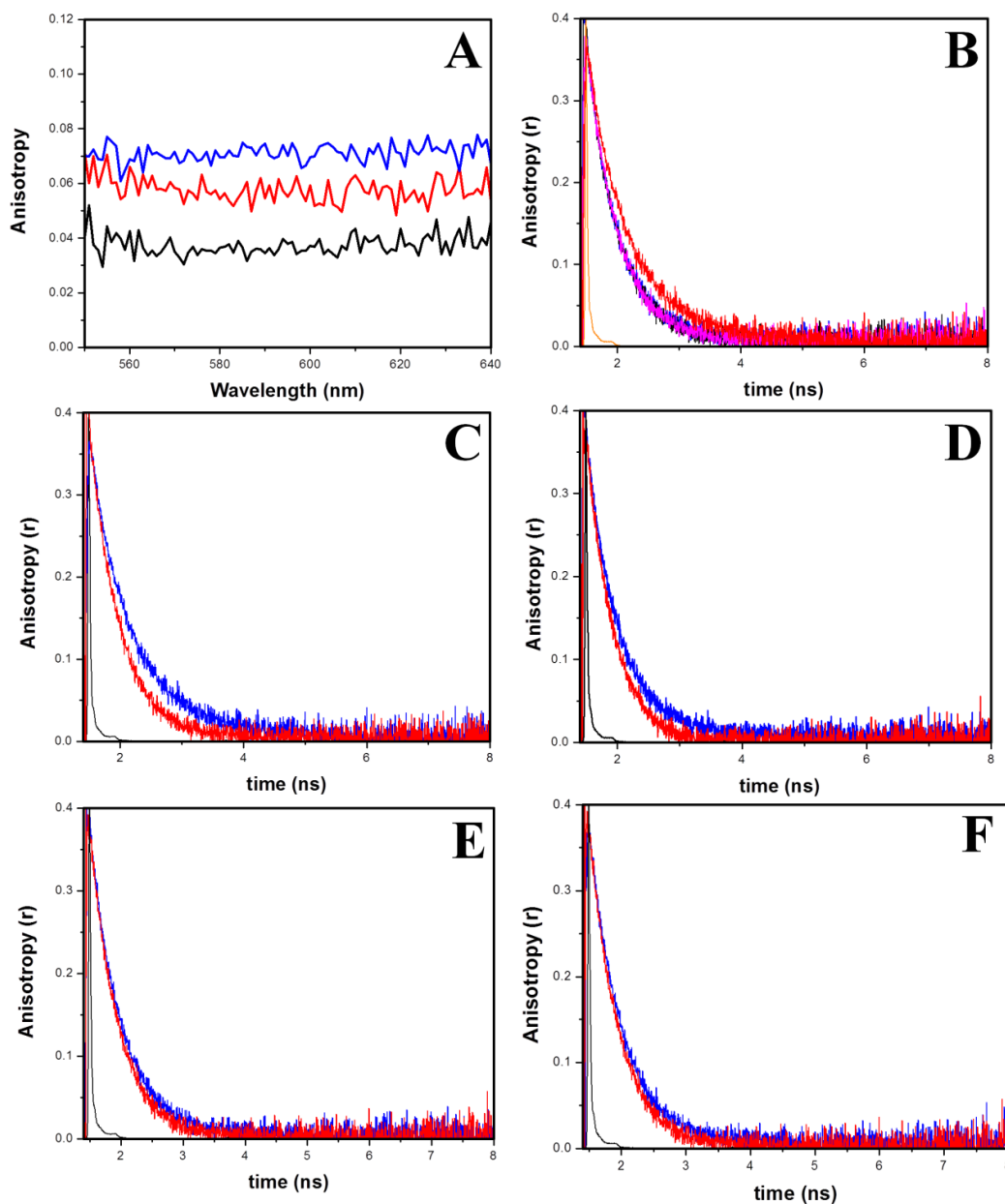
Figure 3.10. Comparison of steady state and time resolved anisotropy decays of Cy3B in dNMP solutions and iso-viscous glycerol-water solutions. (A) - steady state anisotropy of Cy3B in 250 mM dGMP(blue), iso-viscous solution (red), and buffer (blue). (B)- Time resolved anisotropy decays of Cy3B in 250 mM dGMP(red), dAMP(blue), dCMP(black), and dTMP(magenta). Overlap of time resolved anisotropy decays of the 250 mM dNMP solutions (blue) and the corresponding iso-viscous solutions (red), for dGMP(C), dAMP(D), dCMP(E), dTMP(F). The overlaps of the anisotropies definitely show that the rotational diffusion is slower for the dyes in presence of dNMP solutions compared to iso-viscous solutions.

122

Sample	A1	t1 (ns)	A2	t2 (ns)
visc = 1.41	0.37	0.51		
dGMP	0.3	0.57	0.06	1.78
visc = 1.14	0.36	0.43		
dAMP	0.35	0.49	0.02	3.45
visc = 1.28	0.36	0.46		
dCMP	0.36	0.48	0.01	3.18
dTMP	0.35	0.49	0.01	5.07

Table 3.3. Rotational correlation time of Cy3B in 250 mM dNMP solutions and the iso-viscous solutions. The results indicates presence of two populations of the Cy3B in dNMP solutions, one having the same rotational correlation time of the iso-viscous solutions (free dye) and the second having a much longer rotational correlation time (probably Cy3B-dNMP complexes).

3.3.4. Redox potentials. Photoinduced electron transfer (PET) is one of the most potent pathway for the quenching of the fluorescent dyes.[31-34] To calculate the feasibility of the PET, the ground state redox potentials of the dyes were calculated and presented in table 3.4. Table 3.4 also contains the $E_{0,0}$ and $^*E^A_{red}$ values. The detailed description of the PET and the calculation of these different potential values are described in section 1.3.2.4. The cyclic voltammograms of the three dyes in water is represented in Figure 3.11.

Fluorophore	E^A_{red} (V) vs. NHE	$E_{0,0}$ (V)	$^*E^A_{red}$ (V) vs NHE
TAMRA	-0.57	2.21	1.64
Cy3B	-0.96	2.19	1.23
Alexa 546	-0.76	2.20	1.44

Table 3.4. The reduction potential of the ground state and the first excited singlet state as calculated using the zero-zero transition energy of the three dyes.
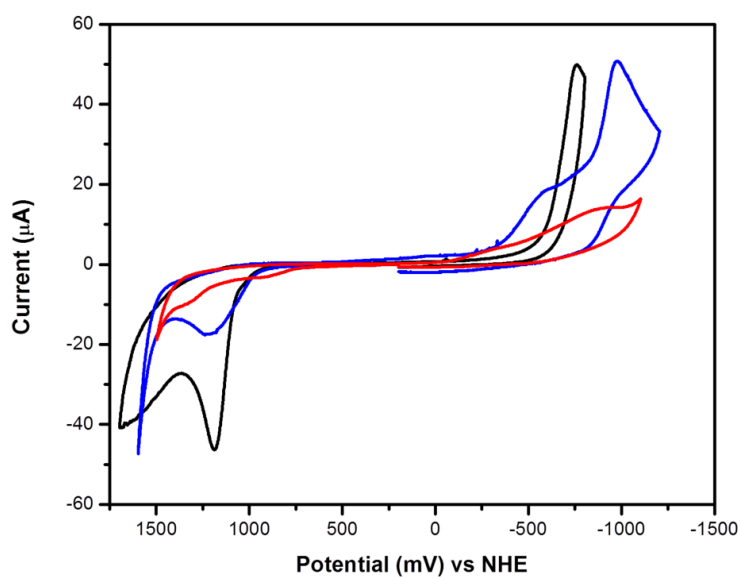
Figure 3.11. Cyclic voltammograms of Alexa 546(Black), Cy3B (red) and TAMRA (blue). The CV measurements were carried out in 10mM TRIS buffer.

3.4. Discussion

Photoinduced electron transfer (PET) is the most efficient way for the quenching of fluorescence.[33, 34] In the presence of a nucleotide, the PET mechanism operates via the transfer of an electron from the nucleotide (nucleotide oxidation) to the first excited state of the fluorophore (fluorophore reduction).[31-33, 45] The most potent quencher among all the DNA and RNA bases is guanine due to its lowest oxidation potential. Therefore, it is not surprising that amongst the four nucleotides under investigation, deoxyguanosine monophosphate, or dGMP, is well suited to cause PET by virtue of its very low E_{ox} value (-1.47 V, NHE scale).[34] The oxidation potentials of the base, G, and the nucleoside, dG, are 1.53 V and 1.19 V (vs. NHE), respectively.[34] In theory, the Rehm-Weller equation (equation 1.17) gives a formulism to calculate the feasibility of the quenching reaction. In practice, this becomes more difficult due to the fact that the cyclic voltammograms of the fluorescent dyes are often irreversible[57-59] and the measured reduction potentials are often dependent on the solvent.[60, 61] As an example, there is a difference of 0.22 V in the measured E^A_{red} values of coumarin when the solvent is changed from water to DMF.[34] The coulombic interaction term, though often neglected, can have great influence on the calculated ΔG value. Including or neglecting the -0.1 V Coulombic term can result in differences in the sign of the ΔG, resulting in a change in the feasibility of the reaction.

A survey of the excited state potentials of the various fluorescent dyes that have been previously published are given in table 3.5.[31-34, 45] These values have been converted from various different scales to the NHE scale for easier comparison.

Dye	$E_{red} + E_{0,0}$ (V) vs NHE	Dye	$E_{red} + E_{0,0}$ (V) vs NHE
Texas Red[1]	1.204	Cy5[2]	1.284
Alexa546[1]	1.443	JA22[2]	1.494
JA133[2]	1.494	Atto647N[2]	1.504
Rh6G[2]	1.574	Rh630[2]	1.584
JA66[2]	1.604	Bodipy FL[1]	1.604
JA66[2]	1.604	TMR[1]	1.64
MR121[2]	1.684	JA51-DS[2]	1.694
5-FAM[1]	1.994	Bodipy R6G[1]	2.094

Table 3.5. Excited state reduction potentials for various fluorescent dyes. The superscripts (1) and (2) refer to measurements in water and acetonitrile respectively.

A closer look at table 3.5 shows that the dyes having excited state reduction potentials ($^*E^A_{red}$) above approximately 1.5 V (vs NHE) are quenched efficiently by guanine or dGMP. TAMRA ($^*E^A_{red} = 1.64$ V), which has a similar $^*E^A_{red}$ value compared to MR121 ($^*E^A_{red} = 1.684$ V) and Rh6G ($^*E^A_{red} = 1.574$ V), is very efficiently quenched by dGMP. Cy3B ($^*E^A_{red} = 1.23$ V), having a similar excited state reduction potential to that of Cy5 ($^*E^A_{red} = 1.28$ V) and Texas red ($^*E^A_{red} = 1.20$ V) is not quenched by dGMP.

The value of the excited state reduction potential of Alexa 546, as derived from the ground state reduction potentials by CV measurements and from the peak of the

absorption and emission spectra, is 1.44 V vs. NHE. This value is slightly lower than the value of $^*E^A_{red}$ obtained for other rhodamines, e.g. Rh6G and TAMRA, who are very efficiently quenched by dGMP. This indicates that the efficiency of quenching of Alexa 546 by dGMP through PET is less feasible than that observed for these other rhodamines. The very small amount of quenching observed for Alexa 546-dGMP can thus be explained by the lower excited state potential of Alexa 546. The other explanation for the small Stern-Volmer constant obtained for Alexa 546 in presence of dGMP can be due to the lack of interaction between Alexa 546 and dGMP, leading to little or no ground state complex formation required for PET. The FCS data suggest that the interactions between Alexa 546 and the dNMPs are very weak at best. This is probably due to the presence of bulky Cl and charged SO^{3-} groups in Alexa 546. These bulky groups can inhibit complex formation through steric hindrance. A similar behavior was observed by Harvey et al.,[44] where the cyanine dye Cy3, with the SO^{3-} groups attached, interacted less with dNMPs compared to the nonnsulfonated version of the same dye, called $DiIC_23$.[44] For PET to occur, the interacting molecules need to be present at a very short distance to each other, and steric hindrance caused by the bulky groups may prevent that. Thus, the low Stern-Volmer constant obtained for the Alexa 546 is a result of both steric and thermodynamic effects. Cy3B does not show any evidence of quenching by PET in presence dGMP. This is expected from the excited state reduction potential of Cy3B (1.23 V), which is comparable to Cy5 (1.28 V), a dye known not to be quenched by dGMP.

FCS was further employed to investigate the interactions of the dyes with dNMPs in absence of sufficient quenching. This technique has previously been used to study the association and dissociation kinetics of the oxazine derivative MR121 with tryptophan,[31]

and rhodamine R6G with dGTP.[62, 63] These fluorophores are completely quenched.

Hence, these studies do not report any change in the diffusion timescales of the

correlation decays. In these cases, the very fast association dissociation kinetics result in

fluctuation of fluorescent intensity and correlation analysis of these fluctuations give

evidence of the interaction. The timescales of these fluctuations are very short, e. g. 30 ns

for Rh6G and 10 mM dGTP. These fluctuations become even faster at a higher

concentration of dGTP due to the bimolecular nature of the association process. These

fluctuations appear at a much faster time than the fluctuations resulting from diffusion

(0.1 to 1 ms) and are shorter than the resolution of the correlator used in these

experiments (250 ns).[62] Consequently, the fluorescent correlation decays obtained in our

experiments can be easily fitted with a diffusion only model.

The origin of the fluorescent correlation decays obtained in these experiments is

the fluctuations in fluorescent intensity arising out of the translational diffusion of the

fluorophores through an inhomogeneously illuminated confocal volume. The origin being

translational diffusion, the pertinent timescale for these fluctuations is $l^2/6D$, where l is

the length scale where the inhomogeneities in the illumination volume become apparent

and D is the diffusion constant of the molecule. The dye being bound to the dNMP for a

fraction of time during its transition through the observation volume appears to move

slower and thus results in a smaller diffusion constant. This makes sense because as long

as the association dissociation equilibrium is much faster than the translational diffusion,

the diffusion of the dye in presence of association will appear slower than that of the free

dye. This is true even if the associated complex between the dye and the dNMP is

absolutely dark. The apparent diffusion constant (D_{app}), which is dependent on the

128

fraction of the time the dye spends free and the fraction it is associated with the dNMPs is given by,

$$D_{app} = \left. \left(D_F + K_{eq}[dNMP] \times D_{FN} \right) \middle/ \left(1 + K_{eq}[dNMP] \right) \right. \qquad (3.2)$$

In the above equation, D_F and D_{FN} are the diffusion constants of the free dye and the dye-dNMP complex, respectively; K_{eq} represents the equilibrium constant for the fluorophore-nucleotide association reaction. The two terms, $1/\left(1 + K_{eq}[dNMP] \right)$ and

$K_{eq}/\left(1 + K_{eq}[dNMP] \right)$ represent the fraction of the time the dye spends in the free and

bound state, respectively. D_{app} is independent of the brightness of the dye in different

states as long as the association dissociation equilibria happen at much shorter timescales

compared to the diffusion phenomena. This equation was derived by Dr. Marcia Levitus

and the derivation is available in the supplementary information of the following paper:

Ranjit, S. and Levitus, M. (2012), Probing the Interaction Between Fluorophores and

DNA Nucleotides by Fluorescence Correlation Spectroscopy and Fluorescence

Quenching. Photochemistry and Photobiology, 88: 782–791. doi: 10.1111/j.1751-

1097.2012.01121.x

As mentioned in the results, the time resolved anisotropy decays for the dye in

dNMP solutions were fitted with a bi-exponential decay and the dye in iso-viscous

solution were fitted with mono-exponential decay. Inclusion of more components did not

result in better χ^2 or randomness of the residuals. The rotational correlation times

obtained for the dye in dNMP solutions can be indicative of the rotational correlation

time of the free dye and the dye-dNMP complexes. Although the faster rotational

correlation time of the dye in different dNMP solutions were different, the faster

rotational correlation times were the same in solutions of the same viscosity. Therefore,

the faster of the two rotational time changes with the solution viscosity only and most

probably represents the rotational correlation time of the free dye itself. The second and

longer correlation time can represent the rotational correlation time of the dye in complex

with the dNMP. This rotational correlation time is different for different dNMPs.

Theoretically, from the amplitude of the bi-exponential decay of an associated

anisotropy, the equilibrium constant can be obtained by using the following relation,

where the bi-exponential decay is defined as,

$$r(t) = Ae^{-t/\tau_{Cy3B}} + (0.38 - A)e^{-t/\tau_{Cy3B-dNMP}}$$

$$r(t) = \frac{1}{1+\frac{\varepsilon_2\varphi_2}{\varepsilon_1\varphi_1}K_{eq}[dNMP]} r^0_{Cy3B}\, e^{-t/\tau_{Cy3B}} + \frac{K_{eq}[dNMP]}{\frac{\varepsilon_1\varphi_1}{\varepsilon_2\varphi_2} + K_{eq}[dNMP]} r^0_{Cy3B-dNMP}\, e^{-t/\tau_{Cy3B-dNMP}}$$

$$= \frac{1}{1+d} r^0_{Cy3B}\, e^{-t/\tau_{Cy3B}} + \frac{1}{1+1/d} r^0_{Cy3B-dNMP}\, e^{-t/\tau_{Cy3B-dNMP}} \qquad (3.3)$$

Where, $d = \frac{\varepsilon_2\varphi_2}{\varepsilon_1\varphi_1} K_{eq}[dNMP]$.

In the above set of expressions ε, φ and r^0 represent the extinction coefficient at

the excitation wavelength, quantum yield and intrinsic fluorescence anisotropy (at t = 0),

respectively. *1* and *2* represent the free Cy3B and Cy3B-dNMP, respectively. The

derivation of this equation is described in the appendix A.

Equation 3.2 and 3.3 provide a way to calculate the equilibrium constant (K_{eq}) of

the dye-dNMP association equilibrium in absence of complete quenching. These

calculations, however, face complications from a different perspective. The analysis and the calculation of the equilibrium constant from the data are crippled from the fact that the nucleotides and nucleobases start to self associate at the high concentrations used in these experiments.[64-67] These phenomena have been extensively studied by NMR methods and yet somehow have been neglected in the field of fluorescence. The data obtained from the self-association of these nucleobases, nucleosides, and nucleotides have been analyzed by different research groups using different sequential models. Two of the most common methods used are isodesmic[66] and semi-isodesmic models.[65] The isodesmic model assumes a single association constant in an indefinite self-association model. Semi-isodesmic model assumes two different equilibrium constants, one for the formation of the dimer and another one for all subsequent steps of the indefinite self-association. According to the self-association model, the equilibrium can be described as,

$$dNMP_n + dNMP \rightleftharpoons dNMP_{n+1}$$

Using the isodesmic model, the concentration of the monomer of NMP, $[NMP]^{2-}$, and higher order structures of NMPs, $[NMP^{2-}]_n$ (n > 1) have been calculated as function of the total concentration, defined as $\sum_{n=1}^{\infty} n \times [NMP^{2-}]_n$. The total particle concentration can then be calculated, where total particle concentration was defined as $\sum_{n=1}^{\infty} [NMP^{2-}]_n$. Finally, the fraction of monomer and the fraction of total particle concentrations were calculated as a function of total concentration. The equations that were derived and used to calculate these concentrations are described in the appendix A. The association constants used for the calculation of the concentrations after self association were 2.1 M^{-1} and 1.3 M^{-1} for AMP^{2-} and GMP^{2-}, respectively, as reported by

Sigel and Griesser.[67] According to this model, only 13% of the AMP (red column) and

15% of GMP (black column) molecules exist as monomers when the total concentration

is 250 mM. This is shown in the left panel of Figure 3.12. The inset of the left panel

shows the fraction of monomers present.
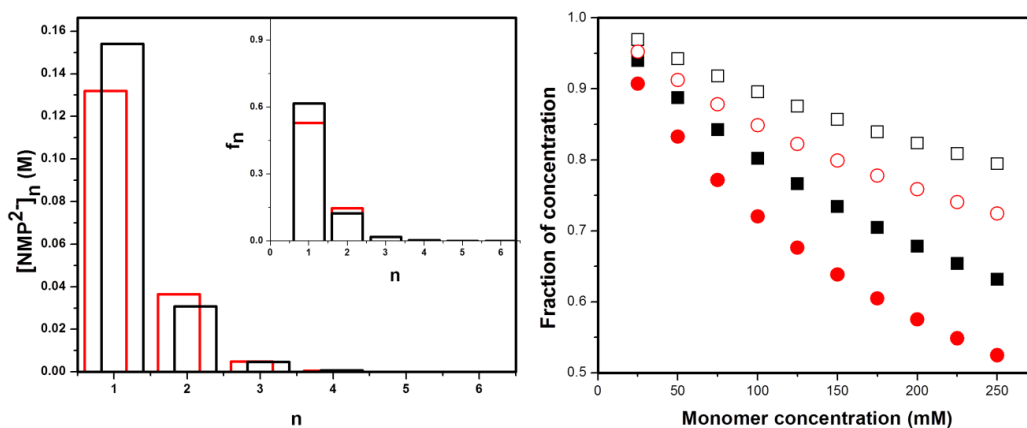
Figure 3.12. Self association of dNMPs in water. The left panel describes the
concentration of monomers and oligomers of $[AMP^{2-}]_n$ (red column) and $[GMP^{2-}]_n$ (black
column) when the total concentration was 250mM. *Inset* shows the fractional
concentrations of the same. The right panel describes the fraction of concentration of
monomer (solid) and the total particle ($\sum_{n=1}^{\infty}[NMP^{2-}]_n$) (open), as a function of total
concentration ($\sum_{n=1}^{\infty}n \times [NMP^{2-}]_n$). The black represents the GMP^{2-} and the red
represents the AMP^{2-} in both the panels.

The right panel in Figure 1.12 describes the fraction of concentration of the

monomer (solid) and the total particle ($\sum_{n=1}^{\infty}[NMP^{2-}]_n$) (open), as a function of total

concentration ($\sum_{n=1}^{\infty}n \times [NMP^{2-}]_n$). In both panels, black represents the GMP^{2-} and red

represents the AMP^{2-}. From the two plots, it is very evident that the fraction of particles

available for complexation to the dye decreases steadily with increasing concentration of

dNMPs. In other words, the available number of dNMP moieties available for the

complex formation with the dyes are much lower that the total concentration ($\sum_{n=1}^{\infty}n \times$

$[NMP^{2-}]_n$) suggests. There have been various studies in the field of fluorescence quenching by dNMPs and nucleobases, and yet the self association equilibria of dNMPs have so far been neglected in this field. Heinlein et al.[33] observed a downward curvature in the Stern-Volmer plot of R6G and dGMP, and attributed this to the ground-state 1:1 complex formation with negligible quantum yield. Sauer et al.[45] reported a similar downward deviation from the straight line in the Stern-Volmer plot of JA51DS against dGMP, which is curiously transformed to a straight line in presence of urea, a denaturing agent. Granting that the ground state complex formation is a feasible explanation for the downward curvature, the curvature can also be explained by the availability of lower number of complex forming entities due to the self association of dNMPs. The data for Cy3B indicated a similar downward curvature and in this case it can be fully explained by the self association.

The data in Figure 3.12 have been calculated assuming a isodesmic model with only one equilibrium constant for each of the self association steps. Other models, including the semi-isodesmic model described earlier, result in different distribution of the oligomeric species.[65, 68, 69] The facts, different models give rise to different number of monomeric species available for binding and dyes can potentially interact with not only monomers but also higher order dNMP structures, make the analysis of the Stern-Volmer, time resolved anisotropy decays, and the autocorrelation decays very complicated. In addition, it has also been observed that purines decrease the diffusion coefficients more than the pyrimidines do (table 3.2 and Figure 3.8). This result, and the fact that the purines self associate better than the pyrimidines, give rise to the possibility that the larger decrease in the diffusion constant of the dyes in presence of purines compared to

pyrimidines can be due to the interaction of the dye with larger moeities of dNMPs, and not due to larger equilibrium constants. Thus, the calculation of the association constant becomes very complicated.

To conclude, the interactions of Cy3B with various nucleotides do not affect the photophysical properties, e. g. quantum yield or lifetime, significantly. The photophysical properties of TAMRA are only affected by dGMP, the most potent quencher amongst all the dNMPs. Other than dGMP, the other nucleotides do not possess the low oxidation potential required for the quenching by photoinduced electron transfer. FCS and time resolved anisotropy techniques uncover evidence of interaction between the dNMPs and these two dyes, albeit their photophysical properties remaining almost unchanged. These interactions lead to lower rotational mobility compared to the free dye, and hence need to be accounted for during the calculation of distances from FRET measurements. These interactions also have the potential to change the structure and stability of DNA. In contrast, Alexa546 does not interact with the dNMPs, as evidenced by the FCS experiments. The bulky Cl and SO_3^{3-} groups may create steric crowding during the interaction with dNMPs and act as a deterrent to the complex formation. The lower excited state reduction potential of Alexa546, compared to other rhodamines, also can inhibit quenching by photo induced electron transfer by dGMP.

The bathochromic shift in the absorption spectra in presence of dNMPs has been used as an indicator of ground state complex formation. The result for Cy3B indicates that, at least for Cy3B, the bathochromic shift of the absorption spectra, in presence compared to in absence of dNMP solutions, can be explained by the changes in the

refractive index of the solution without the need to involve ground state complex

formation. The self association of the dNMPs complicates the analysis of the obtained

correlation decays, time resolved anisotropy decays and quenching data. The propensity

to form higher order structures at a high concentration of dNMPs has been an untouched

subject in the field of fluorescent quenching perhaps because it complicates the analysis

of the procured data.

3.5. References

1.   Huang, B.; Jones, S. A.; Brandenburg, B.; Zhuang, X. W., Whole-cell 3D STORM reveals interactions between cellular structures with nanometer-scale resolution. *Nat. Methods* **2008,** 5, (12), 1047-1052.

2.   Huang, B.; Wang, W. Q.; Bates, M.; Zhuang, X. W., Three-dimensional super-resolution imaging by stochastic optical reconstruction microscopy. *Science* **2008,** 319, (5864), 810-813.

3.   Jares-Erijman, E. A.; Jovin, T. M., Imaging molecular interactions in living cells by FRET microscopy. *Curr. Opin. Chem. Biol.* **2006,** 10, (5), 409-416.

4.   Li, G.; Levitus, M.; Bustamante, C.; Widom, J., Rapid spontaneous accessibility of nucleosomal DNA. *Nat Struct Mol Biol* **2005,** 12, (1), 46-53.

5.   Rasnik, I.; Myong, S.; Cheng, W.; Lohman, T. M.; Ha, T., DNA-binding orientation and domain conformation of the E-coli Rep helicase monomer bound to a partial duplex junction: Single-molecule studies of fluorescently labeled enzymes. *J Mol Biol* **2004,** 336, (2), 395-408.

6.   Yang, M. S.; Millar, D. P., Fluorescence resonance energy transfer as a probe of DNA structure and function. *Method Enzymol* **1997,** 278, 417-444.

7.   Ying, B. W.; Fourmy, D.; Yoshizawa, S., Substitution of the use of radioactivity by fluorescence for biochemical studies of RNA. *Rna* **2007,** 13, (11), 2042-2050.

8.   Willemse, J.; van Wezel, G. P., Imaging of Streptomyces coelicolor A3(2) with Reduced Autofluorescence Reveals a Novel Stage of FtsZ Localization. *Plos One* **2009,** 4, (1).

9.   Schwille, P.; Korlach, J.; Webb, W. W., Fluorescence correlation spectroscopy with single-molecule sensitivity on cell and model membranes. *Cytometry* **1999,** 36, (3), 176-82.

10.   Rothenberg, E.; Ha, T., Single-molecule FRET analysis of helicase functions. *Methods Mol Biol* **2010,** 587, 29-43.

11.   Tomishige, M.; Stuurman, N.; Vale, R., Single-molecule observations of neck linker conformational changes in the kinesin motor protein. *Nat Struct Mol Biol* **2006,** 13, (10), 887-894.

12.   Heilemann, M.; Dedecker, P.; Hofkens, J.; Sauer, M., Photoswitches: Key molecules for subdiffraction-resolution fluorescence imaging and molecular quantification. *Laser Photonics Rev* **2009,** 3, (1-2), 180-202.

13.   Huang, B.; Bates, M.; Zhuang, X. W., Super-Resolution Fluorescence Microscopy. *Annu. Rev. Biochem.* **2009,** 78, 993-1016.

14.   Delgadillo, R. F.; Parkhurst, L. J., Spectroscopic Properties of Fluorescein and Rhodamine Dyes Attached to DNA. *Photochem Photobiol* **2010,** 86, (2), 261-272.

15.   Majumdar, Z. K.; Hickerson, R.; Noller, H. F.; Clegg, R. M., Measurements of internal distance changes of the 30 S ribosome using FRET with multiple donor-acceptor pairs: Quantitative spectroscopic methods. *J Mol Biol* **2005,** 351, (5), 1123-1145.

16.   Harvey, B. J.; Perez, C.; Levitus, M., DNA sequence-dependent enhancement of Cy3 fluorescence. *Photoch Photobio Sci* **2009,** 8, (8), 1105-1110.

17.   Sanborn, M. E.; Connolly, B. K.; Gurunathan, K.; Levitus, M., Fluorescence properties and photophysics of the sulfoindocyanine Cy3 linked covalently to DNA. *J. Phys. Chem. B* **2007,** 111, (37), 11064-11074.

18.   Kolmakov, K.; Belov, V. N.; Bierwagen, J.; Ringemann, C.; Muller, V.; Eggeling, C.; Hell, S. W., Red-Emitting Rhodamine Dyes for Fluorescence Microscopy and Nanoscopy. *Chem-Eur J* **2010,** 16, (1), 158-166.

19.   Willig, K. I.; Harke, B.; Medda, R.; Hell, S. W., STED microscopy with continuous wave beams. *Nat. Methods* **2007,** 4, (11), 915-918.

20.   Dale, R. E.; Eisinger, J.; Blumberg, W. E., Orientational Freedom of Molecular Probes - Orientation Factor in Intra-Molecular Energy-Transfer. *Biophys J* **1979,** 26, (2), 161-193.

21.   Dosremedios, C. G.; Moens, P. D. J., Fluorescence Resonance Energy-Transfer Spectroscopy Is a Reliable Ruler for Measuring Structural-Changes in Proteins -

Dispelling the Problem of the Unknown Orientation Factor. *J. Struct. Biol.* **1995,** 115, (2), 175-185.

22.   Ranjit, S.; Gurunathan, K.; Levitus, M., Photophysics of Backbone Fluorescent DNA Modifications: Reducing Uncertainties in FRET. *J. Phys. Chem. B* **2009,** 113, (22), 7861-7866.

23.   VanBeek, D. B.; Zwier, M. C.; Shorb, J. M.; Krueger, B. P., Fretting about FRET: Correlation between kappa and R. *Biophys J* **2007,** 92, (12), 4168-4178.

24.   Lakowicz, J. R., *Principles of fluorescence spectroscopy*. Springer: 2006; Vol. 1.

25.   Valeur, B., *Molecular Fluorescence: Principles and Applications*. Wiley-VCH: Weinheim, Germany, 2001.

26.   Stryer, L.; Haugland, R. P., Energy Transfer - a Spectroscopic Ruler. *Proc. Natl. Acad. Sci. U. S. A.* **1967,** 58, (2), 719-&.

27.   Iqbal, A.; Arslan, S.; Okumus, B.; Wilson, T. J.; Giraud, G.; Norman, D. G.; Ha, T.; Lilley, D. M. J., Orientation dependence in fluorescent energy transfer between Cy3 and Cy5 terminally attached to double-stranded nuclelic acids. *Proc. Natl. Acad. Sci. U. S. A.* **2008,** 105, (32), 11176-11181.

28.   Lewis, F. D.; Zhang, L. G.; Zuo, X. B., Orientation control of fluorescence resonance energy transfer using DNA as a helical scaffold. *J Am Chem Soc* **2005,** 127, (28), 10002-10003.

29.   Iqbal, A.; Wang, L.; Thompson, K. C.; Lilley, D. M. J.; Norman, D. G., The structure of cyanine 5 terminally attached to double-stranded DNA: Implications for FRET studies. *Biochemistry* **2008,** 47, (30), 7857-7862.

30.   Urnavicius, L.; McPhee, S. A.; Lilley, D. M. J.; Norman, D. G., The Structure of Sulfoindocarbocyanine 3 Terminally Attached to dsDNA via a Long, Flexible Tether. *Biophys J* **2012,** 102, (3), 561-568.

31.   Doose, S.; Neuweiler, H.; Sauer, M., Fluorescence Quenching by Photoinduced Electron Transfer: A Reporter for Conformational Dynamics of Macromolecules. *Chemphyschem* **2009,** 10, (9-10), 1389-1398.

32.   Dunn, D. A.; Lin, V. H.; Kochevar, I. E., The Role of Ground-State Complexation in the Electron-Transfer Quenching of Methylene-Blue Fluorescence by Purine Nucleotides. *Photochem Photobiol* **1991,** 53, (1), 47-56.

33.   Heinlein, T.; Knemeyer, J. P.; Piestert, O.; Sauer, M., Photoinduced electron transfer between fluorescent dyes and guanosine residues in DNA-hairpins. *J. Phys. Chem. B* **2003,** 107, (31), 7957-7964.

34.   Seidel, C. A. M.; Schulz, A.; Sauer, M. H. M., Nucleobase-specific quenching of fluorescent dyes .1. Nucleobase one-electron redox potentials and their correlation with static and dynamic quenching efficiencies. *J Phys Chem-Us* **1996,** 100, (13), 5541-5553.

35.   Torimura, M.; Kurata, S.; Yamada, K.; Yokomaku, T.; Kamagata, Y.; Kanagawa, T.; Kurane, R., Fluorescence-quenching phenomenon by photoinduced electron transfer between a fluorescent dye and a nucleotide base. *Anal Sci* **2001,** 17, (1), 155-160.

36.   Jovanovic, S. V.; Simic, M. G., One-Electron Redox Potentials of Purines and Pyrimidines. *J Phys Chem-Us* **1986,** 90, (5), 974-978.

37.   Yao, T.; Wasa, T.; Musha, S., Linear-Sweep Voltammetry and Simultaneous Determination of Purine-Bases and Their Nucleosides in Glassy Carbon Electrode. *B Chem Soc Jpn* **1977,** 50, (11), 2917-2920.

38.   Marme, N.; Knemeyer, J. P.; Sauer, M.; Wolfrum, J., Inter- and intramolecular fluorescence quenching of organic dyes by tryptophan. *Bioconjugate Chem* **2003,** 14, (6), 1133-1139.

39.   Vaiana, A. C.; Neuweiler, H.; Schulz, A.; Wolfrum, J.; Sauer, M.; Smith, J. C., Fluorescence quenching of dyes by tryptophan: Interactions at atomic detail from combination of experiment and computer simulation. *J Am Chem Soc* **2003,** 125, (47), 14564-14572.

40.   Jones, B. E.; Beechem, J. M.; Matthews, C. R., Local and global dynamics during the folding of Escherichia coli dihydrofolate reductase by time-resolved fluorescence spectroscopy. *Biochemistry* **1995,** 34, (6), 1867-1877.

41.   Tournier, E. J. M.; Wallach, J.; Blond, P., Sulfosuccinimidyl 4-(N-maleimidomethyl)-1-cyclohexane carboxylate as a bifunctional immobilization agent. Optimization of the coupling conditions. *Anal Chim Acta* **1998,** 361, (1-2), 33-44.

42.   Sortino, M.; Filho, V. C.; Correa, R.; Zacchino, S., N-Phenyl and N-phenylalkyl-maleimides acting against Candida spp.: Time-to-kill, stability, interaction with maleamic acids. *Bioorganic & Medicinal Chemistry* **2008,** 16, (1), 560-568.

43.   Ramsahoye, B. H., Measurement of genome wide DNA methylation by reversed-phase high-performance liquid chromatography. *Methods* **2002,** 27, (2), 156-161.

44.   Harvey, B. J.; Levitus, M., Nucleobase-Specific Enhancement of Cy3 Fluorescence. *J Fluoresc* **2009,** 19, (3), 443-448.

45.   Sauer, M.; Han, K. T.; Müller, R.; Nord, S.; Schulz, A.; Seeger, S.; Wolfrum, J.; Arden-Jacob, J.; Deltau, G.; Marx, N. J.; Zander, C.; Drexhage, K. H., New fluorescent dyes in the red region for biodiagnostics. *J Fluoresc* **1995,** 5, (3), 247-261.

46.   Kittler, L.; LÃ¶ber, G.; Gollmick, F. A.; Berg, H., 352 - Redox processes during photodynamic damage of DNA III. Redox mechanism of photosensitization and radical reaction. *Bioelectrochemistry and Bioenergetics* **1980,** 7, (3), 503-511.

47.   Li, X.; Zhu, R. X.; Yu, A. C.; Zhao, X. S., Ultrafast Photoinduced Electron Transfer between Tetramethylrhodamine and Guanosine in Aqueous Solution. *J Phys Chem B* **2011,** 115, (19), 6265-6271.

48.   Noordzij, J. G.; de Bruin-Versteeg, S.; Verkaik, N. S.; Vossen, J. M.; de Groot, R.; Bernatowska, E.; Langerak, A. W.; van Gent, D. C.; van Dongen, J. J., The immunophenotypic and immunogenotypic B-cell differentiation arrest in bone marrow of RAG-deficient SCID patients corresponds to residual recombination activities of mutated RAG proteins. *Blood* **2002,** 100, (6), 2145-52.

49.   Bayliss, N. S., The Effect of the Electrostatic Polarization of the Solvent on Electronic Absorption Spectra in Solution. *J. Chem. Phys.* **1950,** 18, (3), 292-296.

50.   Bayliss, N. S.; Mcrae, E. G., Solvent Effects in Organic Spectra - Dipole Forces and the Franck-Condon Principle. *J Phys Chem-Us* **1954,** 58, (11), 1002-1006.

51.   Arbeloa, F. L.; Arbeloa, T. L.; Estevez, M. J. T.; Arbeloa, I. L., Photophysics of Rhodamines - Molecular-Structure and Solvent Effects. *J Phys Chem-Us* **1991,** 95, (6), 2203-2208.

52.	Arbeloa, F. L.; Ojeda, P. R.; Arbeloa, I. L., Fluorescence Self-Quenching of the Molecular-Forms of Rhodamine-B in Aqueous and Ethanolic Solutions. *J Lumin* **1989,** 44, (1-2), 105-112.

53.	Culbertson, M. J.; Williams, J. T. B.; Cheng, W. W. L.; Stults, D. A.; Wiebracht, E. R.; Kasianowicz, J. J.; Burden, D. L., Numerical fluorescence correlation spectroscopy for the analysis of molecular dynamics under nonstandard conditions. *Anal Chem* **2007,** 79, (11), 4031-4039.

54.	Gendron, P. O.; Avaltroni, F.; Wilkinson, K. J., Diffusion Coefficients of Several Rhodamine Derivatives as Determined by Pulsed Field Gradient-Nuclear Magnetic Resonance and Fluorescence Correlation Spectroscopy. *J Fluoresc* **2008,** 18, (6), 1093-1101.

55.	Muller, C. B.; Loman, A.; Pacheco, V.; Koberling, F.; Willbold, D.; Richtering, W.; Enderlein, J., Precise measurement of diffusion by multi-color dual-focus fluorescence correlation spectroscopy. *Europhys. Lett.* **2008,** 83, (4), 46001.

56.	Petrasek, Z.; Schwille, P., Precise measurement of diffusion coefficients using scanning fluorescence correlation spectroscopy. *Biophys J* **2008,** 94, (4), 1437-1448.

57.	Austin, J. M.; Harrison, I. R.; Quickenden, T. I., Electrochemical and photoelectrochemical properties of Rhodamine B. *The Journal of Physical Chemistry* **1986,** 90, (9), 1839-1843.

58.	Fischer, A. B.; Bronsteinbonte, I., Photoinduced Electron-Transfer Quenching of Rhodamine-B in Polymer-Films. *Journal of Photochemistry* **1985,** 30, (4), 475-485.

59.	Jones, G.; Griffin, S. F.; Choi, C. Y.; Bergmark, W. R., Electron Donor-Acceptor Quenching and Photoinduced Electron-Transfer for Coumarin Dyes. *J Org Chem* **1984,** 49, (15), 2705-2708.

60.	Taras-Goslinska, K.; Jonsson, M., Solvent effects on the redox properties of thioethers. *J. Phys. Chem. A* **2006,** 110, (30), 9513-9517.

61.	Wilford, J. H.; Archer, M. D., Solvent Effects on the Redox Potentials of Benzoquinone. *J. Electroanal. Chem.* **1985,** 190, (1-2), 271-277.

62.   Li, X.; Zhu, R.; Yu, A.; Zhao, X. S., Ultrafast Photoinduced Electron Transfer between Tetramethylrhodamine and Guanosine in Aqueous Solution. *The Journal of Physical Chemistry B* 115, (19), 6265-6271.

63.   Widengren, J.; Dapprich, J.; Rigler, R., Fast interactions between Rh6G and dGTP in water studied by fluorescence correlation spectroscopy. *Chem. Phys.* **1997,** 216, (3), 417-426.

64.   Lam, Y. F.; Kotowycz, G., Nuclear Magnetic-Resonance Studies of Nucleotide - Metal-Ion Interactions .8. Nuclear Magnetic-Resonance Studies on Self-Association of Adenosine 5'-Triphosphate in Aqueous-Solutions. *Canadian Journal of Chemistry-Revue Canadienne De Chimie* **1977,** 55, (20), 3620-3630.

65.   Rymden, R.; Stilbs, P., Nucleotide Aggregation in Aqueous-Solution - a Multicomponent Self-Diffusion Study. *Biophys Chem* **1985,** 21, (2), 145-156.

66.   Scheller, K. H.; Hofstetter, F.; Mitchell, P. R.; Prijs, B.; Sigel, H., Macrochelate Formation in Monomeric Metal-Ion Complexes of Nucleoside 5'-Triphosphates and the Promotion of Stacking by Metal-Ions - Comparison of the Self-Association of Purine and Pyrimidine 5'-Triphosphates Using Proton Nuclear Magnetic-Resonanc. *J Am Chem Soc* **1981,** 103, (2), 247-260.

67.   Sigel, H.; Griesser, R., Nucleoside 5 '-triphosphates: self-association, acid-base, and metal ion-binding properties in solution. *Chem. Soc. Rev.* **2005,** 34, (10), 875-900.

68.   Martin, R. B., Comparisons of Indefinite Self-Association Models. *Chem. Rev. (Washington, DC, U. S.)* **1996,** 96, (8), 3043-3064.

69.   Stokkeland, I.; Stilbs, P., A Multicomponent Self-Diffusion Nmr-Study of Aggregation of Nucleotides, Nucleosides, Nucleic-Acid Bases and Some Derivatives in Aqueous-Solution with Divalent Metal-Ions Added. *Biophys Chem* **1985,** 22, (1-2), 65-75.

Chapter 4

Investigation of the solution stability and dynamics of DNA sliding clamps using FCS and smFluorescence

The solution stability and conformational equilibrium between open and closed states of two different sliding clamps, β clamp from *E. coli* and PCNA from *S. cerevisiae*, have been studied in this project using various fluorescence techniques. The experiments show that there is an equilibrium between the open and closed state of the β clamp. The presence of equilibriums between different oligomeric states of the β clamp and PCNA has also been established. The dissociation constant of the monomerization reaction (K_D) was determined to be in the pM and nM^2 range for the β clamp and for the PCNA, respectively. This difference is indicative of the very different solution stability of the two clamps.

4.1 Introduction

Sliding clamps are ring shaped proteins that are part of DNA replication machinery responsible for DNA replication and repair of damaged DNA.[1-6] The main set of proteins involved in replication of DNA are called DNA polymerases. DNA polymerases bind to DNA and make copies of the DNA using each DNA strand as a template, resulting in the continuation of the genetic information. These polymerases consist of several individual proteins. One of them is the core particle, the protein machinery responsible for the DNA replication. The other set of proteins are the accessory proteins - sliding clamp and clamp loaders.[4] Clamp loaders, in the presence of

ATP, are known to attach to the sliding clamp, transfer them to DNA, and then dissociate from the clamp-DNA complex following the hydrolysis of ATP (Figure 4.1), leaving the clamp encircling the DNA.[7] The core particle can then bind to the clamp and continue replication. In absence of these processivity factors (clamp and clamp loader), the DNA polymerase dissociates easily from the template DNA and results in ineffectual replication. Sliding clamps not only help to stabilize the replication machinery and DNA complex but also increase the speed and processivity of replication by orders of magnitude.[6, 8]
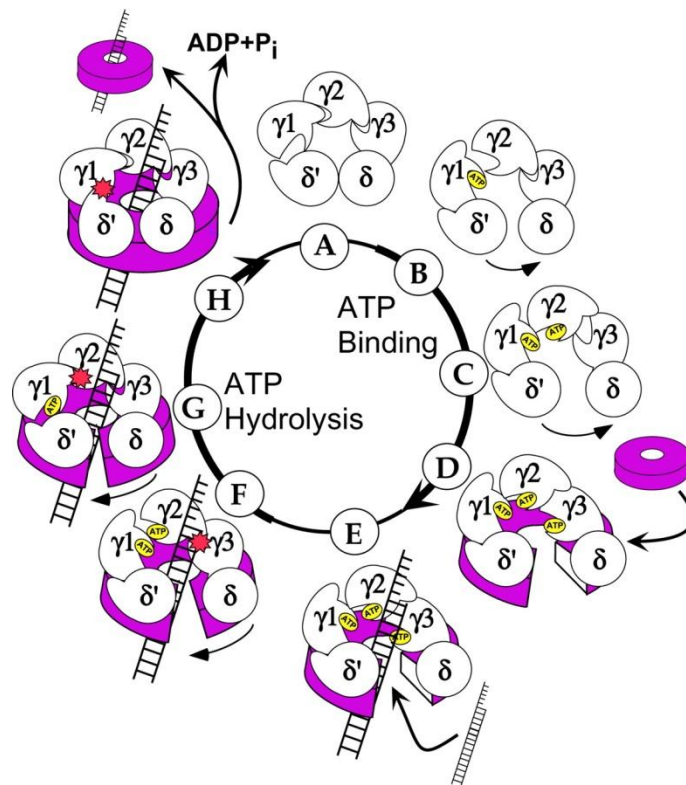

Figure 4.1. Sequential ATP binding and hydrolysis during the loading of the clamp onto the DNA. The clamp loader (shown as a pentameric unit) binds to the clamp (in purple) and transfers the open clamp to the DNA. The hydrolysis of ATP causes the clamp to close and separation of the clamp loader from the clamp-DNA complex. This figure was adopted from Johnson et al.[7]

144

These clamps are present in all types of organisms that use DNA as their genetic material, including gp45 from T4 phage (a virus), β clamp from *E. coli* (a bacteria), PCNA from *S. cerevisiae* (an eukaryote), PCNA form *S. sulfolobus* (an archea) and even human PCNA.[2, 9] All of these proteins are structurally very similar. They are ring-like proteins consisting of two or three monomeric units. Although these proteins are topologically very similar, they have very little sequence homology.[2, 9] Though most of the clamps are homo-oligomers, hetero-oligomeric clamps do exist in nature.[10] The sliding clamps are known to interact with not only DNA polymerase but also various other proteins. PCNA, for example, is known to interact with proteins responsible for replication, mismatch DNA repair, base excision repair, translesion synthesis and controlling cell cycles.[11]
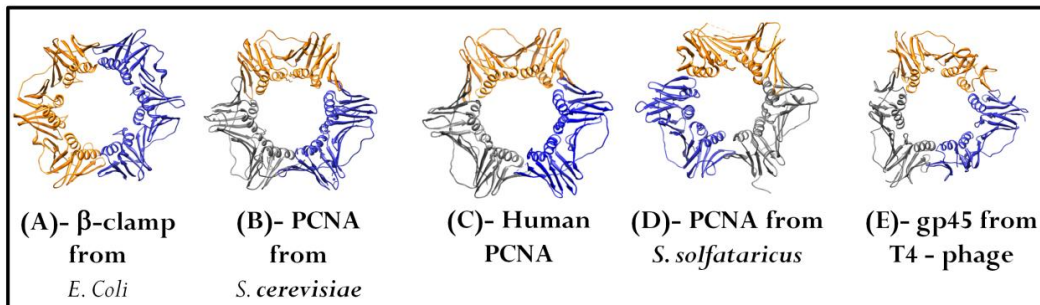
Figure 4.2. Sliding clamps across biology. This figure was prepared from the crystal structure data in PDB data bank using the visualization software Chimera. This figure presents the ring like structure and the topological similarity between clamps from bacteria *E. coli* (A) (PDB ID. 1MMI), eukaryotes *S. cerevisiae* (B) (PDB ID. 1PLQ) and human *H. sapiens* (C) (PDB ID. 1AXC), archaea *S. solfataricus* (D) (PDB ID. 2IX2) to viruses T4 phage (E) (PDB ID. 1CZD).

The two sliding clamps investigated in this study are β clamp from *E. coli* and PCNA from *S. cerevisiae* (Baker's yeast). The crystal structures of both these proteins are

reported: the *E. coli* β clamp is a homodimer and the PCNA is a homotrimer (as can be seen from Figure 4.2 and 4.3).[12, 13] In both cases the monomers are attached in a head to tail fashion. The crystal structures of these proteins encircling the DNA have also been established.[14, 15] These structures show that there is an angle between the axis of the clamp and the helical axis of the DNA. This angle is 22° for the β clamp and 40° for the PCNA. Although the clamps involved in this study are homooligomers, hetero-oligomeric sliding clamps are also present in nature.[10]

According to the crystal structure, both of these clamps are in a closed conformation where the hydrophobic interaction at the area of contact between the monomers is responsible for the conformation. A single mutation at the area of contacts can have significant implication in the stability of the clamp.[16] Each monomer in the β clamp consists of six α helices and six β sheets. Each monomer of PCNA contains four α helices and four β sheets. The α helices are found at the inner surface of the ring while the β sheets are present in the outer surface of the rings. The diameters of the inner rings of the β clamp and the PCNA are 35 Å and 34 Å, respectively.[14, 15] This is much larger than the diameter of the B form of DNA (~21 Å).[17] Thus, the inner cavity of the ring is large enough to accommodate B-DNA comfortably.
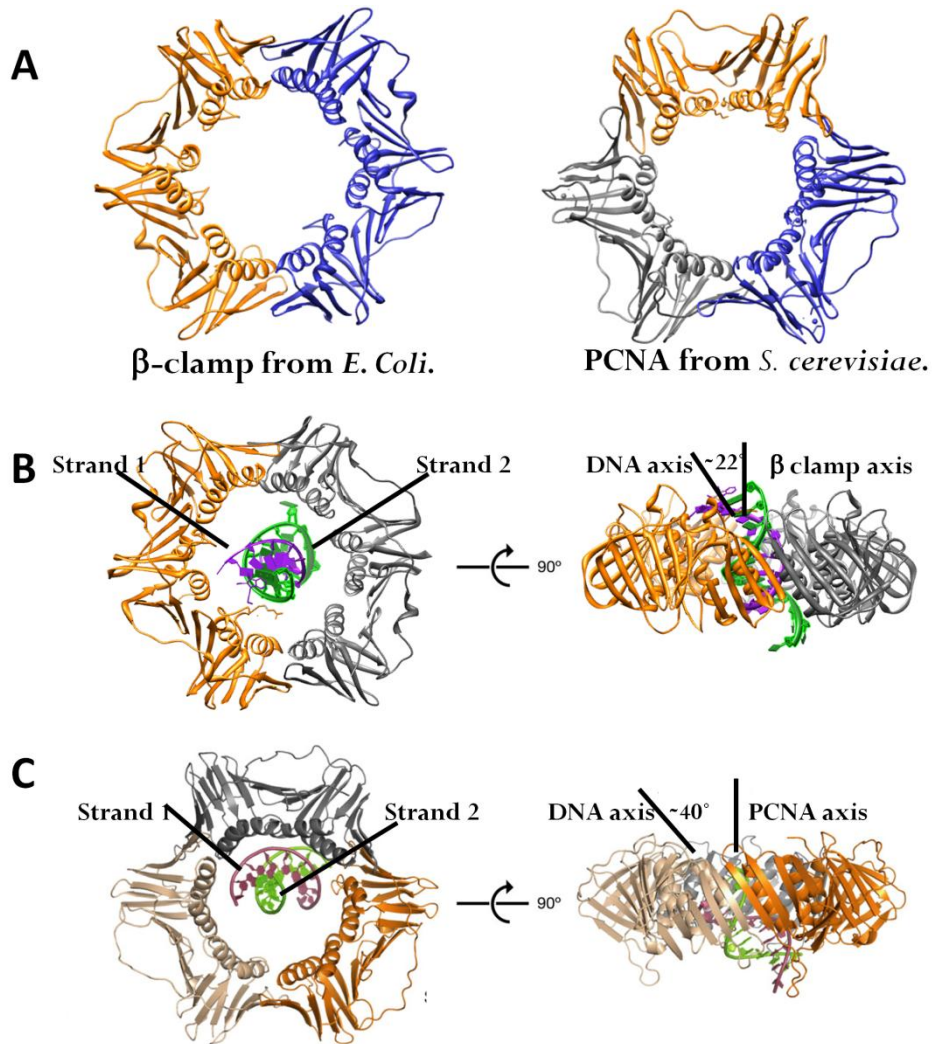
Figure 4.3. The crystal structure of (A) *E. coli* β clamp and (B) PCNA from *S. cerevisiae*. The crystal structure of the β with DNA (B) and the PCNA with DNA(C). The helical axis of the DNA creates an angle with the central axis of the clamp. These pictures were modified from Georgescu et al. and McNally et al.[14, 15] using the software Chimera.

While the crystal structure provides information on the conformation of the clamps, little information is available on the solution stability and dynamic behavior, which is crucial for a complete understanding of how the clamps work. Yao et al. reported the K_D for the monomerization equilibrium of the β clamp and PCNA: 61 pM

and 27 nM, respectively.[18] However, there are many problems with this paper including: the fact that the experiments and rationale behind the calculation of the dissociation constant of the β clamp are not explained, the units of the dissociation constant of the trimer to monomer equilibrium in PCNA should be nM^2 and not nM, and the analysis of the dissociation equilibrium is mathematically incorrect.[18] Other papers have shown that PCNA can exist as monomers at low concentrations, but no quantitative information about the dissociation equilibrium is provided. The very low K_D values for these clamp monomerizations indicate that the time evolution to the system to the equlibrium at nM concentration should be very slow. Any information about the time evolution of the system is also absent in these papers. In addition, different oligomeric states and presence of open and closed clamps in solution have been observed for the gp45 clamp from T4 phage.[19, 20] These open conformations and different oligomeric states can have very important implications in the pathway these clamps bind to clamp loader and get transported to DNA. The stability of these clamps are also very important for these binding pathways. The more stable complex will be harder to open when it interacts with the clamp loader and that can have important influence on the pathway of these interactions.

Not only are more experiments needed that examine both the solution stability and the dynamic behavior of the sliding clamps, but these experiments also need to be quantified. A major focus of this project is just that- investigating the monomerization equilibria as well as quantifying the spontaneous equilibrium between the open and closed structures. Even though the crystal structures show these proteins to be in the closed conformation, there is still the possibility that a small fraction of clamps are in the

open conformation. This open conformation can play an important role in the binding of the clamp loader and sequential binding around DNA. Therefore, proving the existence, or non-existence, of open clamps in solution and characterizing the conformational dynamics of these clamps is an important goal of this project. Furthermore, the presence of monomeric and oligomeric structures in these clamps can have very important implications on how they interact with the clamp loaders and other proteins. It has been proposed that β clamp and PCNA interact with the clamp loader in a similar way.[21] The different stability of these two clamps can indicate that they probably requires different amount of energy for the opening of the ring and may have different pathways of interaction with the clamp loaders.

To investigate these questions, the clamps were mutated and fluorescently labeled with TMR. Two different types of mutants for both β clamp and PCNA were created. In the first type, called single labeled or TMR1, one residue in each subunit close to the interface between two monomers was modified to a cysteine and labeled with TMR. In the second type of modifications, two amino acids in each monomer were mutated to cysteines and labeled with TMR. The two mutations were positioned to be at both the head and tail of each monomer so that the closed structure of the clamp is self quenched due to the dyes from each adjacent monomeric unit being close to each other and forming an H dimer.[22-25] Either opening of the ring or dissociation of the clamp to its monomeric form results in increased distance between the two dyes and recovery of fluorescence. In the single labeled samples, the dyes are far from one another in the closed form of the clamp and do not participate in H dimer formation, meaning that the brightness of each monomer and the total fluorescence intensity does not change due to ring opening or

149

dissociation. The monomerization equilibrium and the dynamics of ring opening and closing were studied using both of these probes and various fluorescence techniques including FCS, smFluorescence, fluorescence lifetime and steady state fluorescence.

4.2 Materials and methods

4.2.1. Modification of sliding clamps and fluorescence labeling. The mutation of the sliding clamps and labeling of these clamps with TMR dyes was carried out in Dr. Linda Bloom's lab at University of Florida, Gainesville. The experimental details in section 4.2.1.1, 4.2.1.2 and 4.2.2, and Figure 4.5 and 4.6 are courtesy of Lauren Douma, who carried out these experiments.

4.2.1.1. Modification and labeling of the PCNA. PCNA was modified by site-directed mutagenesis of the PCNA coding sequence using the QuickChange mutagenesis kit (Stratagene) and following manufacturer instructions. Cysteine residues 22, 68, and 81 were converted to Ser, and either ILE-181 or ILE-111 and 181 were modified to cysteine using this method. Wild type PCNA and the mutants were expressed in *Escherichia coli* BL121(DE3) cells, grown at 37˚C. The cells were grown to A_{600} of 0.6 - 0.7 and then the temperature was reduced to 15˚C and isopropyl β-D-1-thiogalactopyranoside was added to a final concentration of 1 mM to induce protein expression.[25] These *E. coli* cells were lysed using a French press. Lysate was cleared by centrifugation, and the precipitate after the addition of 0.2 g/ml ammonium sulfate to the clarified lysate was discarded. The precipitate after addition of additional ammonium sulfate (0.15 g/ml) to the supernatant was recovered through centrifugation and then resuspended in 20 mM Tris-HCl (pH = 7.5) buffer containing 0.5 mM EDTA, 50 mM NaCl, and 2 mM DTT and 10% (v/v) glycerol (Buffer B). The solution was dialyzed and then eluted with a sucrose gradient of 50-700 mM NaCl using Hi-Trap Q-Sepharose (GE Healthcare) columns. The PCNA was then further purified using S-Sepharose and MonoQ columns. The purified PCNA was

151

dialyzed against 30 mM HEPES (pH= 7.5) 150 mM NaCl, 8 mM MgCl$_2$ 2 mM DTT (buffer A) and stored in -80˚C.

The purified PCNAs I111C/I181C and I181C were incubated for 5 min at room temperature with 1 mM (final concentration) TCEP solution in Tris buffer (pH = 8.0). The PCNA/TCEP solution was then incubated with excess TMR-maleimmide at room temperature for four hours. The labeled protein was purified from the excess fluorophore using a Bio-rad P6 DG desalting column equilibrated with buffer A and then a Hi-Trap Q sepharose column. In the gel electrophoresis experiment, 1.7 nmol and 0.5 nmol of labeled PCNAwas run along with a ladder in a 12% SDS-PAGE gel. These clamps were run along with the marker to determine the molecular weight from the R_f value. The purity of the labeled protein was further checked via HPLC. After labeling, the I181C mutation is called single labeled PCNA or TMR1 PCNA, and the I111C/I181C modification is called double labeled PCNA or TMR2 PCNA.

4.2.1.2. Modification and labeling of the β clamp. The β clamp mutations were prepared by introducing mutations in the *dnaN* coding sequence by site directed mutagenesis and the proteins were expressed in *E. coli* BL21(DE3) cells.[24] The different mutations were I305C/C260S/C333S and R103C/ I305C/C260S/C333S. In both of these mutants, the surface cysteines were mutated to serines and a residue at the head or tail of the monomers was converted to cysteine so to bind to a TMR dye. The mutated β clamps were separated from the cell lysate using published protocol.[26, 27] The purified β clamps were labeled with TMR by incubation of a solution of the β clamp (~60 μM) and TMR maleimide (~1.67 mM) in 50 mM potassium phosphate buffer (pH = 7.4) containing 1

mM TCEP in room temperature for 2 hours and overnight at 4˚C. The excess fluorophore is removed the same way as described for the PCNA experiments. Purity of the labeled β clamp and PCNA were checked by both HPLC and gel electrophoresis. The HPLC chromatogram of the elution of β was monitored at both 560 nm absorption (TMR absorption) and 220 nm (absorption of protein backbone). The 220 nm absorbance was monitored to find the retention time of the clamps since the extinction coefficient at 280 nm is very low. Then, a chromatogram of just the TMR dye was obtained from HPLC under identical elution condition. A comparison of TMR and β clamp at 560 nm observation wavelength proves that there was no excess free TMR in the clamp solution. I305C/C260S/C333S and R103C/ I305C/C260S/C333S modifications after labeling to the TMR are called TMR1 and TMR2 β clamp samples, respectively.

The residues of both PCNA and β clamp that were mutated to cysteine and used for the attachment with the TMR are shown in green in Figure 4.4 panel A. TMR dyes in the TMR2 samples of both β and PCNA are in the H-dimer formation, formed due to stacking of the two dyes which quenches the fluorescence.[22, 23, 25, 28] A pictorial presentation of this H-dimer is shown in Figure 4.4 panel B. This figure is just a pictorial presentation of the H-dimer.

153
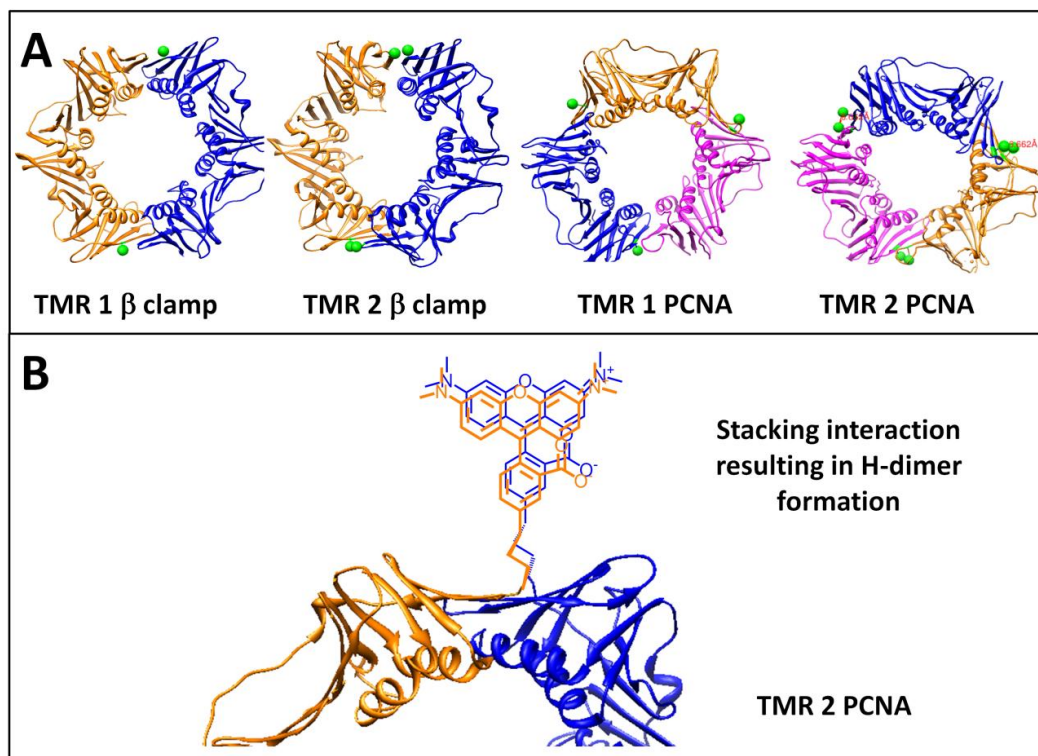
Figure 4.4. Positions of the mutations of both the β clamp and PCNA that were labeled with TMR (panel A). A pictorial presentation of the H-dimer: the stacking interaction that quenches the fluorescence (panel B).

4.2.2. Calculation of labeling efficiency. Concentrations of both the unlabeled clamps were measured using the Gill and von Hippel method.[29] In this method the absorbance of the unlabeled clamp is measured in both native and denaturing conditions, with the same concentration of protein used in both cases. The extinction coefficient at 280 nm under denaturing condition is determined from the wavelength dependent extinction coefficient of tyrosine, tryptophan and cysteine. The concentration of the protein is measured using this extinction coefficient and as the native protein should have the same concentration, the extinction coefficient of the native protein can then be

calculated. In our experiment, the extinction coefficient of β and PCNA were estimated to be 15000 and 6000 $M^{-1} cm^{-1}$, respectively. The β extinction coefficient is the same as that measured by Johanson et al.[27]

To measure the concentration of the TMR labeled samples, the extinction coefficient of the protein at 280 nm cannot be used. TMR has a large absorption in the ultra violet range of the light spectrum and the very low extinction coefficient of these clamps makes the calculation of concentrations based on the absorbance at 280 nm erroneous at best. Thus, concentrations of these proteins are determined using either the Lowry or Bradford assay.[30, 31] In the Bradford assay, the protein was treated with Coumassin Brilliant blue G-250 and the absorbance at 595 nm was measured.[30] In the Lowry assay, the protein was treated with copper and Folin reagent and the absorbance was measured at 750 nm.[31] The standard curve of the absorbance at either 595 nm or 750 nm (depending on the method) was prepared for both β clamp and PCNA using the unlabeled clamps, whose concentration were measured using the Gill and von Hippel method. These standard curves were then used as the calibration curve to measure the concentration of the labeled clamps. The fluorophore concentration corresponding to a known clamp concentration was then determined by measuring the absorbance at the maxima of the fluorophore band under denaturing condition and using the extinction coefficient of TMR (95000 $M^{-1}cm^{-1}$ at 555 nm).

4.2.3. Estimation of the diffusion constants. Diffusion constants of the monomeric and oligomeric sliding clamps were estimated using the program Hydropro.[32, 33] Hydropro is designed to calculate the hydrodynamic properties of the proteins and

DNA based on their atomic level structure or coarse-grained residue-level structure. The input for the calculation of the hydrodynamic properties of the sliding clamps were the crystal structure of the clamp, the molecular weight of the corresponding unit, the density of the solution, and the partial specific volume of the protein. The molecular weight of the trimer and monomer of the PCNA 88036 Da and 29345 Da, respecitively, while the molecular weight of the dimer and monomer of β clamp are 81261 Da and 40630 Da, respectively. As stated previously, the crystal structure of β clamp is a homodimer. The crystal structure of the monomeric β was created by deleting one of the monomeric units. Similarly, the crystal structure of monomeric PCNA was created by deleting two of the monomers from the original trimeric PDB structure of the PCNA. These modified crystal structures were created using the software Chimera. The input for the density of the solution was assumed to be 1 g/cm^3. The partial specific volume of the protein was calculated from the reciprocal of the average density of the protein and the average density of the protein was assumed to be[34]

$$\rho(M) = \left[1.410 + 0.145 \times Exp\left(- {M(kDa)}/{13} \right) \right] \tag{4.1}$$

The estimated diffusion constants for the trimeric and monomeric PCNA and dimeric and monomeric β were 54.65 μm^2/s and 71.49 μm^2/s, 56.67 μm^2/s and 72.10 μm^2/s, respectively.

4.2.4. Fluorescence correlation spectroscopy (FCS). FCS is a method where the temporal fluctuations of intensity of a fluorophore diffusing in and out of an optically restricted inhomogeneously illuminated confocal volume are analyzed and rates of

different processes that can cause these fluctuations are determined from a correlation decay.[35, 36] The detailed description of the theory and instrumentation of FCS is given in section 1.3.4. In absence of a secondary process that produces intensity fluctuations, the autocorrelation decay is indicative only of diffusion. Under the approximation of a Gaussian volume, the autocorrelation decay of a single species can be fitted to equation 1.23 provided the optical parameters r and z are known. The result of this fitting is the determination of the diffusion coefficient of that single species.

4.2.4.1. FCS of PCNA samples: The autocorrelation decays of 1 nM, 10 nM and 100 nM TMR1 PCNA samples in the presence of 1.5 μM BSA were taken immediately after dilution from a concentrated stock solution as well as a function of incubation time. The time dependent autocorrelation decays of 1 nM TMR1 PCNA were also obtained. Each of these autocorrelation involved 5 minutes of acquisition time. There was a gap of 5 minutes between successive runs of the autocorrelations until 2 hours of incubation time, after which the gap time was increased to 10 minutes. Autocorrelation decays of TMR1 PCNA at 1 nM and 10 nM were measured as a function of time with a laser power of ~100 μW. The autocorrelation decay of 250~300 nM TMR1 PCNA sample in presence of 1.5 μM BSA was used to calculate the confocal parameters. To obtain the value of dissociation constant (K_D), TMR1 PCNA was diluted from 10 nM to 100 nM concentration in 10 nM intervals and the FCS decays measured after 24 hours of incubation time.

4.2.4.1.1. Fitting with apparent D. In the FCS experiments involving PCNA, the values of r and z are determined from the fitting of an autocorrelation decay of 250/300

157

nM TMR1 PCNA. This concentration of PCNA is much higher than the expected value
of the dissociation constant (K_D) and thus, the autocorrelation decay should be indicative
of the trimer-only PCNA. The diffusion coefficient of the trimeric PCNA was assumed to
be 54.65 μm^2/s, as derived from the Hydropro calculations. The other autocorrelation
decays at lower concentrations and as a function of time were fitted with the r and z from
the 250/300 nM fit. At concentrations lower than 250 nM, PCNA may dissociate into
different oligomeric forms that have different diffusion coefficients. Under these
circumstances, the obtained diffusion coefficient from the fit of these autocorrelations
using a single component model will have contribution from diffusion of all of these
species. Therefore, the diffusion coefficients obtained from the fit are not actual
diffusion coefficients and are referred to as apparent diffusion coefficient (D_{app}s).

4.2.4.1.2. Fitting with two-component model. The autocorrelation decays of
TMR1 PCNA were further analyzed with a two component diffusion model. The fitting
equation included a triplet term. The final equation is defined as,

$$G(\tau) = \frac{\left(1 - f + f \times Exp\left[-\tau/\tau_{triplet}\right]\right) \times \left[xN_1 G_1(\tau) + (3x + 6x^2)N_3 G_3(\tau)\right]}{(xN_1 + 3xN_3)^2}$$

(4.2)

In the above equation, f and $\tau_{triplet}$ present the fraction of particle in the triplet state
and the triplet relaxation time. The triplet relaxation time of these fits was fixed at 15 μs
and f is shared between all the individual autocorrelation decays. N_1 and N_3 are the
number of monomeric and trimeric PCNA in the confocal volume. x is the average
fraction of labeling. The derivation of this equation is discussed in appendix B. $G_1(\tau)$ and

158

$G_3(\tau)$ present the autocorrelation decay of monomeric and trimeric PCNA, respectively, and are given by,

$$G_1(\tau) = \left(1 + \frac{4 \times 71.49 \times \tau}{r^2}\right)^{-1} \left(1 + \frac{4 \times 71.49 \times \tau}{z^2}\right)^{-\frac{1}{2}} \tag{4.3}$$

$$G_3(\tau) = \left(1 + \frac{4 \times 54.65 \times \tau}{r^2}\right)^{-1} \left(1 + \frac{4 \times 54.65 \times \tau}{z^2}\right)^{-\frac{1}{2}} \tag{4.4}$$

In the above equations, the diffusion constant of the monomeric and trimeric PCNA are assumed to be 71.49 μm^2/s and 54.65 μm^2/s , respectively, based on Hydropro calculations. The time dependent evolution of the autocorrelation decays of 1 nM PCNA samples for each days experiment was then globally fitted with equation 4.5, keeping r and z constant. The value of the optical parameters were obtained from the single diffusion constant fit of 250/300 nM PCNA (TMR1) as described earlier. The labeling efficiency of TMR1 PCNA is 71.3%. Thus, for the fitting of TMR1 PCNA samples with a dual component correlation decay, equation 4.2 can be transformed to,

$$G(\tau) = \frac{\left(1 - f + f \times Exp\left[-\tau/\tau_{triplet}\right]\right) \times \left[0.713 \times N_1 \times G_1(\tau) + 5.189 \times N_3 \times G_3(\tau)\right]}{(0.713 \times N_1 + 2.139 \times N_3)^2} \tag{4.5}$$

The result of this fit is N_1 and N_3, the average number of monomeric and trimeic PCNA in the confocal volume. These number of molecules of various species in the confocal volume were then converted to the concentration of the corresponding species using the value of the confocal volume, obtained from the G(0) of the autocorrelation decay of 3.55 nM TAMRA in water.

4.2.4.2. FCS of β clamp samples. Fluorescence correlation decays of 1 nM, 5

nM, 20 nM TMR1 PCNA and a mixture of 5 nM TMR1 PCNA and 500 nM wt PCNA

were measured after 3 hours of incubation time. The perfusion chambers used to contain

the sample while acquiring the intensity data were incubated with 1.5 μM BSA prior to

the start of the data acquisition. Then, correlation decays of 125 pM, 250 pM, 500 pM

and 1 nM TMR1 β clamp solution were taken right after dilution from concentrated stock

solution and again after 18 hours of incubation time. These decays were overlapped to

show that any changes in the diffusion at these concentrations were insignificant. To

obtain information about the conformational dynamics of ring opening and closing in β

clamp, autocorrelation decays of the clamp at 1 nM concentration were acquired for both

TMR1 and TMR2 samples.

4.2.4.2.1. Decoupling conformational dynamics from diffusion for β clamp.

The fluorescence intensity and brightness of TMR1 β clamp sample is independent of

any conformational change involving ring opening and closing. Thus, the resulting

autocorrelation decay of this sample can be described by a diffusion only model.

However, the fluctuations in fluorescence intensity of the TMR2 β clamp sample can

originate from both the conformational dynamics and diffusion. In the closed

conformation, the TMR is in an H-dimer configuration and is quenched. The opening of

the ring causes increase in the distance between the two fluorophores, disruption of the

H-dimer and increase in fluorescence. Thus, the autocorrelation decay of this sample

includes both the kinetic and diffusion components.[37] To obtain the kinetic information,

these two autocorrelation decays have been analyzed using the method described in section 1.3.4.3.2.

4.2.5. smFluorescence. Single molecule (sm) fluorescence traces of the 10 pM β clamp were measured using the confocal set up described in section 1.3.5 with a laser power of 150 μW. The quenched β clamp (TMR2) was diluted to a final concentration of 10 pM and the time evolution of the single molecule peaks were observed as a function of time. At time zero, the clamps were self quenched. As time progresses, though, more and more dimers form monomers, as is expected to happen if the concentration is below the K_D value. The monomers are bright and should show an increase in the frequency of sm peaks. The time evolution of the smFluorescence signals was then analyzed in two ways. The first one is by creating frequency plots of the frequency of appearance vs. counts/ms. The Y axis of this plot was converted to log scale to better illustrate the data since most of the single molecule traces contain a small background signal contributes to the majority of the acquired intensity data. The second way this data was analyzed involved defining a threshold for the single molecule peak and then counting the number of times there was a peak above that threshold.

4.2.6. Fluorescence lifetime and steady state fluorescence. The extent of quenching by the formation of an H-dimer in double labeled TMR2 clamps was measured by both time resolved and steady state fluorescence methods. The technique, theory and analysis of the fluorescence lifetime is described in section 1.3.3. The intensity decay of 1 μM of the single labeled TMR1 and double labeled TMR2 samples of both PCNA and β clamp were measured with the emission polarizer kept at a constant

angle, the magic angle (54.7˚), compared to the vertical orientation (0˚) of the excitation polarizer. Analysis of the decay provided the lifetime of the samples. In the steady state method, the extent of quenching was determined using a QuantaMaster-4/2005SE spectrofluorometer (PTI, NJ). A concentrated sample of SDS was added to the quenched clamp solution and the fluorescence intensities at 565 nm were measured before and after the denaturation of the protein. The ratio of these two intensities is the extent of quenching by the H-dimer formation.

4.3 Results

4.3.1. Percentage of labeling. The percentage of labeling of the sliding clamp samples has been calculated from the concentration of the labeled protein (determined by Lowry assay or Bradford assay) and concentration of the labeled fluorophore in the denaturing condition as described in section 3.2.2. The labeling efficiencies of these samples are presented in table 4.1.

Type of sliding clamp	Mutation	Conc. of protein (μM)	Conc. of TMR (μM)	% labeling efficiency
TMR1 β	I305C	27.17	36.95	68
TMR2 β	I305C R103C	11.6	49.43	128
TMR1 PCNA	I181C	15.0	32.1	71.3
TMR2 PCNA	I111C I181C	13.2	71.2	89.9

Table 4.1. The labeling efficiency of the sliding clamps. The clamps were modified with TAMRA.

The purity of the labeling was checked by HPLC and denaturing gel electrophoresis. Figure 4.5 shows the HPLC chromatogram obtained after labeling the β clamp with TMR. The first run was monitored at 220 nm (protein backbone modification peak) while the second and third run was monitored at 560 nm (TMR peak). The first two runs show the purified protein and the third illustrates free TMR. The absence of TMR

peaks in the β clamp chromatogram shows that there is no excess free dye after the
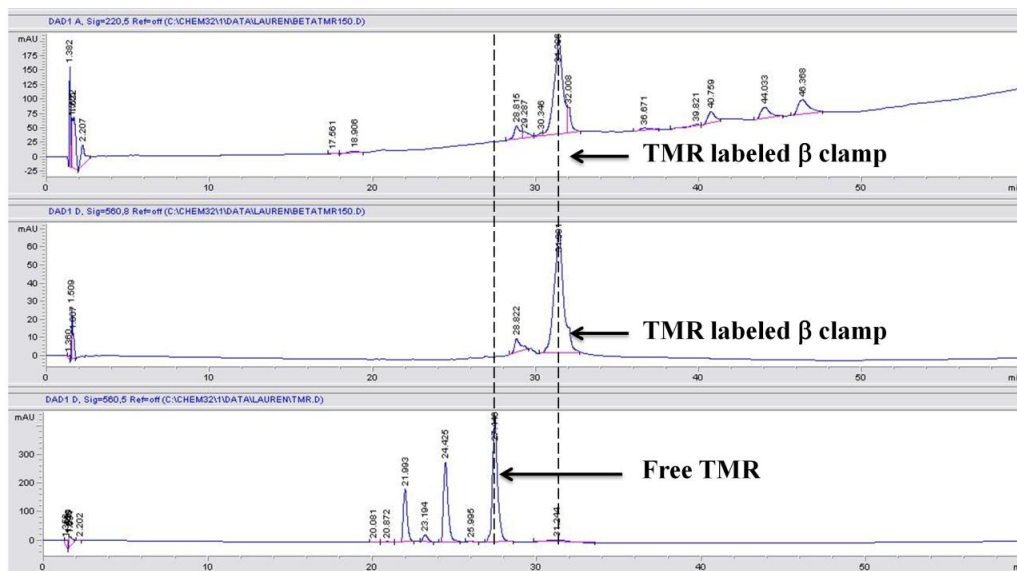
separation column.

Figure 4.5. Chromatogram of labeled β clamp (monitored at 220 nm), labeled β clamp (monitored at 560 nm), free TMR (monitored at 560 nm) (top to bottom). β clamp elutes around 32 minutes and when the chromatogram was monitored at 560 nm, contained no peak corresponding to free TMR. This experiment was carried out by Lauren Douma in Dr. Linda Bloom's lab at University of Florida, Gainesville.

The purified labeled clamps were subjected to 12% SDS-PAGE electrophoresis

and the gel electrophoresis images are shown in Figure 4.6. Panel A shows the image for

the PCNA and panel B demonstrates the image for the β clamp. In panel A, the three

lanes are, from left to right: 0.5 nmol labeled PCNA, 1.7 nmol labeled PCNA, and a

molecular weight standard. The PCNA gel shows that the labeled PCNA has a similar

molecular weight as that of the unlabeled samples (~ 29 kDa). In panel B the lanes for the

β clamp gel were loaded (from left to right) with a molecular weight standard, 1 nmol,

0.5 nmol, and 0.25 nmol of unlabeled β clamp and 0.25 nmol labeled β clamp. The β

clamp gel shows that the labeled sample traverses the same distance as that of the

unlabeled β and has the same expected molecular weight (~ 40 kDa)
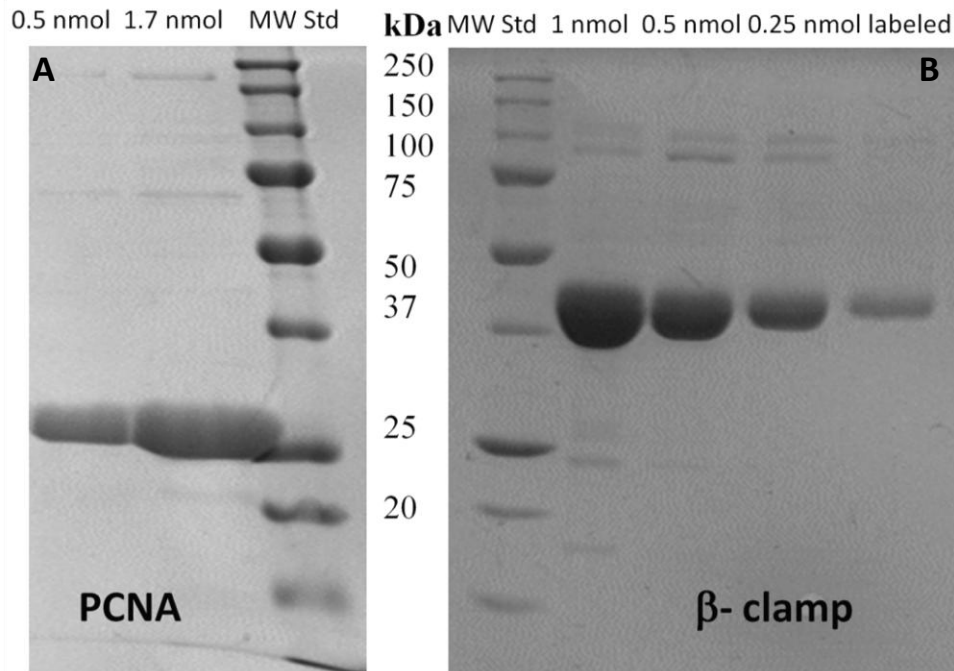
Figure 4.6. Gel electrophoresis image of the purified labeled PCNA (left panel) and β clamp (right panel). Left panel: the three lanes are, from left to right: 0.5 nmol labeled PCNA, 1.7 nmol labeled PCNA, and a molecular weight standard. The PCNA gel shows that the labeled PCNA has a similar molecular weight as that of the unlabeled samples (~ 29 kDa). Right panel: the lanes for the β clamp gel were loaded (from left to right) with a molecular weight standard, 1 nmol, 0.5 nmol, and 0.25 nmol of unlabeled β clamp and 0.25 nmol labeled β clamp. The β clamp gel shows that the labeled sample traverses the same distance as that of the unlabeled β and has the same expected molecular weight (~ 40 kDa). This experiment was carried out by Lauren Douma in Dr. Linda Bloom's lab at University of Florida, Gainesville.

4.3.2. H-Dimer formation and quenching of fluorescence.

4.3.2.1. Absorbance. The formation of H-dimers in the TMR2 clamp is associated with quenching of fluorescence and the appearance of a blue shifted absorption peak.[22, 23] Figure 4.7 shows a plot of the absorbance spectra of both the TMR2 (red) and TMR1 (black) modifications, panel A of β clamp and panel B of PCNA. In both cases, the clear blue shifted peak indicates the formation of an H-dimer.
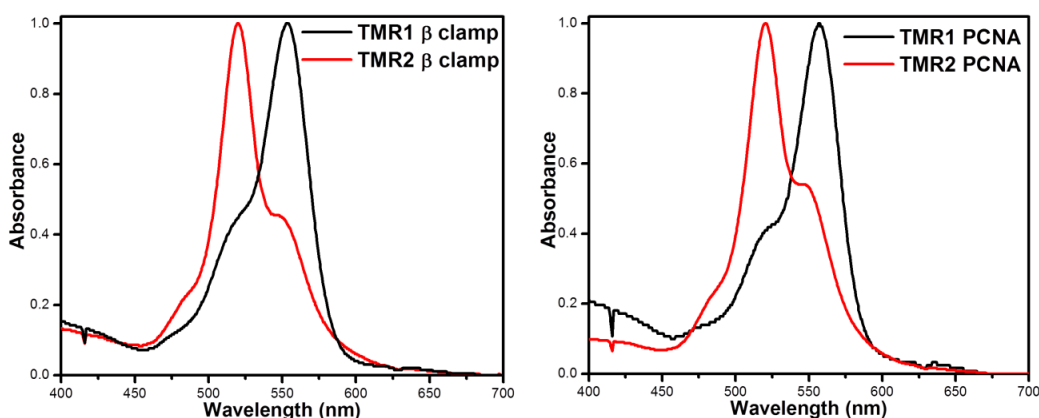

Figure 4.7. Absorption spectra of TMR1 (black) and TMR2 (red) modifications of β clamp (left panel) and PCNA (right panel). The blue shifted peaks in the TMR2 modification of the clamps are indicative of H-dimer formation.

4.3.2.2. Quenching from lifetime and steady state fluorescence. The time resolved intensity decays of TAMRA (green), single labeled TMR1 β clamp (red), single labeled TMR1 PCNA (black), double labeled TMR2 β clamp (purple), double labeled TMR2 PCNA (blue) and the instrument response function (IRF) (orange) are plotted together in Figure 4.8. This figure clearly shows that the TMR2 versions of both the β clamp and PCNA have a much shorter lifetime compared to the TMR1 versions. This can be seen from the calculated lifetimes, Table 4.2. The extent of quenching was also

studied using steady state fluorescence by measuring the changes in fluorescence addition

before and after addition of SDS to the protein. The fluorescence intensity of TMR2 β

clamp and TMR2 PCNA increased approximately 24 times on addition of SDS to the

clamp solution. These increases in fluorescence intensity of the TMR2 clamp samples on

addition of SDS are indicative of the extent of quenching by the formation of the H-
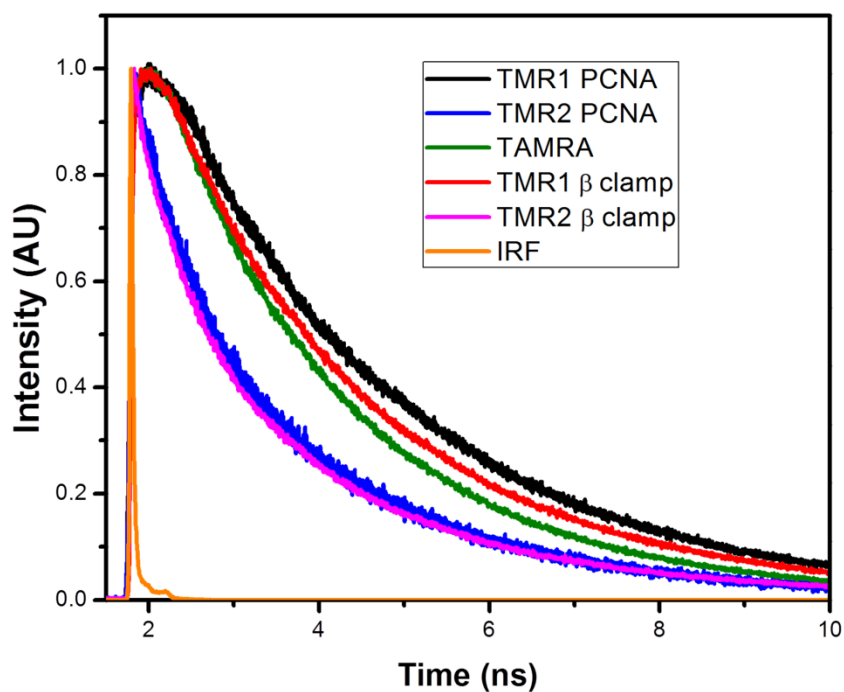
dimer.

Figure 4.8. The fluorescence intensity decays of TAMRA (green), single labeled TMR1 β clamp (red), single labeled TMR1 PCNA (black), double labeled TMR2 β clamp (purple), double labeled TMR2 PCNA (blue), and instrument response function (IRF) (orange). The faster intensity decay is indicative of smaller lifetime. TMR2 samples have shorter lifetime than the TMR1 samples.

Sample	A_1	τ_1 (ns)	A_2	τ_2 (ns)	A_3	τ_3 (ns)	$\langle\tau\rangle$ (ns)
TAMRA dye	71.16	2.54	28.84	1.37			2.20
TMR1 PCNA	100	2.81					2.81
TMR2 PCNA	44.0	2.5	28.1	0.7	27.9	0.12	1.33
TMR1 β clamp	81.52	2.78	18.48	1.04			2.46
TMR2 β clamp	30.83	2.74	28.47	0.94	40.7	0.12	1.16

Table 4.2. Average lifetime and fitting parameters (sum of exponentials) of the intensity decays of the sliding clamps from the intensity decays showed in Figure 4.8.

4.3.3. Results of PCNA monomerization experiments. The monomerization of PCNA was followed using fluorescence correlation experiments. The autocorrelation decays of TMR1 PCNA were measured as a function of time and concentration. This data was then fitted with a single diffusion constant model. These diffusion coefficients were then plotted against concentration as a function of time (Figure 4.9 panel A) or against time as a function of concentration (panel B). Panel A clearly shows that with increasing concentration, the increase in the apparent diffusion constant (D_{app}) over time is much smaller. The other important thing to notice is that even for the first set of correlation decays (time zero), the D_{app} of the 1 nM sample is larger than that of the 100 nM sample.
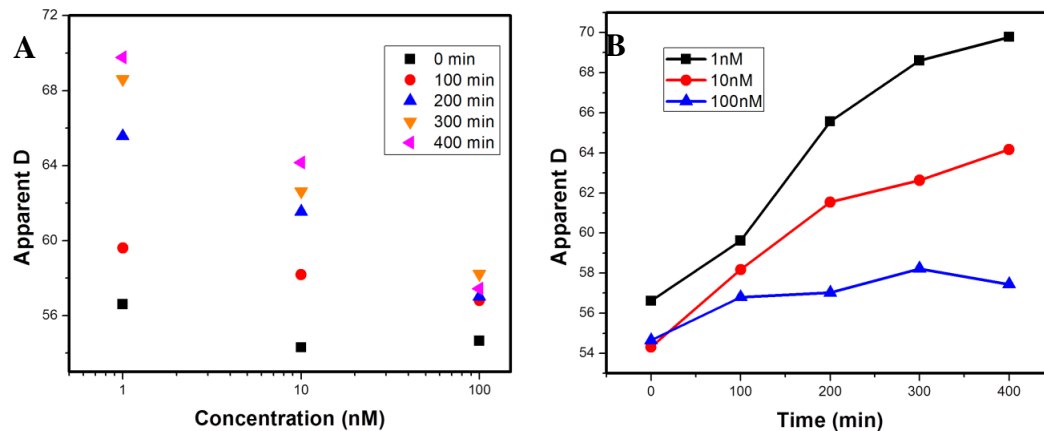
Figure 4.9. The apparent diffusion constant of TMR1 PCNA as a function of concentration (panel A) and as a function of time (panel B). The D_{app}s increase with time, with the extent of increase most prominent for the 1 nM sample.

The changes in the apparent diffusion coefficients were the largest for the 1 nM concentration. Therefore, the autocorrelation decays of the 1 nM sample were collected more intensively with a much shorter time gap between the measurements for a total of 7 hours of incubation time. The experiment was repeated four times and the average of these four experiments are plotted as a function of time in Figure 4.10. This figure clearly shows an increase in the D_{app}s of the 1 nM sample over time.
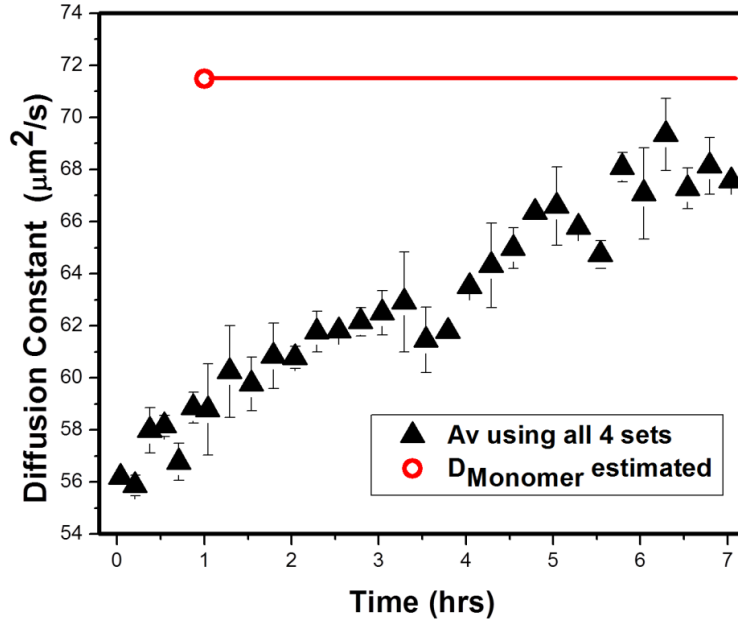
Figure 4.10. Increase in the apparent diffusion constants (black triangles) of TMR1 PCNA as a function of time. The red line presents the diffusion coefficient of monomeric PCNA estimated from Hydropro.

The increase in the apparent diffusion coefficient is indicative of the fact that with more time, more monomers form. The monomeric PCNA is smaller in size compared to the trimeric PCNA and has a faster diffusion, as can be seen from the calculated diffusion coefficients of the monomeric and trimeric PCNA. Although Figure 4.9 and Figure 4.10 indicate that with increasing incubation time more and more monomers are formed, the D_{app} analysis cannot provide any information about how the concentration of the monomeric and trimeric PCNA changes with time. To calculate the number of monomeric and trimeric PCNA molecules in the confocal volume, all the individual autocorrelation decays of the 1 nM PCNA solution were globally fitted with equation 4.5. The result of this fitting is the determination of N_1 and N_3, the number of species of the

monomer and trimer, respectively, in the confocal volume. N_1 and N_3 for four sets of the 1

nM sample correlation experiments are plotted in Figure 4.10. The N_1 increases with

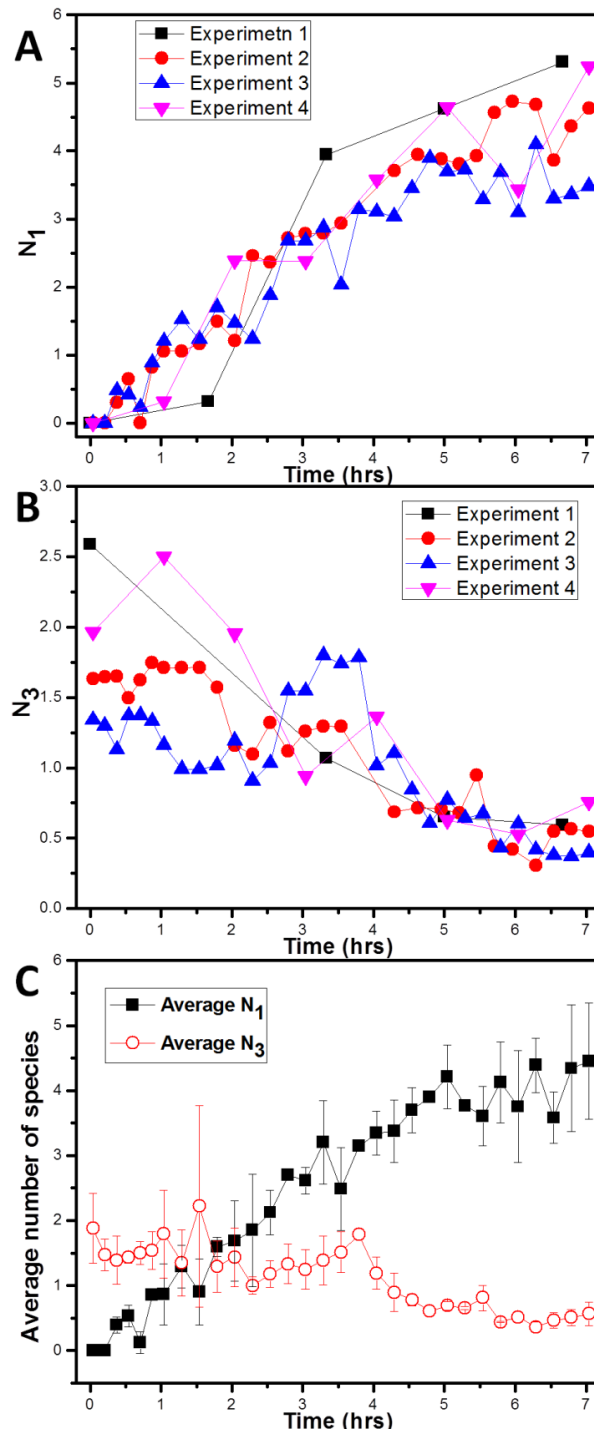time as N_3 decreases with increasing time.

Figure 4.11. Plot of N_1 (A) and N_3 (B) for the four set of time dependent 1 nM TMR1 PCNA autocorrelation experiments. N_1 increases and N_3 decreases with time, showing monomerization of the protein at a 1 nM concentration. The average N_1 (black square) and N_3 (red circle) are shown in panel C.

172

Another way of analyzing the data is to calculate the fraction of monomers in the confocal volume. The fraction of monomers is defined as $N_1/(N_1+3N_3)$. The increase in the average fraction of monomers for 1 nM of PCNA is presented in Figure 4.12. This fraction of monomer plot shows that even after seven hours of incubation, the fraction does not reach equilibrium.
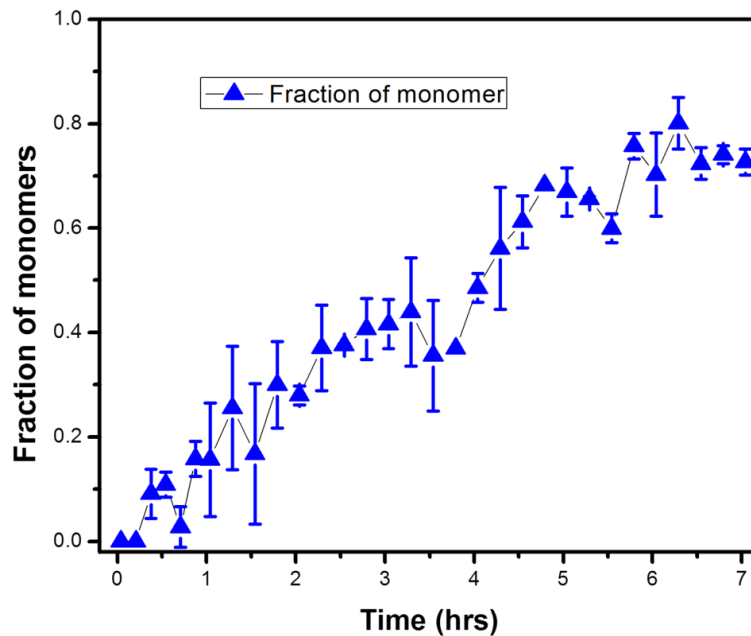
Figure 4.12. Average fraction of monomer [$N_1/(N_1+3N_3)$] of PCNA as a function of time when the initial concentration of the trimer was 1 nM.

One thing to be aware of in these experiments is that the low concentrations used can result in a loss of protein over the incubation time. To investigate any potential loss of protein, the total number of monomers inside the confocal volume (N_1+3N_3) throughout the course of the experiment can be calculated and should not change throughout the experiment. If protein is lost during incubation, then the total number of

173

monomers will decrease. Figure 4.13 shows the total number of monomers plotted as a function of time for the four sets of experiments. This figure clearly illustrates that though the number of total monomers fluctuates around a mean value, it does not show any increase or decrease with time.
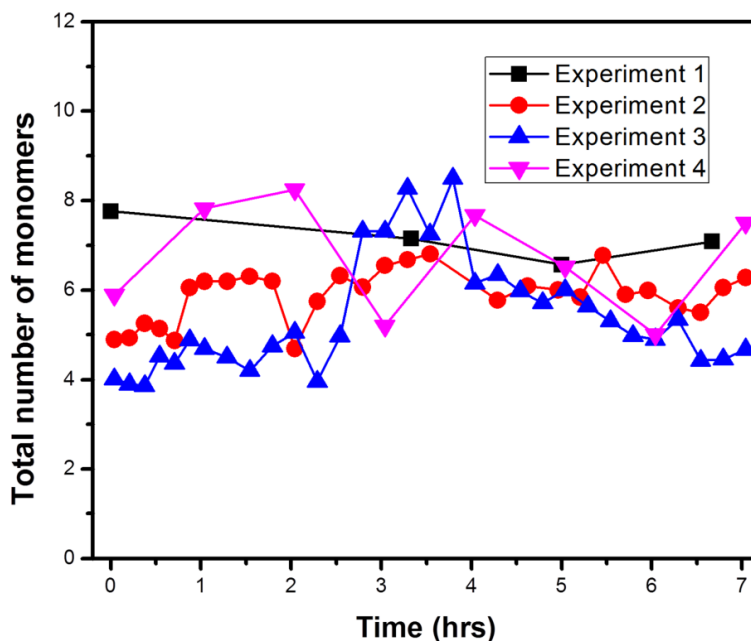
Figure 4.13. The total number of monomers (N_1+3N_3) of PCNA as a function of time for the four sets of experiments. The data shows that the total number of monomers fluctuate around a mean value but is constant over time.

Since the number of PCNA monomers and trimers has been calculated as a function of time for the 1 nM time dependent experiments, the concentration of each species can then be determined by using the number of molecules of each species (N_1 and N_3) and the volume (V) of the confocal, as shown in this equation,

$$C = n/(N_A \times V)$$ (4.6)

In this relation, n and N_A are the number of molecules in the confocal volume and Avogadro's number, respectively. The volume (V) was calculated from the autocorrelation decay of 3.55 nM TAMRA and found to be 5.38 fL. The average concentrations of the monomeric (C_1) and trimeric (C_3) PCNA as a function of the time have been plotted in Figure 4.14.
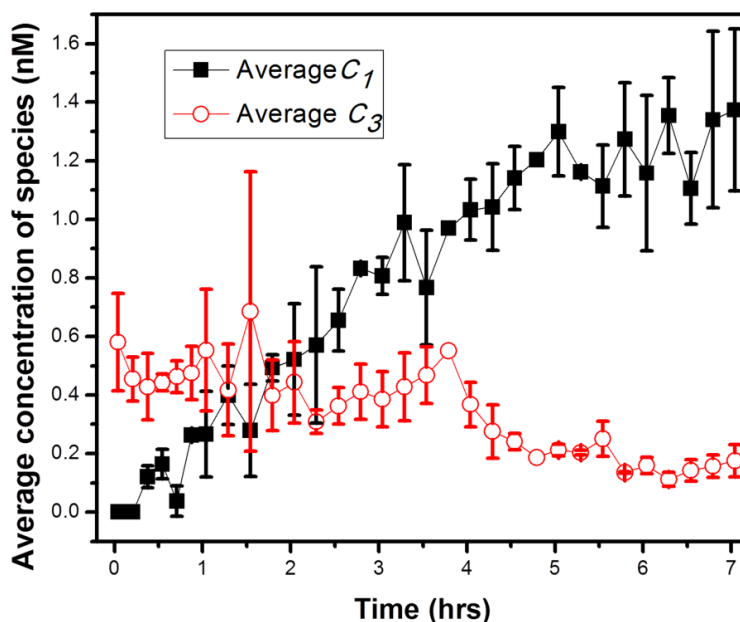
Figure 4.14. Time dependent evolution of the concentrations of the monomers (black square) and trimers (red circles) of PCNA for 1 nM PCNA concentration experiments.

The rates of association and dissociation of the trimer to monomer equilibrium can be calculated from the time evolution of the monomers of PCNA. However, the solution of the differential equation of the trimer to monomer equilibrium is a numeric one. Thus, to estimate the rates of association and dissociation, one of the following parameters, the dissociation constant (K_D), rates of association (k_2) or rates of dissociation (k_1), has to be known. To achieve this, the 10 nM to 100 nM TMR1 PCNA

autocorrelation decays after 24 of incubation hours were fitted with equation 4.5. The result of this analysis was the estimation of N_1 and N_3 at each PCNA concentration after 24 hours of incubation time. Then, N_1 and N_3 were converted to the corresponding concentration (monomer: C_1 and trimer: C_3). Then, the dissociation constant was calculated from the relation, $K_D = C_1^3/C_3$. The average value of K_D obtained using this process was $35\times10^3 \pm 11\times10^3$ nM^2. The plot of the total number of monomers (N_1+3N_3) as a function of concentration after 24 hours of incubation is plotted on Figure 4.15. This figure shows that the total number of monomers (black squares) of TMR1 PCNA increases linearly (red line) with concentration. This is further proof that the protein at these concentrations is not lost even after 24 hours of incubation.
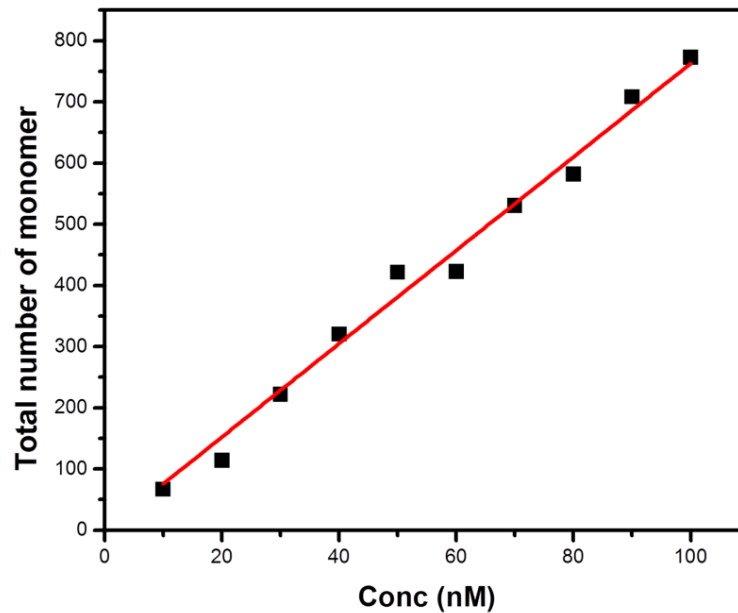

Figure 4.15. Total number of monomers (N_1+3N_3) (black squares) of PCNA as a function of concentration after 24 hours of incubation. The red line presents the linear fit and has a slope of 7.6 ± 0.1. This figure presents the fact that the protein is not lost during the incubation time.

The evolution of the concentration of the monomer was overlapped with the numeric solution of the trimer-monomer equilibrium for different association rates for the calculated K_D value of 35×10^3 nM^2. Figure 3.15 shows the evolution of the concentration of the PCNA monomers (black square) as a function of time similar to Figure 4.14. The purple, blue and red line present simulations of the concentration of monomeric PCNA when the association rates (k_2) are 1×10^{-8} nM^{-2} s^{-1}, 7.8×10^{-9} nM^{-2} s^{-1} and 6×10^{-9} nM^{-2} s^{-1}, respectively, and the K_D is 35×10^3 nM^2. This plot shows that the k_2 value of 7.8×10^{-9} nM^{-2}s^{-1} is the best match to the experimental data amongst the three choices at the given K_D. These values of k_2 were chosen in such an way that the time evolution of the monomers can be simulated at the given K_D. This combination of K_D and k_2 results in the dissociation rate (k_1) of 2.73×10^{-5} s^{-1} and a lifetime of ~10 hours.
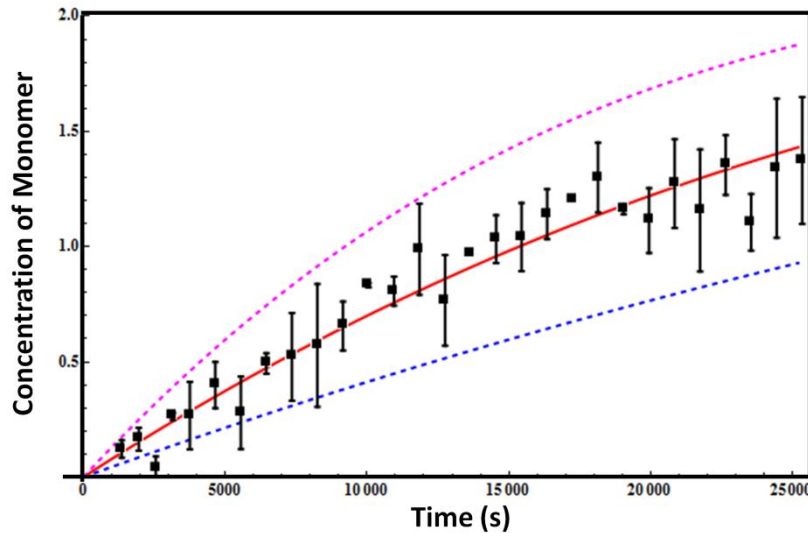
Figure 4.16. The overlap of the concentrations of PCNA monomers as a function of time (black squares) for the 1 nM PCNA experiments and simulations of the evolution of monomers of PCNA. The purple, blue and red line presents the concentration of monomeric PCNA when the association rates are 1×10^{-9} nM^{-2} s^{-1}, 7.8×10^{-9} nM^{-2} s^{-1} and 6×10^{-9} nM^{-2} s^{-1}, respectively, and the K_D is 35×10^3 nM^2. The red line shows the best overlap.

177

4.3.4. Results for the β clamp monomerization experiments. The

monomerization of the β clamp was investigated using both FCS and smFluorescence

methods. The data and results are presented below.

4.3.4.1. Correlation experiments. The monomerization of the β clamp was

followed using FCS autocorrelation decays as a function of time and concentration.

These experiments were similar to the FCS experiments described for PCNA. Figure 4.17

shows the overlap of the correlation of 1 nM (red), 5 nM (green), 20 nM labeled β (blue),

a mixture of 5 nM labeled with 500 nM unlabeled β (magenta), and the TMR dye (black)

after 3 hours of incubation time. The complete overlap of these autocorrelation suggests

that at these concentrations the clamps are not monomeric and exist as dimers.
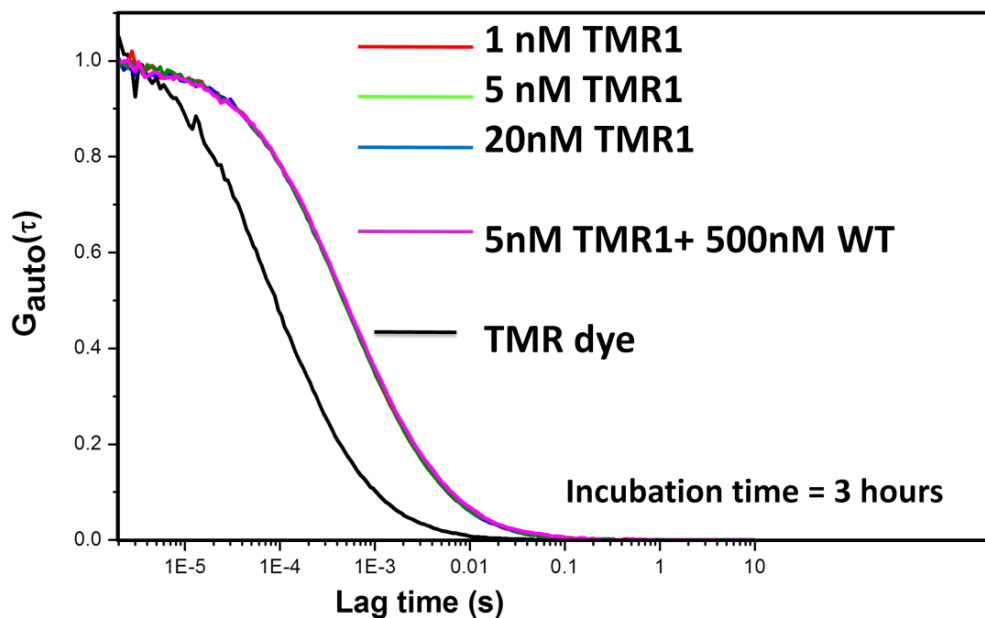
Figure 4.17. Overlap of autocorrelations of β clamp at 5 nM to 500 nM concentration.
The figure presents the normalized correlation decays of 1 nM (red), 5 nM (green), and
20 nM labeled β (blue), 5 nM labeled with 500 nM unlabeled β (magenta), and the TMR
dye (black) after 3 hours of incubation time.

178

As Figure 4.17 indicates, there is no significant monomerization of the β clamp at the concentration levels measured. This was not completely surprising because the β clamp is supposed to be more stable than PCNA. Hence, to see monomerization, the concentration of the β clamp measured as a function of the time would need to be lower than those concentrations used for PCNA monomerization experiments. Figure 4.18 A presents the overlap of normalized autocorrelation decays of TAMRA (black), and 125 pM (red), 250 pM (blue), 500 pM (teal) and 1 nM (magenta) TMR1 β clamp right after dilution and after 18 hours of incubation time. These decays overlap with each other. The correlation of the clamp at 125 pM TMR1 β at zero (black) and 19 hours of incubation time (red) are overlapped and presented in Figure 4.18 B.
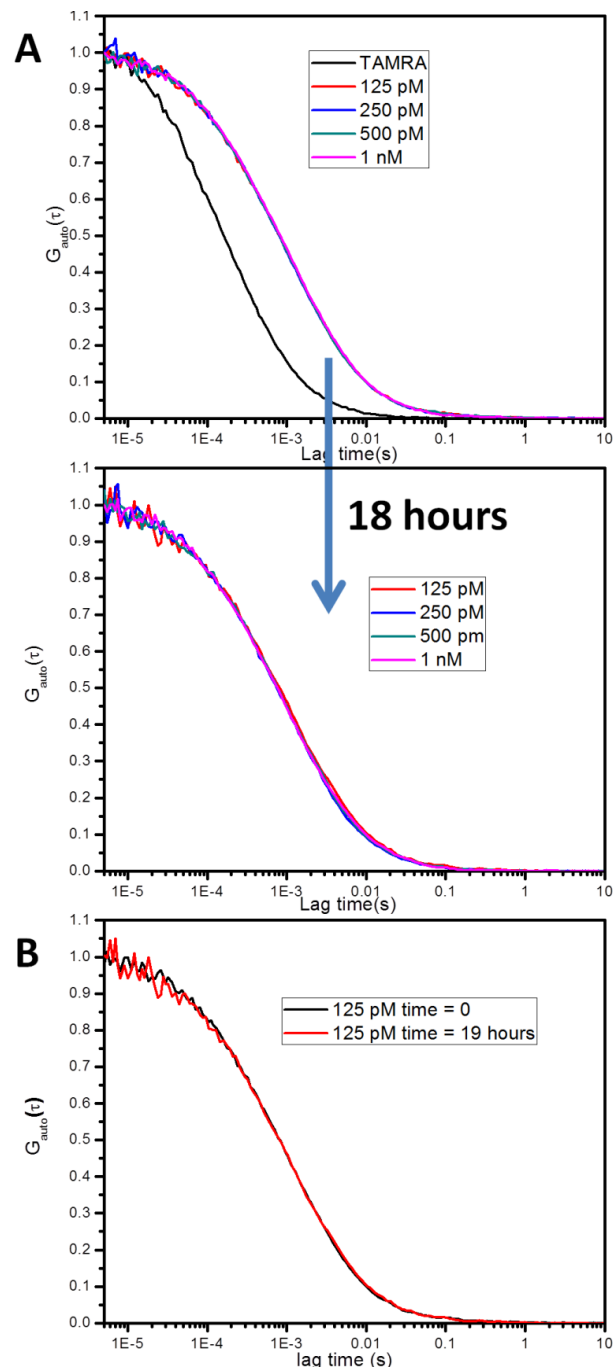
Figure 4.18. Panel A: the overlap of normalized autocorrelation decays of TAMRA (black), and 125 pM (red), 250 pM (blue), 500 pM (teal) and 1 nM (magenta) TMR1 β clamp at time zero and after 18 hours of incubation. Panel B: the correlation of 125 pM TMR1 β clamp at zero (black) and 19 hours of incubation time (red). This figure suggests that there are no observable monomer formation in the 125 pM solution after 19 hours of incubation.

4.3.4.2. Single molecule Fluorescence results. The monomerization of the β

clamp was further studied by smFluorescence. The main logic behind these experiments

these experiments is that right after dilution to a single molecule level (~ pM) from a

much higher concentration (~ μM), TMR2 β clamps will still be quenched and the

smFluorescence signals will resemble the signal from the buffer. With increasing

incubation time, more and more monomers will form and, since monomers are brighter,

the frequency of smFluorescence peaks will increase. First, the smFluorescence signals of

the buffer and 10 pM TMR1 β clamp were measured. TMR1 sample contains β clamps

where two dyes per dimeric clamp and are bright. This results in bright smfluorescence

bursts. Identifying these smFluorescence peaks from TMR1 clamp is crucial to determine

that the instrument has proper optical alignment necessary for single molecule

experiments. Then, the smFluorescence signal of 10 pM TMR2 β-clamp was measured as

a function of time. In the first experiment, the data were taken with an incubation time of

5 hours, 8 hours and 12 hours. Figure 4.19 presents the representative single molecule

signals from these data. The signals arising from buffer (A, teal), 10 pM TMR1 β (B,

black), 10 pM TMR2 β at time zero (C, blue), and 10 pM TMR2 β after 5 hours of

incubation were shown in Figure 4.19. The dissociation to monomer for the TMR2 β

clamp increases the distance between the two monomers and the fluorescence as the H-

dimer is disrupted. The increase in single molecule peaks of TMR2 β over time is thus

indicative of dissociation of the β clamps. The data acquired right after dilution of TMR1

β clamp samples to single molecule concentrations are indicative of a molecule with two

fluorophores. Monomers of TMR2 samples also have two dyes. Thus the height of the

expected peak for TMR1 β right after dilution should be similar to the TMR2 β after

monomerization, as they both contain two dyes.
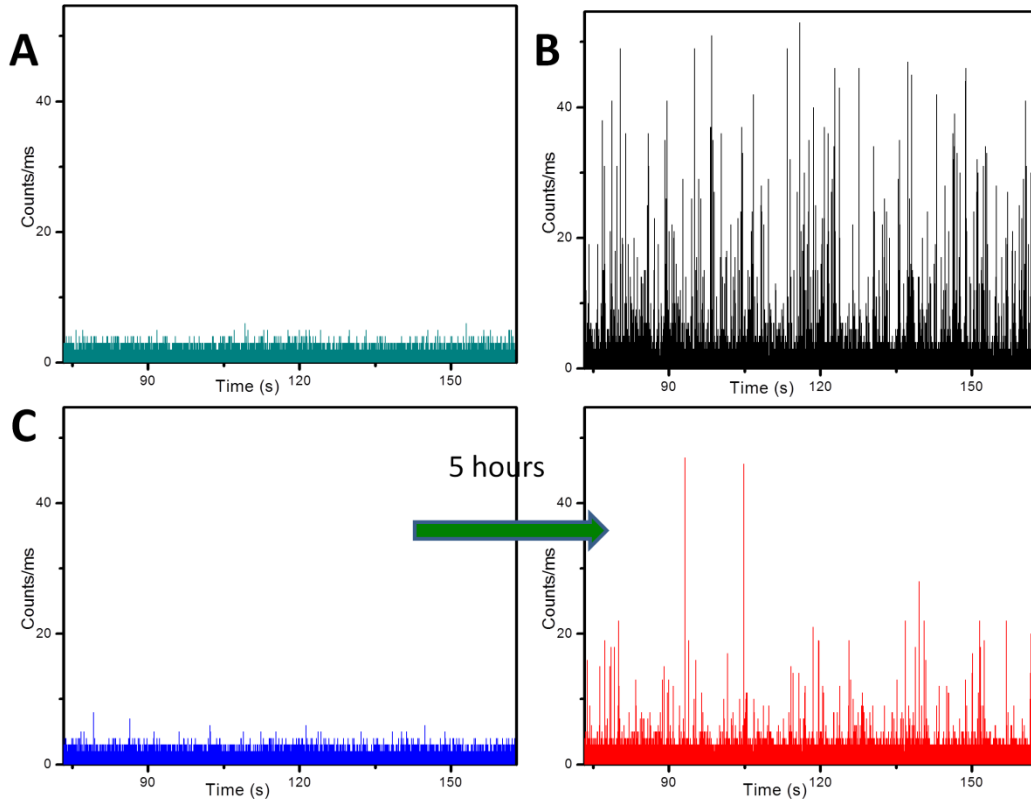
Figure 4.19. smFluorescence signals arising from buffer (A, teal), 10 pM TMR1 β at time zero (B, black), 10 pM TMR2 β at time zero (C, blue), and 10 pM TMR2 β after 5 hours of incubation time.

This time evolution data of smFluorescence peaks for TMR2 β clamp were

analyzed using frequency plots. Figure 4.20 panel A presents the frequency plots of 10

pM TMR2 β clamp as a function of time. This plot shows the changes in the frequency of

appearance of smFluorescence signals right after dilution (blue) and after an incubation

time of 5 hours (red), 8 hours (green) and 12 hours (purple). Panel B describes the time

evolution of 10 pM TMR2 β after a different incubation time scale: for the first 3 hours of incubation time. All of this frequency data was analyzed with a smFluorescence peak being defined as a signal above 6 counts/ms, which is shown in panel C. The frequency plots in panels A and B indicate that an incubation time longer than 3 hours is needed to see any dissociation of the β clamp but after 8 hours, the continuous evolution peaks arising from 10 pM TMR2 β clamp reaches a plateau.

Figure 4.20. Frequency plots of evolution of single molecule peaks of 10 pM TMR2 β clamp of 12 hours incubation (A) and three hours of incubation (B). Panel C describes the frequency of times a signal higher than 6 counts/ms appears.
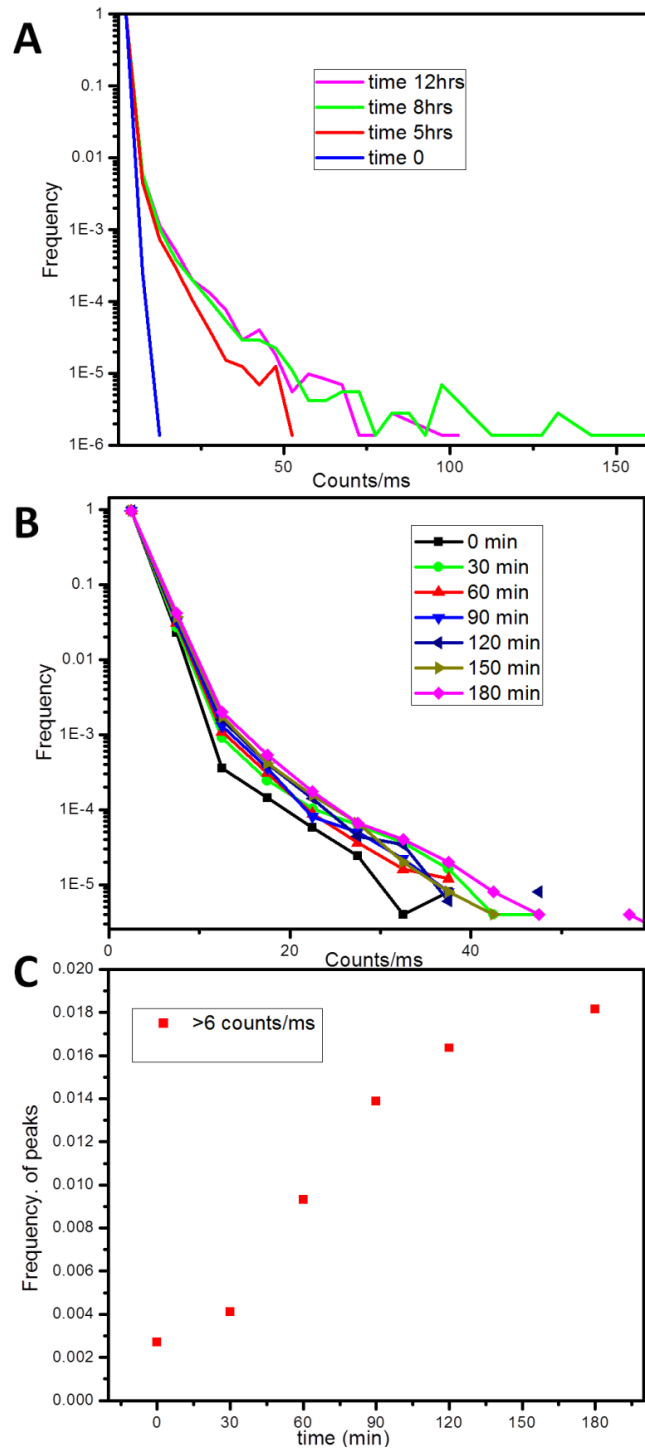
184

4.3.4.3. Results from the ring opening and closing experiments. Figure 4.21

panel A shows the autocorrelation function of TMR2 (black) and TMR1 (red) β clamp

autocorrelation functions. The blue dotted line is the normalized TMR1 β clamp

autocorrelation function where it was been overlapped at the diffusion timescales of the

correlation decay of TMR2. Panel B shows the ratio of TMR2/TMR1 correlation decays

(black). The presence of a decay in this plot could be indicative of a ring opening-closing

equilibrium. This decay cannot be fitted with a monoexponential decay (blue dotted line,

panel B) and requires a stretched exponential ($y = y_0 + Exp[-t^\beta]$) with a β value of

0.417.
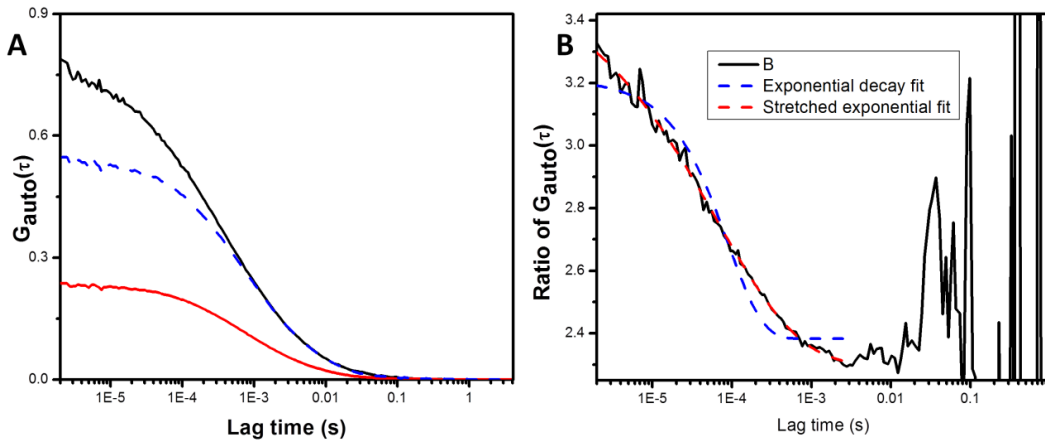
Figure 4.21. **Panel A.** β clamp autocorrelation and ratio of autocorrelations of TMR2 to TMR1 β clamp. Autocorrelation decays of TMR1 β clamp (red), TMR2 β clamp (black) and normalized autocorrelation decay of TMR1 β clamp (blue). The normalization was done in a way that TMR1 and TMR 2 β clamp autocorrelation decays overlap at the timescales of diffusion. **Panel B.** The ratio of autocorrelations of TMR2 β clamp to the TMR1 β clamp (black). The ratio was fitted to a single exponential decay (blue, dashed) and a stretched exponential decay (red, dashed), with the stretched exponential decay resulting in the best fit of the experimental data.

4.4 Discussion

Both the fluorescence lifetime and steady state fluorescence data describe the extent of quenching in the double labeled TMR2 sliding clamps. The difference in the absorption spectra of the TMR1 and TMR2 version of the clamps shows that the distinctive blue shifted peak for the TMR2 version of the clamp is absent TMR1 clamps. This blue shifted peak is indicative of the H-dimer formation and proves that this dimer formation is indeed the quenching pathway in the TMR2 samples.[22, 23] In addition, the experiments with SDS prove that increasing the distance between the two dyes involved in the H-dimer formation results in disruption of dimer formation and subsequent increase in fluorescence. Our collaborators have also treated the TMR2 clamps with clamp loader proteins and have observed increase in fluorescence (data not shown), consistent with the fact that these clamps are known to exist in an open conformation when bound to the clamp loader.

4.4.1. PCNA monomerization. PCNA monomerization was studied by analyzing the autocorrelation decays of TMR1 PCNA samples as a function of concentration and time. Figure 4.9 shows that even at the start of the incubation time, the diffusion coefficient of the 1 nM TMR1 PCNA is larger than that of the 100 nM sample. This is due to the fact that the acquisition of the correlation decay requires five minutes after the dilution to 1 nM concentration, and during this time of data acquisition, there can be some monomerization of the PCNA. This is also apparent from the values of the D_{app} and at how it increases due to more contribution from the monomers. The larger the extent of increase in the diffusion constant over time, the larger the contribution of the monomers

to the diffusion coefficient. The monomers are smaller compared to the trimeric PCNA and thus, have much faster diffusion as indicated from the diffusion coefficient calculations from Hydropro. Figure 4.9 also shows how the extent of increase in D_{app}s over time is highest for the 1 nM sample. This is reflective of the fact that for a given K_D, the lower the concentration of the protein, the higher the extent of monomerization. This PCNA monomerization, although observed before, has not been quantified until now.

To obtain the rate of association and dissociation of the trimer-monomer equilibrium in PCNA, the time evaluation of the monomeric species at a given concentration can be fitted with numerical solutions involving the evolution of that particular species. Thus, the monomerization of 1 nM TMR1 trimeric PCNA was followed in more detail with correlation decays collected every ten or fifteen minutes for a total seven hours, as shown in Figure 4.10. The difficulty is that to determine the rates of association and dissociation as well as the K_D, the concentrations of the monomers and trimers must be known. To obtain the number of monomers (N_1) and trimers (N_3) of PCNA in the confocal volume, the autocorrelation functions were globally fitted with a two component model, as described in equation 4.5. Figure 4.11 shows the results of the fits: N_1 increases and N_3 decreases over time. Figure 4.13 and Figure 4.14 demonstrate that there was no loss of protein during the course of incubation and measurement of the FCS decays. Figure 4.12 and 4.14 suggest that the equilibrium between the monomers and trimers of the PCNA was not reached after seven hours of the incubation times for the 1 nM TMR1 PCNA autocorrelation experiments. Thus, the value of K_D was obtained from the 24 hours of the incubation experiments and it was determined to be $35 \times 10^3 \pm 11 \times 10^3$ nM^2. The overlap of the evolution of concentration of the monomers of PCNA

and the simulated PCNA monomer evolution in Figure 4.16 shows that the association

rate is ~ 7.8×10^{-9} nM^{-2} s^{-1} and the dissociation rate is ~ 2.73×10^{-5} s^{-1}. This small value of

K_D indicates is that PCNA is stable at concentrations higher than nM. Given the

dissociation rate, to reach equilibrium between monomers and trimers of PCNA at 1 nM

concentration requires almost four days of incubation. Even at a trimer PCNA

concentration of 300 nM, the required equilibrium time is greater than seven hours. In

general, the literature supports these results qualitatively but not quantitatively. As an

example, previous works have reported the presence of monomeric PCNA in the nM to

μM concentration range .[38, 39] However, the incubation time used was insufficient for the

system to reach equilibrium and no study, till now, has looked into the time evolution of

the monomeric species.

4.4.2. β clamp monomerization. The monomerization of the β clamp was first

studied the same way as the PCNA sample using autocorrelation decays. The plot of

normalized autocorrelations of 1 nM to 20 nM TMR1 β clamp and a mixture of 5 nM

TMR1 and 500 nM wt β clamp solution after three hours of incubation time overlap with

each other. This means that β clamp is much more stable than the trimeric PCNA and

even at 1 nM concentration, the β clamp does not dissociate after an incubation time of 3

hours. Additionally, autocorrelation decays were measured at β clamp concentrations of

125 pM to 1 nM both right after dilution and after 18 hours of incubation. The

normalized autocorrelations of the four concentrations in this experiment: 125 pM, 250

pM, 500 pM and 1 nM, overlap with each other at both time zero and 18 hours later or

even 19 hours later in the case of 125 pM TMR1 β clamp. This proves that even at 125

pM concentration, there is no monomerization after 19 hours of incubation time. The absence of evidence of monomerization of the β clamp in the correlation experiments proves that β clamp is more stable than PCNA. PCNA starts monomerizing in the nM-concentration range. However, even in the pM-concentration range, the β clamp has little monomerization. This proves that the stability of these two clamps is very different, which could have very important implications in binding and unbinding with the clamp loader and DNA. Therefore, to study the monomerization of the β clamp, a different type of experiment that can detect and study lower concentration than 125 pM would need to be done.

smFluorescence experiments were conducted to look at the monomerization of the β clamp. A 10pM TMR1 sample was first tested to determine the sensitivity of the measurements. The TMR1 samples are bright and contain two TMRs in a dimeric β clamp, making this a good sample to use to determine the sensitivity of the instrument. The monomeric TMR2 β clamp, since it has two TMRs, should have the same brightness and should be detected with similar intensity as that of the TMR1 dimeric β clamp. The TMR1 β clamp smFluorescence peaks at 10 pM concentration and the absence of peaks in the buffer sample (Figure 4.19) dictate a good signal to noise ratio and sensitive condition to conduct the monomerization experiment of TMR2 β clamp.

Then, the evolution of smFluorescence peaks of a 10 pM TMR2 β clamp was studied as a function of time. Comparison of the signals from TMR2 β at time zero and the buffer show that at time zero, the TMR2 sample behaves as buffer and the clamp is a dimer. This is expected since the TMR2 sample is quenched and so should have a low

189

fluorescence efficiency. As time progresses, however, the dimers should dissociate into monomers and as the monomers are brighter, more and more single molecule peaks should appear, as seen in Figure 4.19. This data was analyzed using the frequency plots and the frequency plots show that more and more smFluorescence peaks appear with increasing incubation time. The frequency of sm peaks does not change after 8 hours. Therefore, it is believed that the sample reaches an equilibrium.

This data can also be analyzed as the frequency of appearance of greater than 6 counts/ms, as described earlier. This show similar trend as that of the frequency plots. This type of analysis is visually easier to demonstrate the saturation of the sm peaks. These experiments demonstrate that the β clamp is very stable and requires concentrations in the pM range for monomerization to occur. However, quantification of the smFluorescence data to determine the K_D is much more complicated. The frequency of single molecule peaks changes based on the definition of the peak height. Furthermore, the conversion between the frequency of peaks and number of molecules is not straight forward, the diffusion time of the clamps and the frequency of labeling and the changes in the detection efficiency of the smFluorescence experiments complicate this conversion. This makes quantification of the observed single molecule data very complicated.

4.4.3. Evidence of ring opening and closing of β clamp. As stated previously, another way to look at conformational dynamics of a protein is to compare the ratio of the correlations between a sample that is defined solely by diffusion (TMR1) to a sample that has both diffusion and dynamic behavior (TMR2). The ratio of the correlations of TMR2

190

to TMR1 for the β clamp is indicative of the ring opening and closing, as seen in Figure 4.21. It is very clear that the decay in the ratio does not fit to a monoexponential decay. Monoexponential decays are indicative of a two step process. This decay ratio, however, fits to a stretch exponential function with a β value of 0.417. This suggests the presence of some other complex mechanism involving more than two steps. There are many photophysical processes as well as other conformational processes not related to protein dynamics that could be responsible for the non-monoexponential decay. As an example, the dynamics of the linker can also cause the H-dimer to open and create fluctuations in the observed fluorescence intensity. Further work is underway to produce a mutant β clamp where the two monomers are bound to each other and thus it cannot open. This will provide a better control of a ring without any open conformation. Absence of a decay in the ratio of TMR2 to TMR1 correlations of this closed clamp will validate the above mentioned results.

In summary, the experiments with the sliding clamps show that the stability of the two sliding clamps under investigation, β clamp from *E. coli* and PCNA from *S. cerevisiae*, is dramatically different. PCNA starts dissociation in the ~nM concentration range, while β clamp needs ~pM concentration to show any evidence of monomerization. The difference in the stability of PCNA and β clamp suggests that although these proteins are topologically very similar, they may have very different pathways to interact with DNA and other proteins. As an example, this difference in stability could also have a pronounced effect on the binding and transfer pathway to the DNA and interactions with the clamp loader. While it is known that the sliding clamps

191

exist in an open structure when they are bound to the clamp loaders, how the sliding clamps binds to the clamp loaders is still an open question. There are a number of different hypotheses as to how this happens, including: 1) If there are any intrinsic open clamp structures in solution, however miniscule the amount, the clamp loader might bind specifically to them and help stabilize the clamp in the open conformation or 2) The clamp loader could bind to any closed clamp and pry it open. Our studies suggest that there is a rapid spontaneous equilibrium between the open and the closed clamp. Future work into the understanding the conformations of these clamps would help in understanding more of how these clamps are loaded onto DNA.

4.5. References

1.   Bloom, L. B., Loading clamps for DNA replication and repair. *DNA Repair (Amst)* **2009,** 8, (5), 570-8.

2.   Indiani, C.; O'Donnell, M., The replication clamp-loading machine at work in the three domains of life. *Nat. Rev. Mol. Cell Biol.* **2006,** 7, (10), 751-761.

3.   Kamlet, M. J.; Abboud, J. L. M.; Abraham, M. H.; Taft, R. W., Linear Solvation Energy Relationships .23. A Comprehensive Collection of the Solvatochromic Parameters, Pi-Star, Alpha and Beta, and Some Methods for Simplifying the Generalized Solvatochromic Equation. *J Org Chem* **1983,** 48, (17), 2877-2887.

4.   Kornberg, A.; Baker, T. A., *Dna Replication*. Univ Science Books: 2005.

5.   Kuriyan, J.; Bowman, G. D.; Goedken, E. R.; Kazmirski, S. L.; O'Donnell, M., DNA polymerase clamp loaders and DNA recognition. *FEBS Lett.* **2005,** 579, (4), 863-867.

6.   Kuriyan, J.; Odonnell, M., Sliding Clamps of DNA-Polymerases. *J Mol Biol* **1993,** 234, (4), 915-925.

7.   Johnson, A.; O'Donnell, M., Ordered ATP hydrolysis in the gamma complex clamp loader AAA plus machine. *J Biol Chem* **2003,** 278, (16), 14406-14413.

8.   Bloom, L. B., Dynamics of loading the Escherichia coli DNA polymerase processivity clamp. *Crit Rev Biochem Mol Biol* **2006,** 41, (3), 179-208.

9.   Georgescu, R. E.; Yao, N. Y.; O'Donnell, M., Single-molecule analysis of the Escherichia coli replisome and use of clamps to bypass replication barriers. *Febs Letters* **2010,** 584, (12), 2596-2605.

10.   Dionne, I.; Nookala, R. K.; Jackson, S. P.; Doherty, A. J.; Bell, S. D., A heterotrimeric PCNA in the hyperthermophilic archaeon Sulfolobus solfataricus. *Mol Cell* **2003,** 11, (1), 275-282.

11.   Torimura, M.; Kurata, S.; Yamada, K.; Yokomaku, T.; Kamagata, Y.; Kanagawa, T.; Kurane, R., Fluorescence-quenching phenomenon by photoinduced electron transfer between a fluorescent dye and a nucleotide base. *Anal Sci* **2001,** 17, (1), 155-160.

12.   Krishna, T. S.; Kong, X. P.; Gary, S.; Burgers, P. M.; Kuriyan, J., Crystal structure of the eukaryotic DNA polymerase processivity factor PCNA. *Cell* **1994,** 79, (7), 1233-43.

13.   Oakley, A. J.; Prosselkov, P.; Wijffels, G.; Beck, J. L.; Wilce, M. C.; Dixon, N. E., Flexibility revealed by the 1.85 A crystal structure of the beta sliding-clamp subunit of Escherichia coli DNA polymerase III. *Acta Crystallogr D Biol Crystallogr* **2003,** 59, (Pt 7), 1192-9.

14.   Georgescu, R. E.; Kim, S. S.; Yurieva, O.; Kuriyan, J.; Kong, X. P.; O'Donnell, M., Structure of a sliding clamp on DNA. *Cell* **2008,** 132, (1), 43-54.

15.   McNally, R.; Bowman, G. D.; Goedken, E. R.; O'Donnell, M.; Kuriyan, J., Analysis of the role of PCNA-DNA contacts during clamp loading. *BMC Struct Biol* **2010,** 10, 3.

16.   Freudenthal, B. D.; Gakhar, L.; Ramaswamy, S.; Washington, M. T., A charged residue at the subunit interface of PCNA promotes trimer formation by destabilizing alternate subunit interactions. *Acta Crystallographica Section D-Biological Crystallography* **2009,** 65, 560-566.

17.   Kochaniak, A. B.; Habuchi, S.; Loparo, J. J.; Chang, D. J.; Cimprich, K. A.; Walter, J. C.; van Oijen, A. M., Proliferating Cell Nuclear Antigen Uses Two Distinct Modes to Move along DNA. *J Biol Chem* **2009,** 284, (26), 17700-17710.

18.   Yao, N.; Turner, J.; Kelman, Z.; Stukenberg, P. T.; Dean, F.; Shechter, D.; Pan, Z. Q.; Hurwitz, J.; O'Donnell, M., Clamp loading, unloading and intrinsic stability of the PCNA, beta and gp45 sliding clamps of human, E. coli and T4 replicases. *Genes Cells* **1996,** 1, (1), 101-13.

19.   Millar, D.; Trakselis, M. A.; Benkovic, S. J., On the solution structure of the T4 sliding clamp (gp45). *Biochemistry* **2004,** 43, (40), 12723-7.

20.   Alley, S. C.; Shier, V. K.; Abel-Santos, E.; Sexton, D. J.; Soumillion, P.; Benkovic, S. J., Sliding clamp of the bacteriophage T4 polymerase has open and closed subunit interfaces in solution. *Biochemistry* **1999,** 38, (24), 7696-709.

21.   Kazmirski, S. L.; Zhao, Y.; Bowman, G. D.; O'Donnell, M.; Kuriyan, J., Out-of-plane motions in open sliding clamps: molecular dynamics simulations of eukaryotic and archaeal proliferating cell nuclear antigen. *Proc. Natl. Acad. Sci. U. S. A.* **2005,** 102, (39), 13801-6.

22.   Hamman, B. D.; Oleinikov, A. V.; Jokhadze, G. G.; Bochkariov, D. E.; Traut, R. R.; Jameson, D. M., Tetramethylrhodamine dimer formation as a spectroscopic probe of the conformation of Escherichia coli ribosomal protein L7/L12 dimers. *J Biol Chem* **1996,** 271, (13), 7568-7573.

23.   Hernando, J.; van der Schaaf, M.; van Dijk, E. M. H. P.; Sauer, M.; GarcÃa-ParajÃ³, M. a. F.; van Hulst, N. F., Excitonic Behavior of Rhodamine Dimers:â€‰ A Single-Molecule Study. *The Journal of Physical Chemistry A* **2002,** 107, (1), 43-52.

24.   Paschall, C. O.; Thompson, J. A.; Marzahn, M. R.; Chiraniya, A.; Hayner, J. N.; O'Donnell, M.; Robbins, A. H.; McKenna, R.; Bloom, L. B., The Escherichia coli Clamp Loader Can Actively Pry Open the beta-Sliding Clamp. *J Biol Chem* **2011,** 286, (49), 42704-42714.

25.   Thompson, J. A.; Marzahn, M. R.; O'Donnell, M.; Bloom, L. B., Replication Factor C Is a More Effective Proliferating Cell Nuclear Antigen (PCNA) Opener than the Checkpoint Clamp Loader, Rad24-RFC. *J Biol Chem* **2012,** 287, (3), 2203-2209.

26.   Anderson, S. G.; Thompson, J. A.; Paschall, C. O.; O'Donnell, M.; Bloom, L. B., Temporal correlation of DNA binding, ATP hydrolysis, and clamp release in the clamp loading reaction catalyzed by the Escherichia coli gamma complex. *Biochemistry* **2009,** 48, (36), 8516-27.

27.   Johanson, K. O.; Haynes, T. E.; McHenry, C. S., Chemical characterization and purification of the beta subunit of the DNA polymerase III holoenzyme from an overproducing strain. *J Biol Chem* **1986,** 261, (25), 11460-5.

28.   Pachall, C. O.; Thompson, J. A.; Marzahn, M. R.; Chiraniya, A.; Hayner, J. N.; O'Donnell, M.; Robbins, A. H.; McKenna, R.; Bloom, L. B., The E. coli clamp loader can actively pry open the beta-sliding clamp. *submitted* **2011**.

29.   Gill, S. C.; Vonhippel, P. H., Calculation of Protein Extinction Coefficients from Amino-Acid Sequence Data. *Anal Biochem* **1989,** 182, (2), 319-326.

30.   Bradford, M. M., A rapid and sensitive method for the quantitation of microgram quantities of protein utilizing the principle of protein-dye binding. *Anal Biochem* **1976,** 72, (1–2), 248-254.

31.   Lowry, O. H.; Rosebrough, N. J.; Farr, A. L.; Randall, R. J., Protein Measurement with the Folin Phenol Reagent. *J Biol Chem* **1951,** 193, (1), 265-275.

32.   de la Torre, J. G.; Huertas, M. L.; Carrasco, B., Calculation of hydrodynamic properties of globular proteins from their atomic-level structure. *Biophys J* **2000,** 78, (2), 719-730.

33.   Ortega, A.; Amoros, D.; de la Torre, J. G., Prediction of Hydrodynamic and Other Solution Properties of Rigid Proteins from Atomic- and Residue-Level Models. *Biophys J* **2011,** 101, (4), 892-898.

34.   Mader, O.; Reiner, K.; Egelhaaf, H. J.; Fischer, R.; Brock, R., Structure property analysis of pentamethine indocyanine dyes: Identification of a new dye for life science applications. *Bioconjugate Chem* **2004,** 15, (1), 70-78.

35.   Elson, E. L.; Magde, D., Fluorescence Correlation Spectroscopy .1. Conceptual Basis and Theory. *Biopolymers* **1974,** 13, (1), 1-27.

36.   Schwille, P.; Korlach, J.; Webb, W. W., Fluorescence correlation spectroscopy with single-molecule sensitivity on cell and model membranes. *Cytometry* **1999,** 36, (3), 176-82.

37.   Li, G.; Levitus, M.; Bustamante, C.; Widom, J., Rapid spontaneous accessibility of nucleosomal DNA. *Nat Struct Mol Biol* **2005,** 12, (1), 46-53.

38.   De Biasio, A.; Sanchez, R.; Prieto, J.; Villate, M.; Campos-Olivas, R.; Blanco, F. J., Reduced Stability and Increased Dynamics in the Human Proliferating Cell Nuclear Antigen (PCNA) Relative to the Yeast Homolog. *Plos One* **2011,** 6, (2).

39.   Schurtenberger, P.; Egelhaaf, S. U.; Hindges, R.; Maga, G.; Jonsson, Z. O.; May, R. P.; Glatter, O.; Hubscher, U., The solution structure of functionally active human

proliferating cell nuclear antigen determined by small-angle neutron scattering. *J Mol Biol* **1998,** 275, (1), 123-132.

APPENDIX A

SUPPLEMENTARY INFORMATION FOR CHAPTER 3

A.1. Derivation of the equation 3.3 for fitting of the time resolved anisotropy decays of cy3b-dnmp complex.

Time resolved associated fluorescence anisotropy decay is defined as the type of anisotropy decay, where the decay arises from two separate independent components. The associated anisotropy decay is defined as:[1]

$$r(t) = \sum_{i=1}^{n} f_i \times r_i(t) = f_1 r_1(t) + f_2 r_2(t) \tag{A.1.1}$$

Here f_1 and f_2 are the fractional intensities of free Cy3B and Cy3B-dNMP complex, respectively. $r_1(t)$ and $r_2(t)$ are the fluorescence anisotropy decays of the Cy3B and Cy3B-dNMP respectively.

The fluorescence anisotropy decays of each component can be described as,

$r_i(t) = r_i^0 \times e^{-t/\tau_{r_i}}$, where r_i^0 is the intrinsic fluorescent anisotropy of the species i, and τ_{r_i} is the fluorescent lifetime of the same.[2]

So, $r(t) = f_1 \times r_1^0 \times e^{-t/\tau_{r_1}}, + f_2 \times r_2^0 \times e^{-t/\tau_{r_2}} \tag{A.1.2}$

Let's assume that the association equilibrium is given by,
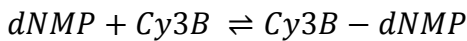
$$dNMP + Cy3B \rightleftharpoons Cy3B - dNMP$$

The association constant is then given by, $K = \dfrac{[Cy3B-dNMP]}{[Cy3B] \times [dNMP]}$

Now,

$$[Cy3B]_0 = [Cy3B] + [Cy3B - dNMP] = [Cy3B] + K \times [Cy3B] \times [dNMP],$$

So, $[Cy3B]_0 = [Cy3B](1 + K \times [dNMP])$.

$$[Cy3B] = \frac{[Cy3B]_0}{\{1 + K \times [dNMP]\}} \tag{A.1.3}$$

$$[Cy3B - dNMP] = \frac{K \times [Cy3B]_0 \times [dNMP]}{\{1 + K \times [dNMP]\}} \tag{A.1.4}$$

After addition of dNMP to the Cy3B solution, the intensity of fluorescence,

$$I_F = I_{Cy3B} + I_{Cy3B-dNMP},$$

Intensity of free Cy3B is given by,

$$I_{Cy3B} = 2.303 \cdot I_0 \cdot \epsilon_1 \cdot [Cy3B] \cdot l \cdot \varphi_1 \cdot \eta_D = b \cdot \epsilon_1 \cdot \varphi_1 \cdot \frac{[Cy3B]_0}{1 + K \times [dNMP]} \tag{A.1.5}$$

In the above equation $I_0, l, \eta_D, \epsilon_1, \varphi_1$ are the intensity of the incident light, length of the path of light through the sample, detector efficiency of the spectrofluorometer, extinction coefficient of Cy3B at the wavelength of the excitation and the quantum yield of Cy3B, respectively. b is a constant which is given by, $b = 2.303 \cdot I_0 \cdot l \cdot \eta_D$

Intensity of the complex is given by,

$$I_{Cy3B-dNMP} = 2.303 \cdot I_0 \cdot \epsilon_2 \cdot [Cy3B - dNMP] \cdot l\varphi_2\eta_D = b \cdot \epsilon_2 \cdot \varphi_2 \cdot \frac{K \times [Cy3B]_0 \times [dNMP]}{1 + K \times [dNMP]}$$

The total fluorescence of the system is given by,

$$I_F = \frac{b \cdot [Cy3B]_0}{1 + K \cdot [dNMP]} \times \{\epsilon_1\varphi_1 + \epsilon_2\varphi_2 \cdot K \cdot [dNMP]\}$$

The fractional intensity of Cy3B is given by,

$$f_{Cy3B} = \frac{\epsilon_1\varphi_1}{\epsilon_1\varphi_1 + \epsilon_2\varphi_2 \cdot K \cdot [dNMP]} = \frac{1}{1 + \frac{\epsilon_2\varphi_2}{\epsilon_1\varphi_1} \cdot K \cdot [dNMP]}$$

The fractional intensity of the anisotropy decays is given by,

$$f_{Cy3B-dNMP} = \frac{\epsilon_2\varphi_2 \cdot K \cdot [dNMP]}{\epsilon_1\varphi_1 + \epsilon_2\varphi_2 \cdot K \cdot [dNMP]} = \frac{K \cdot [dNMP]}{\frac{\epsilon_{21}\varphi_1}{\epsilon_2\varphi_2} + K \cdot [dNMP]}$$

So, the time resolved anisotropy decay is given by,

$$r(t) = \frac{1}{1 + \frac{\epsilon_2\varphi_2}{\epsilon_1\varphi_1}K_{eq}[dNMP]} r^0_{Cy3B} e^{-t/\tau_{Cy3B}} + \frac{K_{eq}[dNMP]}{\frac{\epsilon_1\varphi_1}{\epsilon_2\varphi_2} + K_{eq}[dNMP]} r^0_{Cy3B-dNMP} e^{-t/\tau_{Cy3B-dNMP}}$$

(A.1.6)

$$r(t) = \frac{1}{1+d} r^0_{Cy3B} e^{-t/\tau_{Cy3B}} + \frac{1}{1+1/d} r^0_{Cy3B-dNMP} e^{-t/\tau_{Cy3B-dNMP}} \qquad \text{(A.1.7)}$$

Where, $d = \frac{\epsilon_2\varphi_2}{\epsilon_1\varphi_1} K_{eq} [dNMP]$

    Equation A.1.6 or A.1.7 can be used to fit the time resolved anisotropy decays shown in Figure 3.10. If r_0 for the complex and the free dye is known, then K_{eq} can be calculated from the amplitude of the biexponential fits of the anisotropy decays.

A.2. Calculation of concentrations of monomers of dnmps after self association using isodesmic model.

The self association of the dNMPs was simulated using the isodesmic model of indefinite self association.[3] According to this model, the nucleotide (N) association can be depicted as follows:

$$N + N \rightleftharpoons N_2$$

$$N_2 + N \rightleftharpoons N_3$$

$$N_3 + N \rightleftharpoons N_4 \ldots\ldots\ldots\ldots\text{so on.}$$
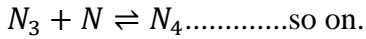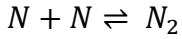
The association constant is the same in each steps, and is given by K.

So,

$$\frac{[N_2]}{[N]^2} = K, \qquad \frac{[N_3]}{[N_2] \times [N]} = K, \qquad \frac{[N_4]}{[N_3] \times [N]} = K \ldots\ldots\ldots\ldots\ldots$$

$$\therefore [N_2] = K \times [N]^2$$

$$[N_3] = K \times [N_2] \times [N] = K^2 \times [N]^3$$

$$[N_4] = K \times [N_3] \times [N] = K^3 \times [N]^4$$

So the total concentration is given by,

$$[N]_{total} = \sum_{n=1}^{\infty} n \times [N_n] = [N] + 2 \cdot [N_2] + 3 \cdot [N_3] + 4 \cdot [N_4] + 5 \cdot [N_5] +$$

$$\ldots\ldots\ldots \qquad\qquad\qquad\qquad\qquad\qquad\qquad\qquad \text{(A.2.1)}$$

$$[N]_{total} = [N] + 2 \cdot K \cdot [N]^2 + 3 \cdot K^2 \cdot [N]^3 + 4 \cdot K^3 \cdot [N]^4 + 5 \cdot K^4 \cdot [N]^5 + \ldots\ldots\ldots$$

$$[N]_{total} = [N] \cdot (1 + 2 \cdot K \cdot [N] + 3 \cdot K^2 \cdot [N]^2 + 4 \cdot K^3 \cdot [N]^3 + 5 \cdot K^4 \cdot [N]^4 + \ldots)$$

$$[N]_{total} = [N] \times \sum_{n=1}^{\infty} n \times (K \cdot [N])^{n-1} = \frac{[N]}{(1-K\cdot[N])^2} \tag{A.2.2}$$

Using Taylor's theorem, $\sum_{n=1}^{\infty} n \times (K \cdot [N])^{n-1} = \frac{[N]}{(1-K\cdot[N])^2}$

Rearranging the above relation for the total concentration gives rise to the following quadratic equation:

$$K^2 \cdot [N]_{total} \cdot [N]^2 - (2K[N]_{total} + 1) \cdot [N] + [N]_{total} = 0$$

Solution of this quadratic equation results in the equation used for the calculation of the monomer concentration and is give by,

$$[N] = \frac{(2\,K\,[N]_{total}+1) \pm \sqrt{1+4\,K\,[N]_{total}}}{2\,K^2\,N_{total}} \tag{A.2.3}$$

The concentrations of all the other oligomers are directly related to the monomeric concentration and can be calculated accordingly.

1. Lakowicz, J. R., *Principles of fluorescence spectroscopy*. Springer: 2006; Vol. 1.

2. Valeur, B., *Molecular Fluorescence: Principles and Applications*. Wiley-VCH: Weinheim, Germany, 2001.

3. Scheller, K. H.; Hofstetter, F.; Mitchell, P. R.; Prijs, B.; Sigel, H., Macrochelate Formation in Monomeric Metal-Ion Complexes of Nucleoside 5'-Triphosphates and the Promotion of Stacking by Metal-Ions - Comparison of the Self-Association of Purine and Pyrimidine 5'-Triphosphates Using Proton Nuclear Magnetic-Resonanc. *J Am Chem Soc* **1981,** 103, (2), 247-260.

APPENDIX B

SUPPLEMENTARY INFORMATION FOR CHAPTER 4

B.1. Derivation of the two component fitting equation (equation 4.5) for the TMR1 PCNA FCS decays.

FCS decays of TMR1 PCNA after 24 hours of incubation time and the time evolution of FCS decays of 1 nM TMR1 PCNA solution were fitted with equation 4.5. The derivation of this equation is described below.

FCS decay of a sample with multiple species with multiple brightness can be described as[1]

$$G(\tau) = \left(\sum_{i=1}^{n} N_i B_i^2 G_i(\tau)\right) / \left(\sum_{i=1}^{n} N_i B_i\right)^2 \tag{B.1}$$

Here B_i and N_i represent the brightness and the number of molecule inside the confocal volume of the ith species.

If there is any contribution from the triplet state to the FCS decays, then the correlation decay can be described as,[2]

$$G(\tau) = X_{triplet} \times D_{diffusion} \tag{B.2}$$

In the above equation $X_{triplet}$ is the triplet term and $D_{diffusion}$ is the diffusion term. The triplet term can be described by,[2]

$$X_{triplet} = 1 - f + f \times Exp\left[-\tau/\tau_{triplet}\right] \tag{B.3}$$

where f is the fraction of molecules in the triplet state and $\tau_{triplet}$ is the triplet relaxation time.

If the average labeling efficiency is given by x and the total numbers of monomers of PCNA at any point of time is N_1 then the number of labeled monomers are xN_1 and the number of unlabeled monomers are $(1-x)N_1$.

The number of trimers having a particular numbers of labels can be calculated from the binomial distribution and the efficiency of labeling (x). Assuming that at a certain time the total average of trimeric PCNA in the confocal volume is N_3, the number of trimers having n labels is given by,[3]

$$N_3^n = \binom{n}{3} x^n (1-x)^{3-n} N_3 = \frac{3!}{n! \times (3-n)!} x^n (1-x)^{3-n} N_3 \qquad \text{(B.4)}$$

So, the number of trimers with one label $= N_3^1 = 3x(1-x)^2 N_3$

The number of trimers with two label $= N_3^2 = 3x^2(1-x) N_3$

The number of trimers with one label $= N_3^3 = x^3 N_3$

the number of trimers without any label $= N_3^0 = (1-x)^3 N_3$

Considering only the fluorescent species contribute to the FCS decays, the numerator of equation B.1 becomes,

$$\sum_{i=1}^{n} N_i B_i^2 G_i(\tau)$$

$$= xN_1 G_1(\tau) + [3x(1-x)^2 + 3 \times 4 \times x^2(1-x) + 9 \times x^3] N_3 G_3(\tau)$$

$$= xN_1 G_1(\tau) + [3x + 6x^2] N_3 G_3(\tau) \qquad \text{(B.5)}$$

The denominator of equation B.1 becomes

$$\left(\sum_{i=1}^{n} N_i B_i \right)^2$$

$$= [xN_1 + [3x(1-x)^2 + 3 \times x^2(1-x) \times 2 + 3 \times x^3]N_3]^2$$

$$= [xN_1 + 3xN_3]^2 \tag{B.6}$$

So, the final form of equation B.1 becomes,

$$G(\tau) = \frac{[xN_1G_1(\tau) + (3x + 6x^2)N_3G_3(\tau)]}{(xN_1 + 3xN_3)^2} \tag{B.7}$$

If there is a triplet component in the correlation decay, then the final fitting equation transforms to,

$$G(\tau) = \frac{(1 - f + f \times Exp[-\tau/\tau_{triplet}]) \times [xN_1G_1(\tau) + (3x + 6x^2)N_3G_3(\tau)]}{(xN_1 + 3xN_3)^2} \tag{B.8}$$

TMR1 PCNA has a labeling efficiency of 71.3%. Thus, the value of x in the equation B.8 is 0.713 and equation B.8 transforms to,

$$G(\tau) = \frac{(1 - f + f \times Exp[-\tau/\tau_{triplet}]) \times [0.713N_1G_1(\tau) + 5.189N_3G_3(\tau)]}{(0.713N_1 + 2.139N_3)^2} \tag{B.9}$$

Equation B.9 is represented as equation 4.5 in the main text and used as the fitting equation of the TMR1 PCNA decays with a $\tau_{triplet}$ value of 15 μs.

1.   Lakowicz, J. R., *Principles of fluorescence spectroscopy*. Springer: 2006; Vol. 1.

2.   Schwille, P.; Kummer, S.; Heikal, A. A.; Moerner, W. E.; Webb, W. W., Fluorescence correlation spectroscopy reveals fast optical excitation-driven intramolecular dynamics of yellow fluorescent proteins. *Proc. Natl. Acad. Sci. U. S. A.* **2000,** 97, (1), 151-156.

3.	Chakraborty, M.; Kuriata, A. M.; Henderson, J. N.; Salvucci, M. E.; Wachter, R. M.; Levitus, M., Protein Oligomerization Monitored by Fluorescence Fluctuation Spectroscopy: Self-Assembly of Rubisco Activase. *Biophys J* **2012,** 103, (5), 949-958.

APPENDIX C

CO-AUTHOR APPROVAL

I verify that the following co-authors have approved of my use of our publications

in my dissertation.

Dr. Marcia Levitus (Arizona State University)

Dr. Kaushik Gurunathan (University of Michigan)